

Vilnius University  
and  
Center for Physical Sciences and Technology

Romualdas Trusovas

Formation and Modification of Graphene Layers Using Laser  
Irradiation

Doctoral dissertation  
Technological Sciences, Material Engineering (08T)

Vilnius, 2015

The research was performed in the Department of Laser Technologies of the Center for Physical Sciences and Technology in 2010-2014.

**Scientific supervisor:**

Dr. Gediminas Račiukaitis (Center for Physical Sciences and Technology, technological sciences, material engineering - 08T).



Vilniaus universitetas  
ir  
Valstybinis mokslinių tyrimų institutas Fizinių ir technologijos mokslų centras

Romualdas Trusovas

Grafeno sluoksnių formavimas ir modifikavimas, panaudojant lazerio  
spinduliuotę

Daktaro disertacija  
Technologijos mokslai, medžiagų inžinerija (08T)

Vilnius, 2015

Disertacija rengta 2010-2014 metais Valstybinio mokslinių tyrimų instituto Fizinių ir technologijos mokslų centre Lazerinių technologijų skyriuje.

**Mokslinis vadovas:**

Dr. Gediminas Račiukaitis (Fizinių ir technologijos mokslų centras, technologijos mokslai, medžiagų inžinerija - 08T).

# Table of Contents

<b>ACKNOWLEDGMENTS .....</b>	<b>8</b>
<b>LIST OF ABBREVIATIONS .....</b>	<b>9</b>
<b>1 INTRODUCTION .....</b>	<b>11</b>
1.1 THE AIM OF THE RESEARCH.....	12
1.2 PRACTICAL VALUE AND NOVELTY .....	12
1.2.1 <i>The novelty of the thesis.....</i>	<i>12</i>
1.2.2 <i>The practical value of the thesis .....</i>	<i>13</i>
1.3 STATEMENTS TO BE DEFENDED .....	13
1.4 APPROBATION .....	14
1.4.1 <i>Scientific papers.....</i>	<i>14</i>
1.4.2 <i>Conference presentations .....</i>	<i>15</i>
1.5 CONTRIBUTIONS.....	18
1.5.1 <i>Author's contribution.....</i>	<i>18</i>
1.5.2 <i>Coauthors' contribution .....</i>	<i>18</i>
<b>2 LITERATURE REVIEW .....</b>	<b>19</b>
2.1 GRAPHENE PROPERTIES AND APPLICATIONS .....	19
2.2 GRAPHENE CHARACTERIZATION APPLYING RAMAN SPECTROSCOPY.....	23
2.3 GRAPHENE PRODUCTION METHODS .....	25
2.4 GRAPHITE OXIDE REDUCTION .....	26
2.5 GRAPHENE PRODUCTION AND MODIFICATION WITH LASER IRRADIATION .....	31
2.5.1 <i>Graphene Oxide Reduction With Laser Irradiation.....</i>	<i>31</i>
2.5.2 <i>Graphene ablation.....</i>	<i>40</i>
<b>3 EXPERIMENTAL SET-UPS AND PROCEDURES.....</b>	<b>44</b>
3.1 SAMPLE PREPARATION .....	44
3.1.1 <i>Samples used in graphite oxide reduction.....</i>	<i>44</i>

3.1.2	<i>Samples used in graphite oxide with Congo Red dye reduction</i>	49
3.1.3	<i>Samples used in graphene-chitosan laser treatment experiments</i>	51
3.2	LASER TREATMENT .....	52
3.3	CHARACTERIZATION .....	55
<b>4</b>	<b>GRAPHITE OXIDE REDUCTION TO GRAPHENE USING PICOSECOND LASER IRRADIATION.....</b>	<b>57</b>
4.1	ELECTRICAL RESISTANCE OF MODIFIED GO LAYER .....	60
4.2	SIMULATION OF HEAT TRANSFER VIA GRAPHENE CHANNELS ...	62
4.3	RAMAN SPECTRA ANALYSIS .....	66
4.4	CONCLUSIONS .....	68
<b>5</b>	<b>GRAPHITE OXIDE/ CONGO RED NANOCOMPOSITE COATINGS REDUCTION.....</b>	<b>70</b>
5.1	INVESTIGATION OF CONGO-RED DYE INFLUENCE ON GO REDUCTION	70
5.2	CHARACTERIZATION OF GO LASER TREATED FILMS WITH OPTIMAL CONGO-RED DYE CONCENTRATION .....	72
5.3	MODELING THE TEMPERATURE DYNAMICS DURING THE GO REDUCTION	81
5.4	CONCLUSIONS .....	86
<b>6</b>	<b>GRAPHENE-CHITOSAN COMPOSITE FILM MODIFICATION USING PICOSECOND LASER IRRADIATION .....</b>	<b>87</b>
6.1	INVESTIGATION OF GRAPHENE-CHITOSAN FILM MORPHOLOGY	87
6.2	RAMAN SPECTROSCOPY MEASUREMENTS ON GRAPHENE - CHITOSAN COMPOSITE FILMS .....	89
6.3	ELECTROCHEMICAL INVESTIGATION OF GRAPHENE-CHITOSAN MODIFIED ITO ELECTRODES.....	93
6.3.1	<i>Cyclic voltammetry</i> .....	93

6.3.2	<i>Electrochemical impedance spectroscopy</i> .....	94
6.4	UNIFORM MODIFICATION OF GRAPHENE-CHITOSAN FILM .....	97
6.5	CONCLUSIONS .....	104
<b>LIST OF CONCLUSIONS .....</b>		<b>105</b>
<b>SUMMARY .....</b>		<b>107</b>
<b>REFERENCES.....</b>		<b>108</b>

## ACKNOWLEDGMENTS

This research was funded by grants No. ATE-06/2010 from the Research Council of Lithuania and No. VP1-3.1-ŠMM-07-K-01-124 European Social Fund under the Global Grant measure.

First of all I am extremely grateful to my scientific supervisor Dr. G. Račiukaitis for his valuable guidance, support, patience and useful advices.

Thanks to Prof. J. Barkauskas and his group for the graphite oxide samples preparations.

Thanks to Dr. G. Niaura and Dr. R. Mažeikienė for the Raman spectra analysis.

Thanks to K. Ratautas for the modelling work.

Thanks to Dr. R. Pauliukaitė, Dr. R. Celiešiūtė and A. Radzevič for the preparation and electrochemical analysis of graphene/chitosan samples.

Thanks for my colleague Dr. M. Gedvilas for the fruitful discussions and useful tips.

Thanks to Dr. P. Gečys, Dr. E. Stankevičius, B. Voisiat, E. Markauskas, S. Indrišiūnas and other colleagues from the Department of Laser Technologies for cozy atmosphere at work.

Thanks to my parents.

Thanks to my friends who encouraged me to take this challenge, supported me and continuously were curious when I will finish my thesis.

## LIST OF ABBREVIATIONS

0D	Zero dimensional;
1D	One dimensional;
2D	Two dimensional/ Graphene Raman peak at $\sim 2700\text{ cm}^{-1}$ ;
3D	Three dimensional;
AFM	Atomic Force Microscopy;
BLG	Bi-layer graphene;
CCD	Charge-coupled device;
CMOS	Complementary metal–oxide–semiconductor;
CR	Congo-Red dye;
CV	Cyclic voltammetry;
CVD	Chemical vapor deposition;
DNA	Deoxyribonucleic acid;
EIS	Electrochemical Impedance Spectroscopy;
FET	Field-effect transistor;
FT-IR	Fourier transform infrared spectroscopy;
FWHM	Full width at half maximum;
GNR	Graphene nanoribbon;
GO	Graphene/graphite oxide;
HOPG	Highly oriented pyrolytic graphite;
ITO	Indium tin oxide;
LED	Light-emitting diode;
LDW	Laser Direct Writing;
Nd:YVO <sub>4</sub>	Neodymium-doped ytterbium vanadate;
NMP	N-Methylpyrrolidone;
PC	Polycarbonate;
PECVD	Plasma enhanced chemical vapor deposition;
PLD	Pulsed laser deposition;
QHE	Quantum Hall effect;
rGO	Reduced graphene oxide;

SEM	Scanning electron microscope;
SLG	Single layer graphene;
SLM	Spatial light modulator;
TEM	Transmission electron microscopy;
UHV	Ultra high vacuum;
XPS	X-ray photoelectron spectroscopy.



# 1 INTRODUCTION

Graphene is one-atom thick two-dimensional crystal, consisted from carbon atoms, joined into a honeycomb lattice. From its discovery in 2004 [1], this material gained huge amount of interest from researchers working in various fields. Graphene has unique physical properties, such as high carrier mobility [2], high thermal conductivity and quantum hall effect at room temperature [3], high optical transpance in visible range [4]. It is also mechanically strong material [5]. These properties made graphene very attractive material for various applications. Graphene can be applied in ultrafast FET transistors [6,7], it can be used as a transparent electrode material [8], applied in various polymer composites, saturable absorbers, biological and medicine applications [9].

Diverse graphene production methods have been developed since the first graphene flake was obtained by mechanical exfoliation method. Nowadays, most of developed methods are based on CVD [10] and various implementations of graphene oxide reduction [11]. So far, these methods are considered to be the most promising for mass-production of graphene.

Some graphene oxide production methods employ laser irradiation. Laser can be useful tool for performing the reduction process, as it helps to avoid using hazardous aggressive materials such as hydrazine in chemical reduction or using complex heating systems, which are used in CVD and thermal GO reduction operations. Focused laser beam enables forming of complex conductive graphene microstructures on insulating substrates. Such fabrication features can be useful in electronics applications such as super capacitors, electrodes or heat removal systems formation [3,8,12-22].

Furthermore, the laser-based modification of GO or graphene layers can be a versatile implementation for fabrication of various devices. Tailoring of different laser microfabrication parameters, such as fluence, scanning rate or focusing spot diameter leads to extensive modification range: from thinning of

material to complete its ablation. Such flexible processing enables controlling of physical properties of graphene/GO materials layers.

## **1.1 THE AIM OF THE RESEARCH**

The aim of this research was to investigate formation and modification of graphene layers applying laser irradiation. This goal was divided into two tasks:

- 1 Reduction of graphite oxide to graphene using laser irradiation, evaluation of the reduction results depending on composition of the graphite oxide film and laser irradiation parameters. The task was intended to fabricate the heat-conductive graphene channels in thermo-insulating graphite oxide substrate.
- 2 Modification of graphene/chitosan composite films with laser irradiation for bio-sensor contacts improving of their electrochemical properties, and evaluation of spectroscopic and electrochemical properties of the contacts depending on laser treatment parameters.

## **1.2 PRACTICAL VALUE AND NOVELTY**

### **1.2.1 THE NOVELTY OF THE THESIS**

Various graphene production methods are under development to be applied in the mass production. Despite that the micromechanical cleavage technique offers the best-quality monolayer graphene flakes, it is not suitable for production due to relatively slow yield, poor repeatability, and small sizes of produced graphene flakes, which are not acceptable for most applications.

Reduction of graphene oxide is one of the strongest candidates in producing graphene for various devices. The laser-induced reduction of graphene oxide allows transformation of graphene oxide locally and precisely forming heat and electro-conductive graphene channels. Among all GO

reduction methods, this approach is new, with just a few trials, and needs a lot of development until commercial application will be feasible.

In this research, doping of GO films with Congo-Red dye molecules and its input to the GO reduction quality was evaluated for the first time.

Laser treatment of the graphene/chitosan composite films is a new technique for fabrication of bio-sensor electrodes. Our new approach showed that, despite of the increasing disorder of graphene layers, laser irradiation of the composite can improve electrochemical activity of the composite electrodes.

### **1.2.2 THE PRACTICAL VALUE OF THE THESIS**

1. Results of conducted experiments and theoretical simulations helped to evaluate the most effective conditions for GO reduction to graphene using the picosecond laser treatment.
2. Thermo-conductive graphene containing channels were formed in the GO layer, which itself possess physical properties of insulator.
3. Laser reduction of GO with different dopants was evaluated and it was shown that Congo-Red molecules link graphene sheets together.
4. Experiments on the graphene/chitosan composite films modification with laser irradiation, allowed improving electrochemical properties of graphene/chitosan contacts on ITO substrate for their use in bio-sensing applications.

### **1.3 STATEMENTS TO BE DEFENDED**

- 1 Irradiation of graphite oxide with a picosecond laser can lead to its reduction to graphene, which is evident from development of the 2D line, intrinsic to graphene, in Raman spectra of laser treated films in particular range of the processing parameters, a decrease of the electrical resistance and increase of thermal conductivity.

- 2 Product of the pulse energy and the number of laser pulses per spot efficiently describes the process of GO reduction to graphene during the laser treatment. These parameters determine the temperature in the irradiation zone and the time the material is heated. Influence of this product is clearly visible in Raman spectra of laser treated graphite oxide films.
- 3 Laser treatment improves electrochemical characteristics of graphene/chitosan composite films which are used as electrodes for bio-sensing applications. Picosecond laser irradiation forms nanocrystalline graphene and exposes graphene flakes after chitosan ablation which leads to enlargement of the active surface area of the electrode.

## 1.4 APPROBATION

Results of the research, presented in the thesis, were published in 5 scientific papers and together with coauthors the results were presented in 18 contributions to conferences.

### 1.4.1 SCIENTIFIC PAPERS

- A1. **R. Trusovas**, G. Račiukaitis, J. Barkauskas, R. Mažeikienė, Laser Induced graphite oxide/graphene transformation, *JLMN* **7** (2012) 49-53.
- A2. J. Barkauskas, J. Dakševič, R. Juškėnas, R. Mažeikienė, G. Niaura, G. Račiukaitis, A. Selskis, I. Stankevičienė, **R. Trusovas**, Nanocomposite films and coatings produced by interaction between graphite oxide and Congo red, *J. Mater. Sci.* **47** (2012) 5852-5860.
- A3. **R. Trusovas**, K. Ratautas, G. Račiukaitis, J. Barkauskas, I. Stankevičienė, G. Niaura, R. Mažeikienė, Reduction of the graphite oxide to graphene with laser irradiation, *Carbon* **52**,(2013) 574-582.
- A4. I. Matulaitienė, J. Barkauskas, **R. Trusovas**, G. Račiukaitis, R. Mažeikienė, O. Eicher-Lorka, G. Niaura, Potential dependence of SERS

spectra of reduced graphene oxide adsorbed on self-assembled monolayer at gold electrode, *Chem. Phys. Lett.* **590** (2013) 141–145.

- A5. R. Celiešiūtė, **R. Trusovas**, G. Niaura, V. Švedas, G. Račiukaitis, Ž. Ruželė, R. Pauliukaite, Influence of the laser irradiation on the electrochemical and spectroscopic peculiarities of graphene-chitosan composite film, *Electrochim. Acta* **132** (2014) 265-276.

#### 1.4.2 CONFERENCE PRESENTATIONS

1. **R. Trusovas**, G. Račiukaitis, J. Barkauskas, R. Mažeikienė Reduction of the graphite oxide to graphene with a laser irradiation, XIX Belarussian - Lithuanian seminar Lasers and optical nonlinearity, Minsk, Belarus, May 16-18, 2011, (oral).
2. R. Trusovas, **G. Račiukaitis**, J. Barkauskas, R. Mažeikienė, Laser induced graphite oxide/graphene transformation, The 12th International Symposium on Laser Precision Microfabrication (LPM2011), Takamatsu, Japan, June 7-10, 2011 (poster).
3. **R. Trusovas**, G. Račiukaitis, J. Barkauskas, R. Mažeikienė, Reduction of the graphite oxide to graphene with laser irradiation, 12th Int. Conference Electronics and related properties of organic systems, ERPOS-12, Vilnius, July 11-13, 2011 (poster).
4. **J. Barkauskas**, I. Stankevičienė, J. Dakševič, R. Trusovas, G. Račiukaitis, R. Mažeikienė, Interaction between graphite oxide/graphene nanoparticles and functionalized molecules: a way to produce and/or stabilize graphene coatings, International Conference on Carbon, Carbon 2011, Shanghai, China, July 24 – 29, 2011.
5. R. Trusovas, G. Račiukaitis, R. Mažeikienė, **J. Barkauskas**, I. Stankevičienė, J. Dakševič, Thermal conductivity of laser-treated graphene/graphite oxide coatings, International Conference on Carbon, Carbon 2011, Shanghai, China, July 24 – 29, 2011.

6. **R. Trusovas**, G. Račiukaitis, J. Barkauskas, R. Mažeikienė, Graphite oxide conversion to graphene by laser treatment, The 13th International Conference-School Advanced materials and technologies, Palanga, Lithuania, August 27-31, 2011 (poster).
7. **R. Trusovas**, G. Račiukaitis, J. Barkauskas, R. Mažeikienė, Graphite Oxide Reduction to Graphene Applying Ultrashort Laser Pulses, The 2nd International Graphene Conference GRAPHENE 2012, Brussels, Belgium, April 10-13, 2012 (poster).
8. **R. Trusovas**, K. Ratautas, G. Račiukaitis, J. Barkauskas, I. Stankevičienė, R. Mažeikienė, Formation of graphene domains in graphite oxide by picosecond laser treatment, 4rd international conference Radiation interaction with material and its use in technologies 2012, Kaunas, Lithuania, May 14 – 17, 2012 (poster).
9. **R. Trusovas**, K. Ratautas, G. Račiukaitis, J. Barkauskas, R. Mažeikienė, Reduction of the graphite oxide to graphene using ultrashort laser pulses, Summer School of Ultrafast Laser Science and Applications (SSCS), Menorca, Spain, June 10-15, 2012 (oral).
10. **R. Trusovas**, K. Ratautas, G. Račiukaitis, J. Barkauskas, R. Mažeikienė, Producing of graphene using graphite oxide reduction by laser irradiation, International summer school - Trends and new developments in Laser Technology, Dresden, Germany, August 27-31, 2012 (oral).
11. **R. Trusovas**, K. Ratautas, G. Račiukaitis, J. Barkauskas, R. Mažeikienė, Fabrication of graphene channels in graphite oxide by applying picosecond lasers, International Conference on Advanced Laser Technologies, Thun, Switzerland, September 2 – 6, 2012 (oral).
12. **R. Pauliukaite**, R. Celiešiūtė, R. Trusovas, Ž. Ruželė, G. Račiukaitis,, Nanostructure formation and enhance of electrical capacitance of electrode modified with graphene oxide employing laser technology, ElecNano2013, Bordo, France, May 15-17, 2013.
13. **R. Trusovas**, P. Gečys, G. Račiukaitis, R. Celiešiūtė, R. Pauliukaite, Modification of graphene containing film using laser treatment,

- International Symposium: Fundamentals of Laser Assisted Micro- & Nanotechnologies (FLAMN-13), Sankt Petersburg, Russia, June 24-28, 2013 (poster).
14. **R. Trusovas**, G. Račiukaitis, R. Celiešiūtė, R. Pauliukaitė, Picosecond-laser treatment of graphene films used in electro-chemical sensors, The 14th International Symposium on Laser Precision Microfabrication (LAMP2013), Niigata, Japan, July 23-26, 2013 (oral).
  15. **R. Pauliukaitė**, R. Celiešiūtė, R. Trusovas, G. Račiukaitis, Ž. Ruželė, Electrochemical behaviour of laser-treated graphene-oxide-chitosan film modified ITO electrode, 11-oji Lietuvos Chemikų Tarptautinė Konferencija/ 11th International Conference Of Lithuania's Chemists, Vilnius, September 27 2013.
  16. **R. Trusovas**, R. Celiešiūtė, R. Pauliukaite, G. Račiukaitis, Modification of Graphene-Chitosan Composite Film Using Picosecond Laser Treatment, XX-th Lithuania- Belarus seminar Lasers and Optical Nonlinearity, Vilnius, Lithuania, November 21–22, 2013(poster).
  17. **Ž. Ruželė**, R. Celiešiūtė, R. Trusovas, G. Niaura, G. Račiukaitis, R. Valiokas, R. Pauliukaite, Laser Fabrication and Hydrogel Modification on Nanocrystalline Graphene Patterns, NanoBio Europe 2014, Munster, Germany, June 2-4 2014 (poster).
  18. **R. Trusovas**, A. Radzevič, R. Celiešiūtė, R. Pauliukaite, G. Račiukaitis, Influence of the picosecond laser irradiation on the electrochemical and spectroscopic properties of graphene-chitosan composite film, International Conference on Advanced Laser Technologies, Cassis, France, October 6-10, 2014 (oral).

## **1.5 CONTRIBUTIONS**

### **1.5.1 AUTHOR'S CONTRIBUTION**

Author's contribution included:

- Construction of experimental setup and conducting of experiments on laser treatment of graphite oxide and graphene-chitosan films.
- Analysis of experimental results exploiting optical microscopy, SEM and Raman spectroscopy.
- Preparation and publishing the results of experiments in scientific papers and conferences.

### **1.5.2 COAUTHORS' CONTRIBUTION**

- Graphite oxide samples were prepared by Prof. Jurgis Barkauskas group in the Laboratory of Carbonaceous Materials, Faculty of Chemistry, Vilnius University.
- GO/chitosan composites were prepared by Raimonda Celiešiūtė and Aneta Radzevič in the Nanoformation and Biochip Technologies Laboratory, Department of Nanoengineering, Center for Physical Sciences and Technology.
- Raman measurements and analysis were performed by habil. Dr. Gediminas Niaura and Dr. Regina Mažeikienė in the Laboratory of Spectroelectrochemistry, Department of Organic Chemistry, Center for Physical Sciences and Technology.
- Simulations of heat transfer via graphene channels and temperature dynamics during GO reduction were performed by Karolis Ratautas in Department of Laser Technologies, Center for Physical Sciences and Technology.



## 2 LITERATURE REVIEW

### 2.1 GRAPHENE PROPERTIES AND APPLICATIONS

Graphene is the most recently discovered carbon allotrope. It is a two-dimensional crystal consisting of one layer of carbon atoms joined into honeycomb lattice. Graphene can be considered a base of some other carbon allotropes. Graphite can be treated like huge amount of stacked graphene layers, carbon nanotubes can be produced by rolling graphene into the tube and fullerenes can be considered as graphene rolled into spheres (Fig. 1).

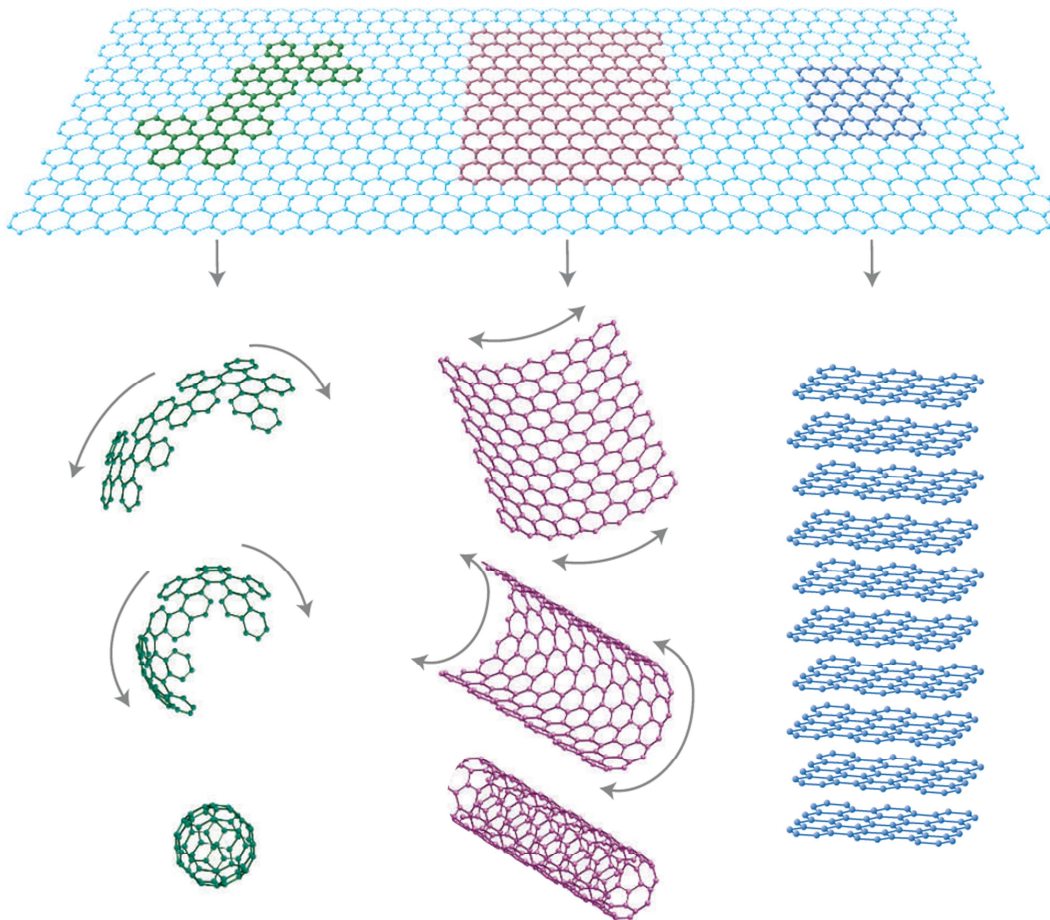


Fig. 1 Graphene is a 2D building material for carbon materials of all other dimensionalities. It can be warped up into 0D buckyballs, rolled into 1D nanotubes or stacked into 3D graphite [23].

Before graphene discovery, freestanding 2D materials assumed to be not existent. Atomic monolayers could only be grown epitaxially on the top of

other material. In 2004, group of scientists in Manchester University lead by A. Geim and K. Novoselov succeeded to obtain graphene monolayer by mechanical exfoliation method [1]. They measured that mobility of graphene charge carriers can reach  $\sim 10000 \text{ cm}^2/\text{Vs}$  at room temperature and ballistic transport takes place in sub-micrometer scales. Such characteristics make graphene an attractive material for FET (Field Effect Transistor) applications. On the other hand, the absence of a band gap restricts direct utilization of graphene in this field.

Despite the fact, that graphene is a gap-less semiconductor, there is an option for introducing the band gap with electric field in multilayer graphene. Zhang et al. [24] demonstrated precise tuning of the band gap in bilayer graphene. They showed that the band gap can be changed from 0 to 250 meV by application of a perpendicular electric field. Lui et al. [25] studied the same effect in three-layer graphene.

Ultra-thin graphene strips - graphene nanoribbons (GNRs) can be used for FET applications. They are quasi-one-dimensional structures with nanometer scale widths and atomically smooth edges. Son et al. [26] investigated energy gaps in GNRs and showed that GNRs with homogeneous armchair and zigzag edges have energy gaps which are inversely proportional to the structure widths. Yang et al. [27] estimated that the band gaps can reach values up to 1-3 eV for 2-1 nm width GNRs. Such band gap values are larger than achieved by tuning the band gap in multilayer graphene [24]. Thus, presence of the band gap, high carrier mobility and fast switching speed makes GNR useful for room temperature FET applications [28,29].

Lee et al. [5] measured Young modulus of defect-free graphene sheet which reaches 1 TPa. The superior mechanical properties of graphene make it attractive for flexible electronics applications [8]. High cost and finite supply of indium forces for searching of indium-tin oxide (ITO) alternatives. Bae et al. [14] have demonstrated roll-to-roll production and wet chemical doping of mostly monolayer graphene films grown by chemical vapor deposition onto flexible copper substrates [14]. They also used layer-by-layer stacking to

fabricate a doped four-layer film which demonstrated properties superior to ITO electrodes. Recent achievements in electronic industry allowed creating novel flexible devices. Flexible screens are important part for such implementations. Graphene stands as a strong candidate of contact material for such applications.

Lack of bandgap determines another interesting peculiarity of graphene. Gap-less material absorbs the light evenly across the whole spectrum demonstrating optical transparency of ~97.7% at whole visible region of spectrum. Such feature makes graphene an ideal candidate for transparent electrode material. J. Wu et al. [30] investigated graphene as a transparent electrode for organic solar cells. GO prepared by Hummers method was spin-coated on a quartz substrate, and then reduction was performed by vacuum annealing at 1100°C or by a combination of a hydrazine treatment and Ar-ion annealing at 400°C. Resistance of prepared graphene films was higher than ITO at the same transparency. This could be explained by incomplete reduction of the GO. Nevertheless, improving of GO reduction quality will allow graphene to compete with ITO.

Thermal conductivity of graphene is dominated by phonon transport, diffusive conduction at high temperature and ballistic conduction at low temperatures [31]. Balandin et al. [32] measured thermal conductivity of a graphene flake prepared with method of mechanical exfoliation by means of Raman spectroscopy. Suspended graphene was used in the experiment; laser beam was focused into the flake and caused heating of graphene. Laser induced heat caused bond softening which reflected in shift of the G-peak position towards larger wavenumbers in Raman spectra. This shift linearly depended on temperature of the sample at used low laser power. Thus, the thermal conductivity in value of 5000 W/m·K was extrapolated from the G-line position dependence on excitation power. CVD graphene and graphene on SiO<sub>2</sub> have lower values of thermal conductivity due to the interaction with substrate.

Thermal conductivity depends on graphene flake dimensions. Heat dissipation from graphene devices and interconnects is limited by their environment and the relatively weak Van der Waals interfaces of graphene. Thermal properties can be highly tunable in graphene composites. Thus graphene is an attractive material for both: heat-sinking and for the high thermal conductivity requiring applications [3].

Goli et al. [33] applied graphene for a heat-sinking setup. They investigated graphene-enhanced Phase Change Materials (PCMs), which consisted of pristine paraffin as the baseline composite and a few layer graphene or graphene as filler. Graphene enhanced thermal conductivity of the composite at room temperature from 0.25 W/m·K to 15 W/m·K.

Graphene enhanced paraffin was applied for heat-sinking of the pack of cylindrical Li-ion batteries (Fig. 2). Temperature was monitored with thermocouples connected to data acquisition system during 10 charge-discharge cycles. Temperature logging results showed that graphene improves thermal conductivity of the paraffin.

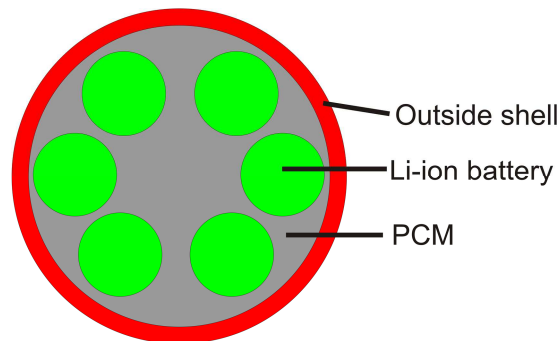


Fig. 2 Top view of the setup of the Li-ion battery pack embedded in the PCM. Adapted from [33].

In the case of no PCM placed between the batteries and the outside shell, the temperature in the cylinders was at its maximum of above 330 K. The outer shell also heated up to ~315 K via conduction through the air. Standard paraffin wax reduced the temperature of the cylinders to around 320 K without heating the outside shell. Thermal management with hybrid graphene PCM resulted in the lowest temperature of the battery cylinders of ~310-315 K with

some increase in the temperature of the outside shell which also resulted in more uniform temperature distribution through the PCM.

A few reasons explain such rise of thermal conductivity of the graphene-enhanced PCMs. The arrangement of graphene flakes creating a network within the composite is ideal for thermal percolation or the strong binding of graphene flakes to the hydrocarbon based matrix. The second possible reason is a good thermal coupling between the fillers and matrix [34].

Superior conducting properties, chemical purity and large surface area make graphene a promising candidate for sensors applications:

- Graphene is a two-dimensional material, thus all carbon atoms in the volume are exposed to the analyte of interest;
- Graphene is highly conductive with low Johnson noise (electronic noise generated by the thermal agitation of the charge carriers (electrons) inside an electrical conductor at equilibrium, which happens regardless of any applied voltage), hence, a small change in carrier concentration can cause a great variation of electrical conductivity;
- Pristine graphene has a small number of crystal defects ensuring a low level of noise caused by thermal switching;
- Four-probe measurements can be made on single crystal graphene device with ohmic electrical contacts having low resistance [35].

## **2.2 GRAPHENE CHARACTERIZATION APPLYING RAMAN SPECTROSCOPY**

Due to nano-range thickness, identification of a single-layer graphene is quite challenging. Several methods can be implied for such purpose. When placed on the certain base – 300 nm thick SiO<sub>2</sub> formed on Si substrate surface, graphene can be detected by means of optical microscopy, due to the change of interference color between monolayer flake and empty substrate [36].

Atomic force microscopy (AFM) is a precise method to identify single or few layer graphene, but it has low throughput. Furthermore it is also limited by the range of substrates on which graphene can be identified as instrumental offset ( $\sim 0.5$  nm) is larger than graphene monolayer, consequently the additional data fitting is required for accurate measurement [37].

Raman spectroscopy is known as a reliable and nondestructive method for identification of carbon allotropes. Graphitic materials show prominent spectral features in  $1000\text{-}3000\text{ cm}^{-1}$  region (Fig. 3). The main features in the Raman spectra of carbons are the G- and D-peaks. Their positions are  $\sim 1560\text{ cm}^{-1}$  and  $1360\text{ cm}^{-1}$ , respectively. Raman spectroscopy can clearly distinguish a single-layer graphene from less than 5 layers graphene [38].

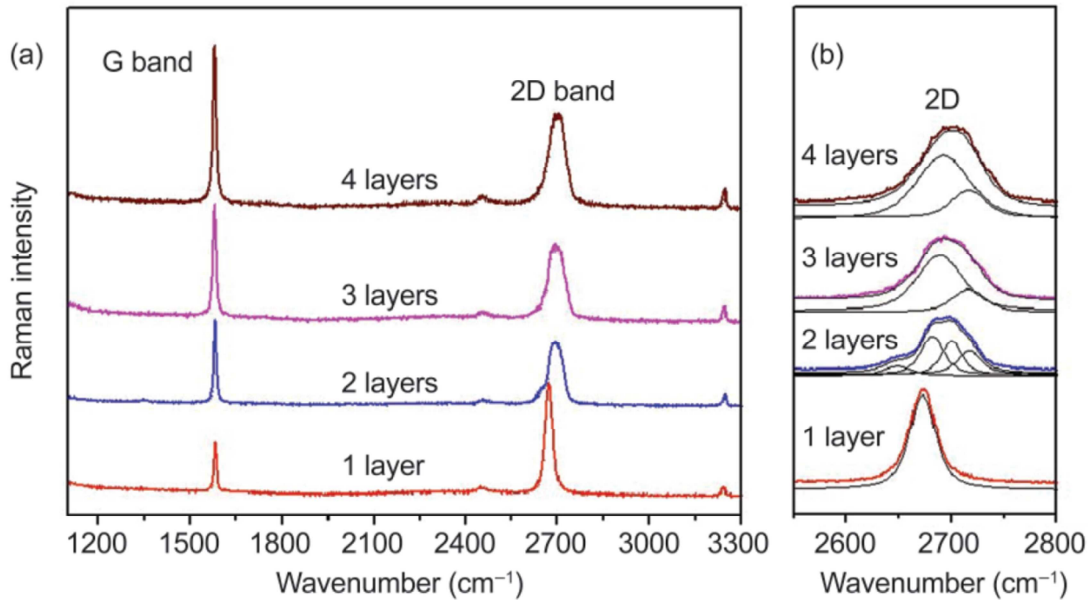


Fig. 3 (a) Raman spectra of graphene with 1, 2, 3, and 4 layers. (b) The enlarged 2D band regions with curve fitting [39].

The G-peak corresponds to the  $E_{2g}$  phonon in the Brillouin zone center, it is characteristic to many carbonous materials. The D-peak at  $\sim 1360\text{ cm}^{-1}$  is due to the breathing modes of  $sp^2$  atoms and requires a defect (vacancy, dislocation etc.) for its activation. Usually, as-prepared graphene without structural defects does not exhibit a strong D-peak because the corresponding Raman mode is active only on edges of flakes. The 2D-peak at  $\sim 2700\text{ cm}^{-1}$  (sometimes denoted as G' peak) – the second order of the D-peak - is the most intrinsic to

graphene [39,40]. This peak is always present in the graphene Raman spectra even in the absence of the D-peak because no defects are required for its activation. In a single-layer graphene, this band can be fitted with sharp and symmetric peak, while in graphite spectra, the 2D-band is not symmetric and can be divided in two peaks  $2D_1$  and  $2D_2$ , which intensities are  $\frac{1}{4}$  and  $\frac{1}{2}$  of the G-peak intensity, respectively [37]. The 2D-peak gets broader and shifts towards greater wavenumbers when number of graphene layers increases. The G-band intensity increases almost linearly with the number of graphene layers. The ratios of the peak intensities are common criterion for graphene investigation. Position of the G-peak and the peak intensity ratio  $I_{2D}/I_G$  determine the number of graphene layers. Shape and position of 2D Raman band are good fingerprints for single and bilayer graphene detection [38,41]. Graphene with significant defects shows an additional disorder related peaks: D' at  $\sim 1620\text{ cm}^{-1}$ , originating from the intra-valley double resonance and (D+D') at  $\sim 2950\text{ cm}^{-1}$ - a combination mode [42].

## 2.3 GRAPHENE PRODUCTION METHODS

Many graphene production methods have been developed since first graphene flake was exfoliated using mechanical cleavage method by Greim et al.[1]. This method implied non sophisticated approach of repetitive peeling of highly oriented pyrolytic graphite (HOPG) with a scotch tape until one-atom thick layer was separated from the material. This method is still widely used in laboratories in order to obtain the high-quality graphene monolayers. It is capable to produce graphene flakes in sizes of hundreds microns. This method is suitable for fundamental investigation of various graphene properties or production of graphene based devices prototypes. However, due to the lack of repeatability, high time consumption and relatively small yield, mechanical exfoliation is not suitable for mass production of graphene.

Chemical graphene exfoliation is based on dispersion and exfoliation of graphite in organic solvents. This approach offers scalability and high yield.

However it is time-consuming and sample contamination from surfactants or solvents utilized is possible [43,44].

Graphene can be epitaxially grown on silicon carbide (SiC) substrates in Ultra High Vacuum (UHV) environment. Epitaxial graphene grows on top of a carbon interface layer and only the second carbon layer on top of this interface acts like monolayer graphene. A bilayer graphene system develops during the process [45,46].

Other promising graphene production method is Chemical Vapor Deposition (CVD) on metal substrate. For this purpose various carbon containing gases are used (methane, propane, butane). Injected into the special chambers, these gases decompose into graphene on catalytic metal substrate at high temperatures. Nickel or copper foils are used as substrates in this method. CVD technique can provide wafer-scale graphene for industrial applications. Bae et al. [14] even have introduced the roll-to-roll production of 30-inch-wide films applying the CVD process. The high-quality monolayer graphene sheets with small amount of lattice defects can be obtained using CVD. Moreover physical graphene properties can be customized by using additives or creating specific defects which can be needed for specific device implementations [10].

## **2.4 GRAPHITE OXIDE REDUCTION**

As discussed above, graphene is produced by using chemical vapor deposition, epitaxial growth on silicon carbide or metal substrates, etc.[10,15,45,47]. There is still a need for new production methods which are distinguished by repeatability and can be implemented in mass production. One branch of graphene fabrication methods is based on the reduction of GO to graphene.

GO is widely used in graphene production technologies. The name “graphite oxide” means the product of the graphite oxidation and does not name separate chemical subject (much like polyethylene covers the whole set of long chain possessing hydrocarbon molecules). There are many theories



which explain GO structure [48]. Despite the intensive studying during recent years, still not much is known about the structure of this compound which can be determined by partially amorphous nature of this material [11]. Lerf and Klinofski proposed structural model of GO [49]. In this model GO consists of honeycomb-like plane of carbon atoms with various oxygen containing functional groups (carboxy, epoxy) attached to the plane (Fig. 4). Carbonyl groups are present as carboxylic acids along the edge of the sheet and as organic carbonyl defects within the plane [11].

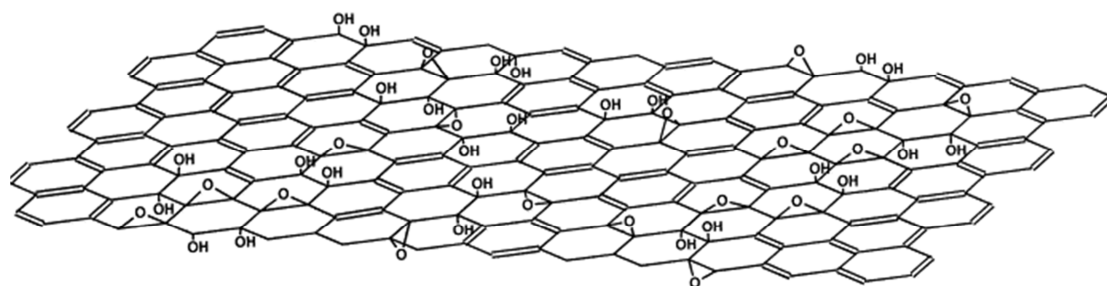


Fig. 4 Structural model for GO; Hydroxyl groups are perpendicular to the graphitic plane, and the inter-planar space contains water molecules [49].

Despite of huge interest in GO, the synthesis methods of this material have not changed much since first variations. In all cases, graphite is exposed to strong oxidizers in acid medium. Most commonly used methods for preparation of GO are Brodie [50], Staudenmaier [51] or Hummers [52] methods or any variations of these methods. Brodie and Staudenmaier used potassium chlorate ( $\text{KClO}_3$ ) and nitric acid ( $\text{HNO}_3$ ), while in Hummers method, potassium permanganate ( $\text{KMnO}_4$ ) and sulfuric acid ( $\text{H}_2\text{SO}_4$ ) are employed for graphite oxidation [31]. Properties of the received product strongly depends on the quality of pristine graphite and reaction conditions [53]. GO has a layered structure like its precursor – graphite; it is formed from hydrophilic layers of graphite oxide. Water molecules can be embedded between these layers, therefore interlayer distance in this structure may vary from 6 Å to 12 Å [54]. GO can be easily dispersed in water by applying sonication [55] or mixing for longer period of time [56]. Dispersed GO

particles obtain negative electric charge. Applying filtration of aqueous GO suspensions, thin GO coatings [57-59] or membranes can be produced [60-62].

Chemical, thermal and photo-induced reduction methods are implied for GO reduction purpose [11,58,63-65]. Several methods based on laser-induced reduction have been described recently [66-71]. This type of procedures permits local reduction of the electrically and thermally insulating GO and formation of conductive graphene domains, which can be used in microelectronics for efficient heat removal or electrical connections.

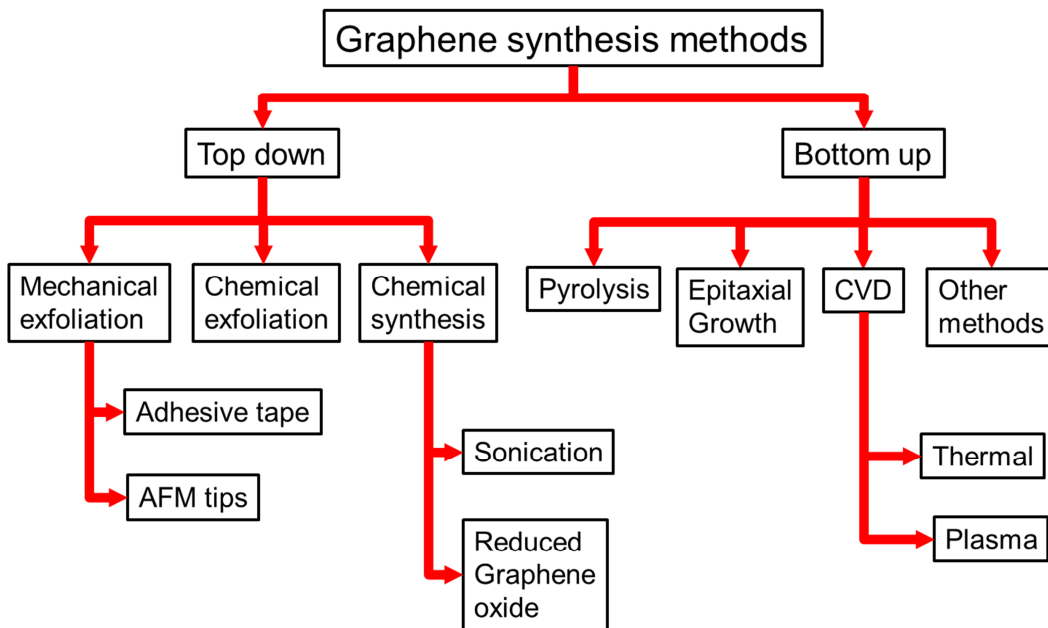


Fig. 5 The schematic represents the different graphene synthesis methods [72].

Many of the current graphene production methods are based on chemical reactions. They often are quite complex, consisting of many stages of production and require certain conditions of production as an extremely sterile environment or production in high vacuum.

One of the simplest and most promising alternatives to such methods is the production of graphene from graphene oxide. This method is based on the reduction of the oxide – breaking oxygen-carbon bond. There are several approaches of graphene oxide reduction:

Table 1 Overview for various synthesis methods of the graphite oxide reduction.

Method	Experimental conditions
GO reduction by alkaline conditions	100 W, 40 kHz, 1 h intense ultrasonication and centrifugation of GO suspension for 2 h at 23,000 rpm and heating in alkaline solutions [73].
Solvo-thermal reduction method	Sonication at 50°C for 60 min. and diluted with NMP, degassed for 60 min., bath sonication at 240°C for 24 h under argon atmosphere, centrifuge at 4500 rpm and annealed at 250, 500 and 1000°C [74].
Thermal exfoliation	The dried graphite oxide is charged into a quartz tube and purged with argon. Rapid heating (>2000°C/min) to 1050°C [75].
Arc discharge exfoliation	GO was rapidly heated by arc discharge in a mixed buffer gas of H <sub>2</sub> (≤10 kPa pressure) and argon (90 kPa pressure). A high-temperature discharge between the two electrodes was generated by a direct current mode ranging from 100 to 150 A. The resulting exfoliated graphite (10 mg) was dispersed in 10 mL of NMP (N-methylpyrrolidone) for 2 h by sonication. Suspension was centrifuged at 15000 rpm for 5 min. to remove thick graphene sheets and non-exfoliated graphite, and to retain thin graphene sheets in the supernatant [76].
Vacuum exfoliation	The as-prepared GO was put into a quartz tube connected to vacuum pump. The tube was heated at the rate of 50°C/min under a high vacuum (<1 Pa) and kept at 200°C for 5 h [77].
Chemical reduction	GO (100 mg) dispersion was sonicated using ultrasonic bath cleaner (150 W). Hydrazine hydrate (1.00 ml, 32.1 mmol) was then added and kept in oil bath at 100 °C under a water-cooled condenser for 24 h over which the reduced GO gradually precipitated and isolated by filtration and washed with water and dried. [43].

Microwave reduction	20 mg of GO were dispersed into 6 mL water under mild ultrasound. Then 30 mL of DMAc was added and sonicated for few minutes and suspension was obtained in the mixture of DMAc/H <sub>2</sub> O. For the microwave thermal reduction experiment, 36 ml of the prepared GO suspension in DMAc/H <sub>2</sub> O (0.56 mg/ml) was put into a microwave oven under dry nitrogen gas, and it was treated for different time in the range of 1–10 min. at 800 W. After washing with ethanol for three times then the mixture was freeze dried at 80 °C for 24 h. [78].
Hydrothermal	25 mL of 0.5 mg/ml GO aqueous solution was transferred to a Teflon-lined autoclave and heated at 180 °C for 6 h. [79].
Electrochemical method	The electrochemical reduction of GO in a three-electrode system (Pt as counter electrode, saturated calomel electrode as reference electrode, GO film coated over GCE as working electrode). Electrochemical reduction experiments were performed on a CHI 1140 electrochemical workstation (CH Instrument Co., USA) at a constant potential (–1.5 or –1.3 V vs SCE) in 10 mmol/l pH 5.0 PBS (K <sub>2</sub> HPO <sub>4</sub> /KH <sub>2</sub> PO <sub>4</sub> ) under stirring for 2 h [17].
Flash reduction	Flash reduction of free-standing GO films can be done with a single, close-up (<1 cm) flash from the Xenon lamp equipped on a common digital camera. Most experiments were done with a Sunpak 383 stand-alone flash unit with a larger window size of around 30 mm × 50 mm [64].

Graphite oxide reduction using laser irradiation can be considered as a thermal case of GO reduction. According to Zh. Wei [80], thermal reduction of GO was manifested at medium temperatures (100-250°C) [80,81]. GO reduction takes place in a wide temperature range from 100 to 1000°C [74,75,79,80,82-84]. According to S. H. Huh [85], evaporation of water molecules occurs at 200°C temperature, removal of the carboxy groups at about 200-600°C, residual carboxyl and hydroxyl groups removal takes place

at 800°C, the removal of hydroxyl groups, partial removal of the epoxy groups and breaking of the aromatic C=C bonds at temperature of about 1000°C. On the other hand the formation of new carbon compounds (CO, CO<sub>2</sub>) occurs, during the reduction process, and they cause structural defects by leaving the basal plane of graphene. That fact reflects in the presence of the D-band Raman spectra of reduced GO. In addition, the phenolic groups stay in the GO even after 1000°C temperatures.

## **2.5 GRAPHENE PRODUCTION AND MODIFICATION WITH LASER IRRADIATION**

### **2.5.1 GRAPHENE OXIDE REDUCTION WITH LASER IRRADIATION**

Focused laser beam has become an important tool for thin-layer surface modification and micro-structuring. The essence of this method is an effective heat zone creation by focusing the laser beam and creating localized transition of physical phase. Use of sufficient laser power enables ablation of materials such as steel, ceramics, nanostructures and biological samples.

Y. Zhou et al. [86] used a focused laser beam micro-structuring of large GO areas to develop and carry out reduction of multi-GO, situated on quartz substrates. The advantage of this method is its reliability, the ability to increase the production scale and relatively low cost. Most importantly, such microstructuring does not require additional substrate preparation. The experiment employed a continuous wave diode laser with a wavelength of 663 nm and a maximum output power of 80 mW. The laser beam diameter was about 3 μm. Fig. 6 schematically illustrates GO structuring procedures and conversion to reduced GO. The film was placed in focus of the laser beam. When the focused beam reached the GO surface, the irradiated area absorbed the laser energy, and local increase in temperature took place. Intense heating raised the temperature of the irradiated zone above 500°C in air and caused a

localized oxidative GO burning with the release of the volatile gases such as CO and CO<sub>2</sub> (Fig. 6, P2 and P3). No clear evidence of graphene phase was confirmed by Raman spectra.

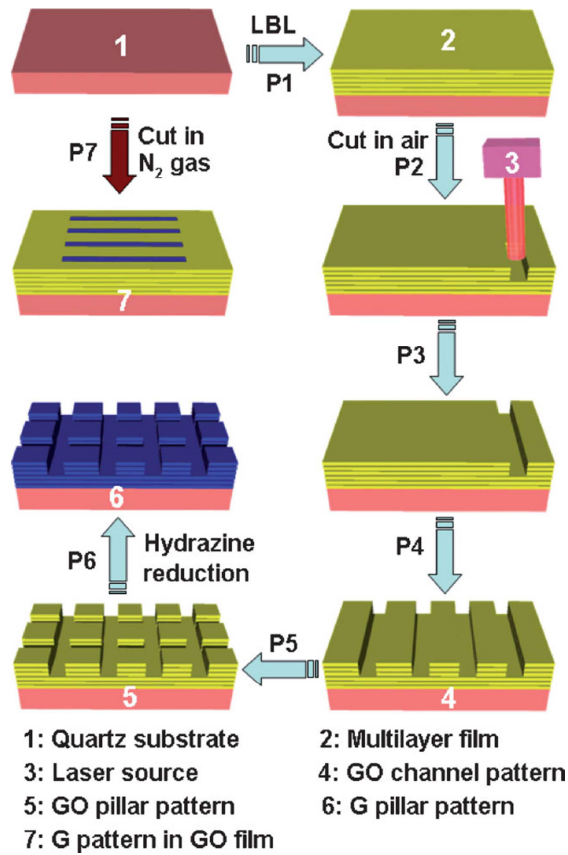


Fig. 6 Scheme of graphene layers microstructuring [86].

In the other research of group [87] an insulator-conductor transformation of graphene oxide films with continuous-wave diode laser (532 nm, 12 mW) was investigated. Increase of the film conductance from 0.012  $\mu\text{S}$  to 2.82  $\mu\text{S}$  was achieved after the laser irradiation. Raman measurements were performed to evaluate laser induced structure changes (Fig. 7). The laser irradiation caused increase of defects as the broadening of D and G peaks in the Raman spectrum. Also the decrease of the 2D peak intensity was observed. Reduction of the film thickness after the laser treatment is explained by two processes: primarily by photo thermal reduction and following oxidative burning.

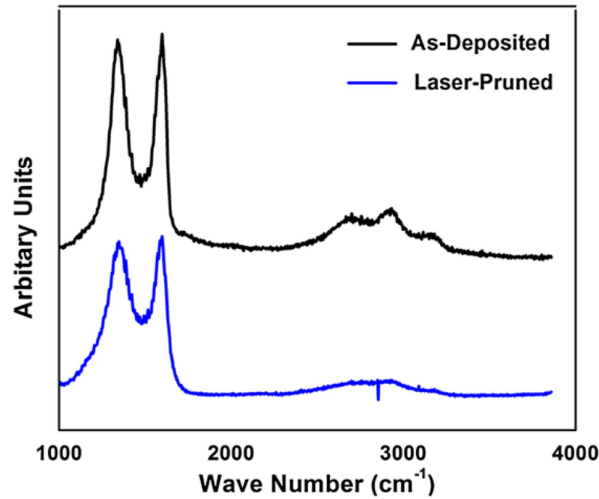


Fig. 7 Raman spectrum of as deposited and laser modified GO [87].

Zhang et al. [67] inscribed microcircuits with a femtosecond laser into the GO layer, spin-coated on glass. However, from the Raman spectra of reduced GO, no evidence of graphene formation was observed as the 2D spectral peak ( $\sim 2700\text{ cm}^{-1}$ ) was absent.

Sokolov et al. [71] used a continuous wave and a pulsed laser excitation of graphene oxide in both air and nitrogen atmosphere. The Raman spectra revealed formation of graphene by appearance of the 2D-line. The results also showed dependence of the process quality on the ambient atmosphere as a decrease of the D-peak intensity in Raman spectra was observed in experiments conducted in the nitrogen atmosphere (Fig. 8). This band represents structural defects in the graphene layer.

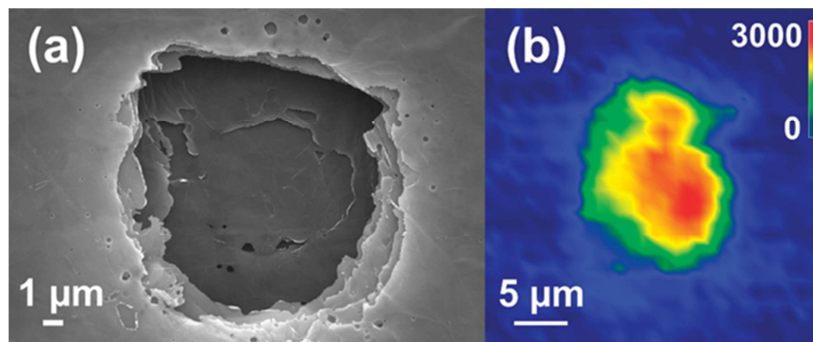


Fig. 8 (a) SEM image of the  $10\text{ }\mu\text{m} \times 5\text{ }\mu\text{m}$  depression produced by 532 nm CW laser irradiation of graphite oxide. The laser energy was 20 mW. Note the outward expansion of the edges and lack of melt zones near the edges. (b) A spatially-resolved map of the Raman 2D band [71].

In later research, Sokolov et. al [88] performed graphene oxide reduction experiments using an excimer laser. The laser irradiation wavelength was 248 nm, pulse duration – 25 ns. Sample was placed into a hermetic chamber and the irradiation was performed in a high vacuum ( $\sim 10^{-6}$  Torr), a low vacuum ( $9.8 \times 10^{-2}$  Torr) and a flowing nitrogen atmosphere. Laser fluence was varied from  $60 \text{ mJ/cm}^2$  to  $400 \text{ mJ/cm}^2$ , furthermore, the pulse number was also varied. 5-8  $\mu\text{m}$  thick GO films were formed on nylon membranes. Raman spectroscopy was employed for investigation of the reduction results (Fig. 9). After laser irradiation, reduction of the D-peak intensity was observed and the 2D-peak emerged. It can be fit with a single Lorentzian with a typical FWHM between  $50\text{--}65 \text{ cm}^{-1}$ . Positions of the D- and G-peaks shifted towards lower wavenumbers, indicating decrease of disorder. Estimated domain sizes after the laser treatment increased from 18 nm to 31.5 nm, indicating transition of reduced graphene to more reduced state. Remaining D-peak in spectra was explained by the influence of untreated GO which lies under reduced layer. 30 pulses at a fluence of  $200\text{--}300 \text{ mJ/cm}^2$  were required to form the high quality graphene in nitrogen and 15–20 laser pulses at  $\sim 150 \text{ mJ/cm}^2$  in the high vacuum. Authors stated that the laser induced reduction requires the use of an oxygen free environment.

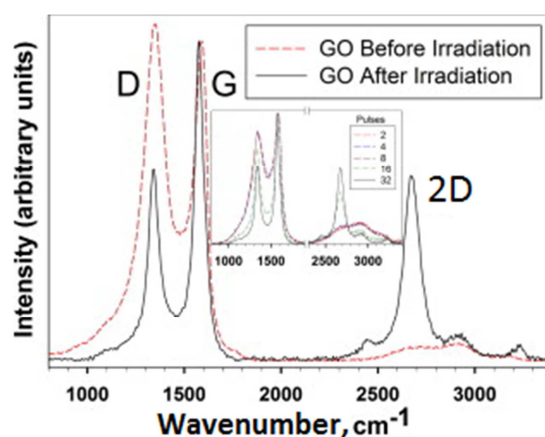


Fig. 9 Raman spectrum of untreated GO compared with a spectrum of an excimer laser-reduced GO produced with 32 pulses at  $\sim 138 \text{ mJ/cm}^2$  laser fluence in the high vacuum ( $\sim 10^{-6}$  Torr). The inset is the pulse dependence of GO reduction at  $138 \text{ mJ/cm}^2$  in the high vacuum ( $\sim 10^{-6}$  Torr) [88].



Yung et al. [89] directly patterned reduced GO circuits on glass using an excimer laser system. Laser with 248 nm radiation wavelength, pulse repetition rate of 1 Hz and pulse duration of 20 ns was employed in the tests. The laser fluence was varied from 60 to 90 mJ/cm<sup>2</sup> during the experiments and the beam scanning speed was constant – 200 μm/s. They achieved  $\sim 1.33 \times 10^4$  S/m conductivity. Formation of the 2D-peak was also observed in the Raman spectra. The FWHM of 2D line was 64 cm<sup>-1</sup>, according to the authors, such value corresponds to the presence of turbostratic graphite, which consists of randomly oriented multiple graphene sheets. The D-peak was also present in the Raman spectra due to remaining oxygen species and edge defects.

Gao et al. [66] performed GO reduction with the direct laser writing for fabrication of supercapacitors. CO<sub>2</sub> laser with 2.4 W power was employed for the reduction process. This technique allowed forming capacitor electrodes in various shape and sizes, and two configurations (“sandwich” and “in plane”) were investigated. Solid GO works as a solid electrolyte and reduced GO serves as an active electrode material. Due to the gases, produced during the reduction process after decomposition of functional groups attached to GO nanosheets, surface of reduced GO became porous after the laser treatment (Fig. 10).

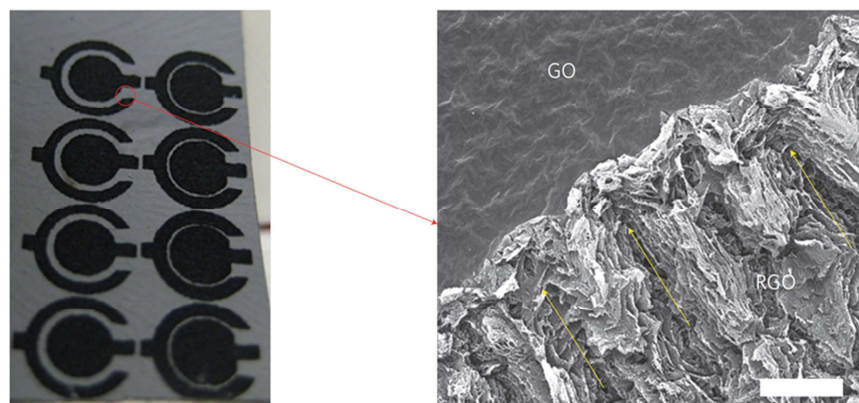


Fig. 10 Photograph of an array of concentric circular patterns fabricated on a free-standing hydrated GO film and SEM image of the interface between GO and RGO (scale bar, 100 nm), with yellow arrows indicating a long-range pseudo-ordered structure generated by laser-beam scanning [66].

Strong et al. [12,13] offered production of laser scribed graphene (LSG) with the standard LightScribe DVD optical drive. Water dispersion of GO was drop-casted on a flexible substrate and irradiated with an infrared laser inside a commercially available LightScribe CD/DVD optical drive. After the laser irradiation the color change of irradiated GO film was observed. SEM inspection of the cross sections of the film showed that the laser irradiation induced exfoliation of the LSG sheets like in [63]. The irradiated films showed a conductivity of 1738 S/m and a high mechanical strength, as the drop of electrical resistance accounted only 1% after 1000 bends cycles. Authors predicted using such films in electrochemical capacitors applications.

Mukherjee et al. [90] demonstrated that photothermally reduced freestanding graphene oxide paper can be applied for lithium-ion batteries. They conducted experiments with flash reduction and laser. Laser setup consisted of the CO<sub>2</sub> laser cutting machine with irradiation power of 4.8 W, irradiation wavelength was 9.3 μm, laser spot size was 100 μm. The laser irradiation induced film expansion (5-10 fold increase of thickness), forming of porous structure and cracks in the film was observed. These effects were explained by the fast increase of pressure caused by escaping oxygen generated during the deoxygenation of material. No forming of porous structure was observed in the laser irradiated samples, which previously were chemically reduced with hydrazine. The authors stated that photo-thermal reduction is suitable for production of porous graphene anodes, since the demonstrated electrical characteristics enabled their operation over a wide range of charge/discharge rates.

Orabona et al. [91] conducted experiments with holographic patterning of GO films. Continuous wave Nd:YVO<sub>4</sub> laser with wavelength of 532 nm, average power of 100 mW and beam diameter of 5 mm was used for photo reduction of GO films. Desirable patterns were formed with Spatial Light Modulator (SLM). Such approach allows reduction of complex patterns in single shot. The FT-IR spectra confirmed the decrease of C-O and C-OH bonds after the reduction experiments.

Li et al. [92] operated with resembling approach in they work. Femtosecond laser with pulse energy of 400  $\mu\text{J}$ , pulse duration of 90 fs, and an adjustable wavelength from 750 nm to 830 nm at an average power of 4.0 W and pulse repetition rate of 10 kHz was chosen for the experiment. Patterns on the GO film were generated with a digital micro mirror device. The number of pulses applied to GO was varied during the experiments. Depending on the number of shots, GO reduction or ablation occurred. The 2D-band was not present at measured Raman spectra. Authors evaluated  $I_G/I_D$  ratio, which depended on the number of shots, and the ratio was maximal (1.067) when 4600 pulses were applied.

Another approach of graphene production applying laser irradiation is based on irradiation of aqueous GO solutions. A few researches have reported on this topic, for example, - Kumar et al. [93] performed GO reduction experiments with the UV irradiation of KrF laser of aqueous GO suspension in a quartz vial. The laser irradiation wavelength was 248 nm, the pulse repetition rate – 5 Hz, the pulse energy – 300 mJ. The authors noticed change in the solution color from yellow to black after the laser irradiation. Moreover, the reduction of carbonyl groups was visible from IR spectra. The authors demonstrated the presence of the D-, G- and 2D-bands in spectra of laser reduced GO. Two-probe resistance measurement showed drop in resistance from 5000  $\Omega/\text{cm}$  in untreated GO to 41  $\Omega/\text{cm}$  after the laser reduction.

Huang et al. [94] irradiated aqueous GO suspensions with the KrF excimer laser (the radiation wavelength 248 nm, the pulse width - 20 ns, the pulse energy - 200 mJ and the pulse repetition rate - 5 Hz, the irradiation time – 5min.). The unfocused beam of dimensions  $24 \times 10 \text{ mm}^2$  was directed to quartz tube with GO suspension. Raman investigations showed minor decrease of structure defects in GO, the 2D-band region ( $\sim 2700 \text{ cm}^{-1}$ ) was not analyzed (Fig. 11). After the laser irradiation, the peak intensity ratio  $I_D/I_G$  decreased from 1.08 to 1.03. The authors determined that this correspond to the decrease of  $sp^2$  cluster size from 4.3 nm to 4.1 nm. The pulsed laser irradiation raised the temperature of the GO flakes above 200°C and resulted in the thermal

deoxygenating reactions for reducing GO as the XPS spectra confirmed elimination of oxygen containing groups (O–H, C = O, and C–O).

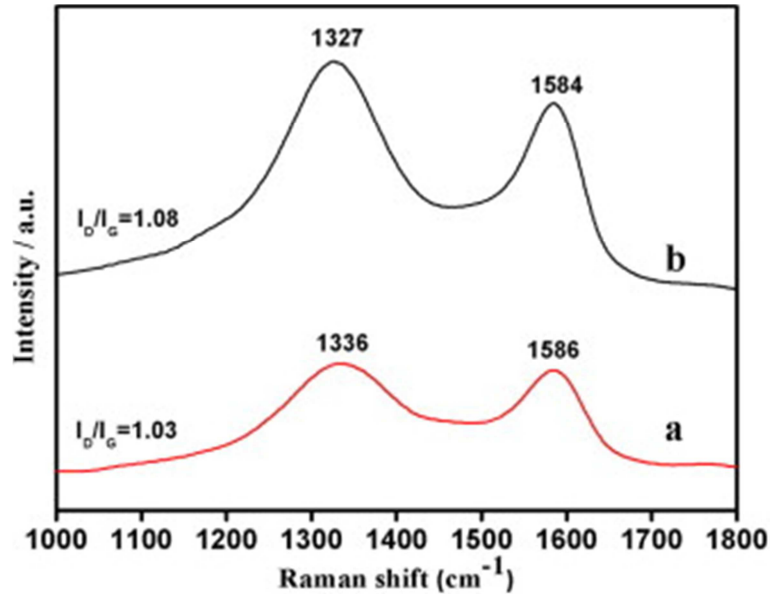


Fig. 11 Raman patterns of (a) GO and (b) pulsed laser irradiated GO powder [94].

Chang et al. [95] employed femtosecond laser for the reduction of GO in aqueous solution. A Ti:Sapphire laser with the central wavelength of 800 nm, the pulse duration of ~120 fs, the repetition rate of 1 kHz, and the laser intensity of  $1.5 \times 10^{15}$  W/cm<sup>2</sup> was used in the experiments. The laser beam was focused into solution using aspheric lenses with the focal distance of 8 mm. Like in Kumar experiment [89], the duration of irradiation was varied during the experiments. The XPS spectra showed that epoxy and carboxy groups were reduced significantly as the laser irradiation time was increased. The atomic C/O ratio increased from 1.7 (untreated GO) up to 81 in reduced GO.

Ghadim et al. [96] also performed irradiation of GO suspensions with the pulsed Nd:YAG laser irradiation. For this experiment, they used a nanosecond laser with following parameters: 532 nm wavelength, 5 ns pulse duration, 10 Hz pulse repetition rate, maximum pulse energy of 300 mJ and 7 mm beam diameter. GO powder was dispersed in ammonia solution. The suspension was placed into a glass tube and stirred with a magneto stirrer while irradiated with unfocused beam. Time of irradiation was varied. The XPS measurements

confirmed the reduction of O/C atoms ratio from 49% to 21% after 10 min. of the laser irradiation which is comparable with 15% after hydrazine treatment. However the changes in the Raman spectra were negligible (Fig. 12). After the laser treatment, the  $I_D/I_G$  ratio decreased from 1.5 to 1.3. Moreover, the intensity of the 2D-band was extremely low, and  $I_{2D}/I_G$  even decreased from 0.038 to 0.025 after the irradiation.

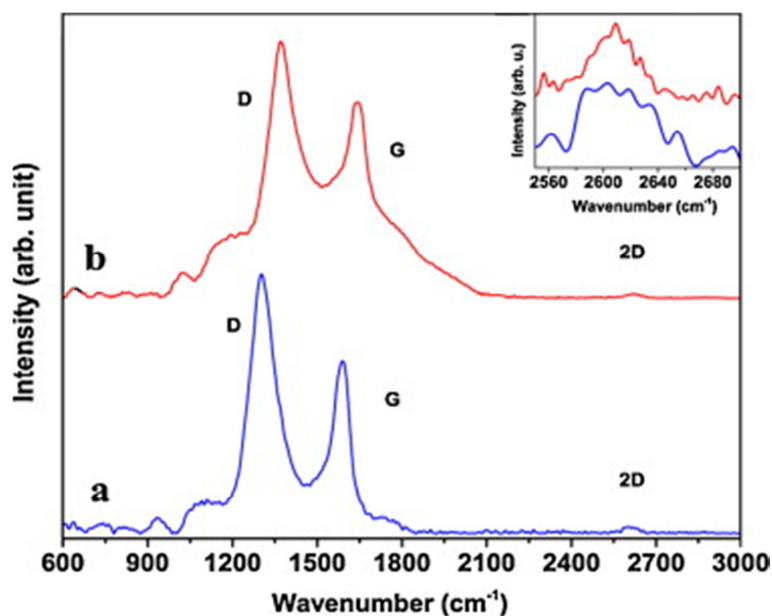


Fig. 12 Raman spectra of (a) GO and (b) pulsed laser-rGO obtained after 10 min. of laser irradiation [96].

Xiong et al. [97] investigated other method of graphene fabrication employing laser irradiation rather than GO reduction. They produced bi-layer graphene applying laser direct writing (LDW) in thin Ni/C films on various insulating substrates (glass and SiO<sub>2</sub>/Si). The sheet resistance of obtained graphene was comparable to GO obtained by laser-assisted CVD and by a magnitude lower than in reduced GO. LDW experiments were conducted with a femtosecond laser, laser beam spot size was 800 nm, beam scanning speed was 500  $\mu\text{m/s}$  and average laser power was varied. The Raman spectroscopy revealed dependences of the graphene film quality on the used laser power (Fig. 13). The intensity ratios  $I_D/I_G$  and  $I_{2D}/I_G$  (Fig. 13 b) clarified the impact of the laser power on the produced graphene structure. Defects tend to decrease till 24 mW where the D-peak intensity reached its minimum, at the same laser

power,  $I_{2D}/I_G$  had its maximum value, larger than 1. Further increase in laser power resulted in decrease of the  $I_{2D}/I_G$  ratio and increase of the D-band intensity due to laser-induced lattice defects. Optimal fluence for this LDW process was  $0.1 \text{ J/cm}^2$ .

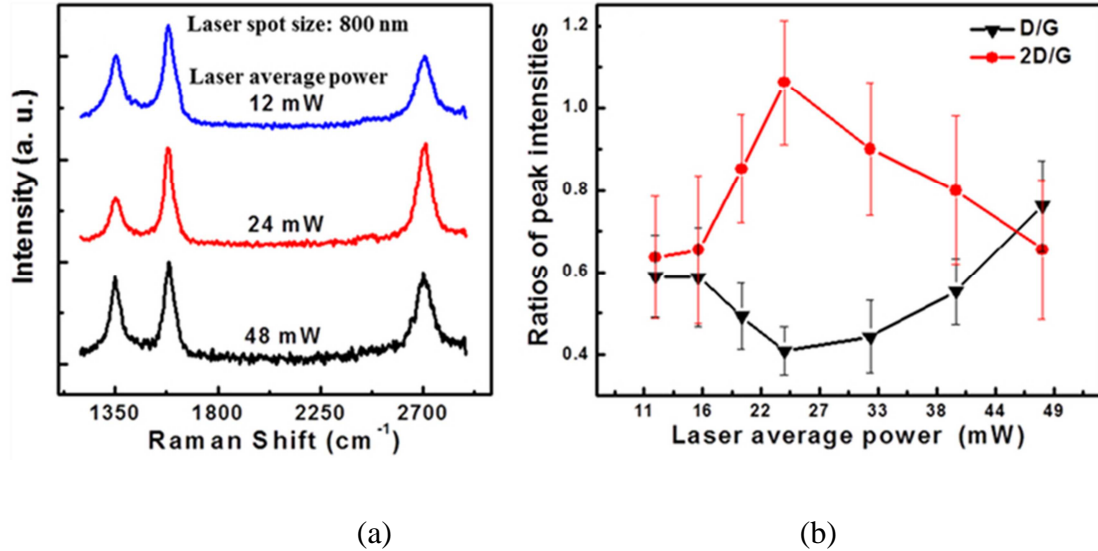


Fig. 13 Raman spectra of the graphene lines fabricated with three different average laser powers – a), and Raman D/G and 2D/G ratios of graphene lines as functions of laser average power – b) [97].

## 2.5.2 GRAPHENE ABLATION

In this section, methods used for patterning or removal of graphene are reviewed.

G. H. Han et al. [98] proposed a method of graphene layers etching by laser irradiation. The upper layers of graphene are completely removed while the lower graphene monolayer remains intact. This is explained by the heat accumulation in the upper layers of graphene during the light absorption. In this case, the  $\text{SiO}_2/\text{Si}$  substrate becomes important, because it works as a heat sink for graphene monolayer in the process, which remains unetched. Etching was controlled by changing thickness of the oxide layer.

Authors analyzed the graphene etching process as a complex heat transfer and dissipation mechanism. Incident light was partially absorbed by the graphene layers, the remaining part of light passed through the layers, and then reflected from the interface with the substrate. In case of a silicon substrate,

two boundaries were formed: one on top of SiO<sub>2</sub>, other underneath the silicon layer. Light was reflected back from these boundaries, leading to a secondary absorption in graphene layers (Fig. 14). Amount of reflected light strongly depended on the refractive index and thickness of silicon and silicon oxide layers. Such complex light propagation with multiple reflections resulted in temperature rise in graphene layers. Heating of graphene layers was determined by the competing processes: accumulation of the heat from the light absorption and heat dissipation through the graphene layers along and perpendicular to the substrate surface.

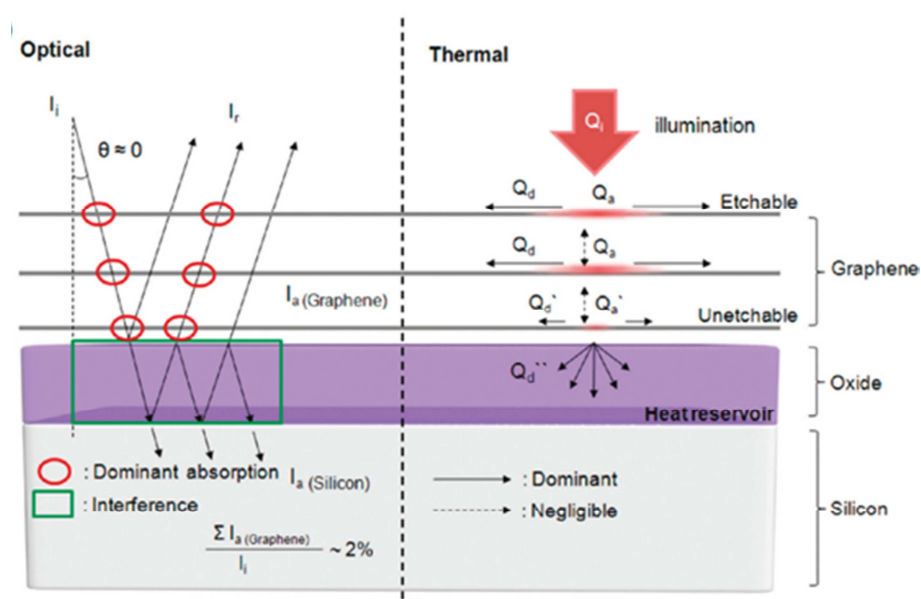


Fig. 14 Phonon softening by accumulated heat with a schematic of the heat accumulation in graphene with different thicknesses. Each graphene layer absorbs light and thus becomes heated. The light is reflected from the bottom substrate. The Si substrate acts as a heat sink [98].

The essence of this method, exploiting graphene substrate as a heat sink was adapted by M. Piazza et al. [99] for post-treatment of CVD graphene layers on Cu substrate. Despite selectivity for formation of graphene monolayer, a few-layer graphene structures are often formed during the process. Various techniques are applied to homogenization of graphene layers produced by CVD technique, Dependence of graphene ablation threshold on the number of layers allow uniform monolayer structure formation. He-Cd blue laser (442 nm) with average power of  $\sim 1$  mW was applied in experiments,

exposition time was varied and in-situ Raman spectra measurements were performed. After 80 s exposure, sharpening of the 2D band and decrease of the  $I_G/I_{2D}$  ratio were visible in Raman spectra which confirmed reduction of graphene layers. However, at the same time, intensity of the D-band rose in proportion to exposure time, indicating increasing number of defects in graphene.

S. Dhar also examined dependence of the laser ablation threshold of graphene on the number of layers [100]. Laser treatment was performed with a 248 nm laser with pulse duration of 20 ns. Authors showed that thick graphene layers (more than 3-5 layers) can be ablated with irradiation energy densities of  $\sim 0.6 \text{ J/cm}^2$ . The obvious difference in the ablation threshold was observed for a single layer ( $0.85 \text{ J/cm}^2$ ) and bi-layer ( $0.55 \text{ J/cm}^2$ ) graphene. A sharp decline of ablation threshold was observed when the number of layers of graphene grows (Fig. 15).

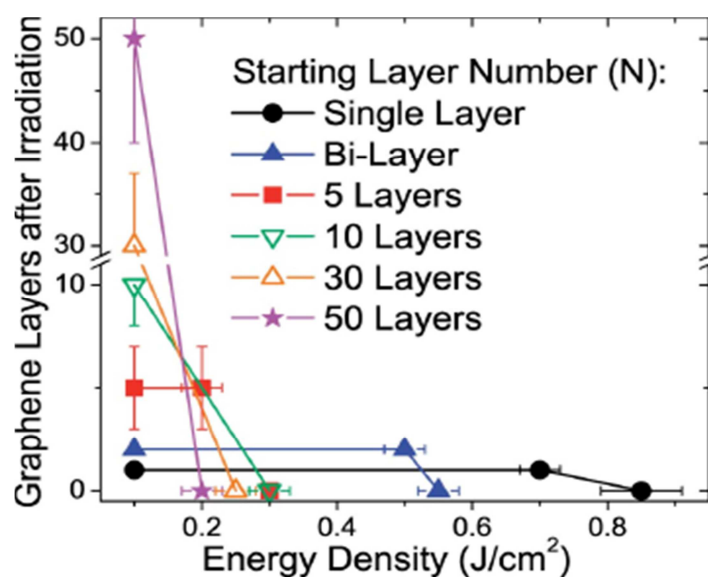


Fig. 15 The ablation of graphene layers as a function of laser energy density and graphene layer-number  $N$  clearly showing the existence of the differences in  $E_{Th}$  between single-, bi-or more layers [100].

Krauss et al. [101] investigated graphene disassembly into nanocrystalline network induced with the laser irradiation. Graphene flakes, prepared with micromechanical cleavage method were placed on Si substrate covered with 300 nm thick  $\text{SiO}_2$  layer. The laser beam with a wavelength of 488 nm and the



average power of 1 mW was focused into 400 nm diameter spot on the sample surface. Graphene layers were irradiated for 18 h, during this time in-situ Raman spectra were being recorded. Drastic changes occurred in the Raman spectra during the experiment (Fig. 16). After 2 hours of the laser treatment, drop of the G-band intensity occurred and intensity continued with a monotonic decrease. The laser irradiation induced breaking of  $sp^2$ -carbon-carbon bonds. The process was followed by gradual detach or single graphene crystal into a network of interconnected graphene nanocrystallites. Rise of the D-band intensity and decrease of 2D band intensity occurred as well. Despite rise of defects the 2D-band still could be fitted with single Lorentz function peak, which implies that no amorphous phase developing. The D+G-band emerged in Raman spectra simultaneously with the strongest D-band development after 12 h of irradiation.

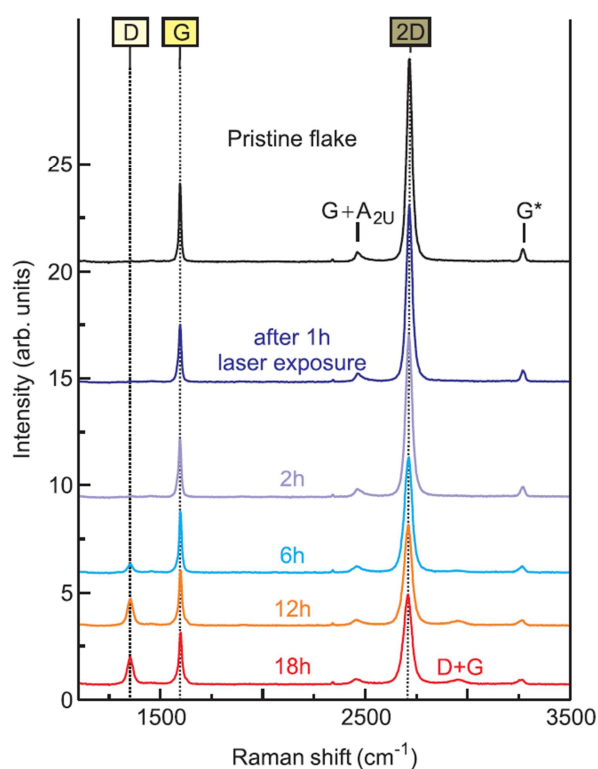


Fig. 16 Laser-induced change in the Raman spectrum. The black line indicate the peak positions in the spectrum of a pristine graphene monolayer. Other Raman spectra were obtained after laser exposure with 1 mW [101].

### **3 EXPERIMENTAL SET-UPS AND PROCEDURES**

#### **3.1 SAMPLE PREPARATION**

##### **3.1.1 SAMPLES USED IN GRAPHITE OXIDE REDUCTION**

Samples of graphite oxide (GO) were synthesized in the Laboratory of Carbonaceous Materials, Vilnius University using the standard Hummers – Offeman [52] and modified synthesis protocols (Fig. 17).

10 g of fine graphite (Merck) and 5 g of NaNO<sub>3</sub> (Reachim) were suspended by mixing and cooling in 230 ml of concentrated H<sub>2</sub>SO<sub>4</sub> (Donau Chemie). During the intensive mixing for 6-8 h, 30 g of KMnO<sub>4</sub> (Merck) was added. During adding of KMnO<sub>4</sub>, the temperature of solution was monitored to keep at 0°C. After all KMnO<sub>4</sub> was added, the compound was kept cool overnight, then it was heated up to temperature of 35°C, after that, it was diluted by 460 ml of water every 30 minutes, simultaneously monitoring that the temperature of the solution would not rise above 70°C. After dilution, the suspension was kept at the temperature of 70°C for 15 min, then it was diluted by 1.4 l of water. Formed MnO<sub>2</sub> and residual KMnO<sub>4</sub> were reduced by concentrated H<sub>2</sub>O<sub>2</sub>. A warm yellowish-brown suspension was filtered through a vacuum filter and washed with distilled water until neutral reaction. Brown GO powder was pumped out and dried in the desiccator. Compound was kept in the fridge. GO prepared in such manner was used in the production of GO coatings and for preparation of modified GO products.

GO coatings of different thickness (20-1200 nm) were deposited on polymer membranes using novel preparation methods developed in the laboratory. Some coatings were treated with the organic reagents containing certain functional groups, which were supposed to join up isolated GO sheets.

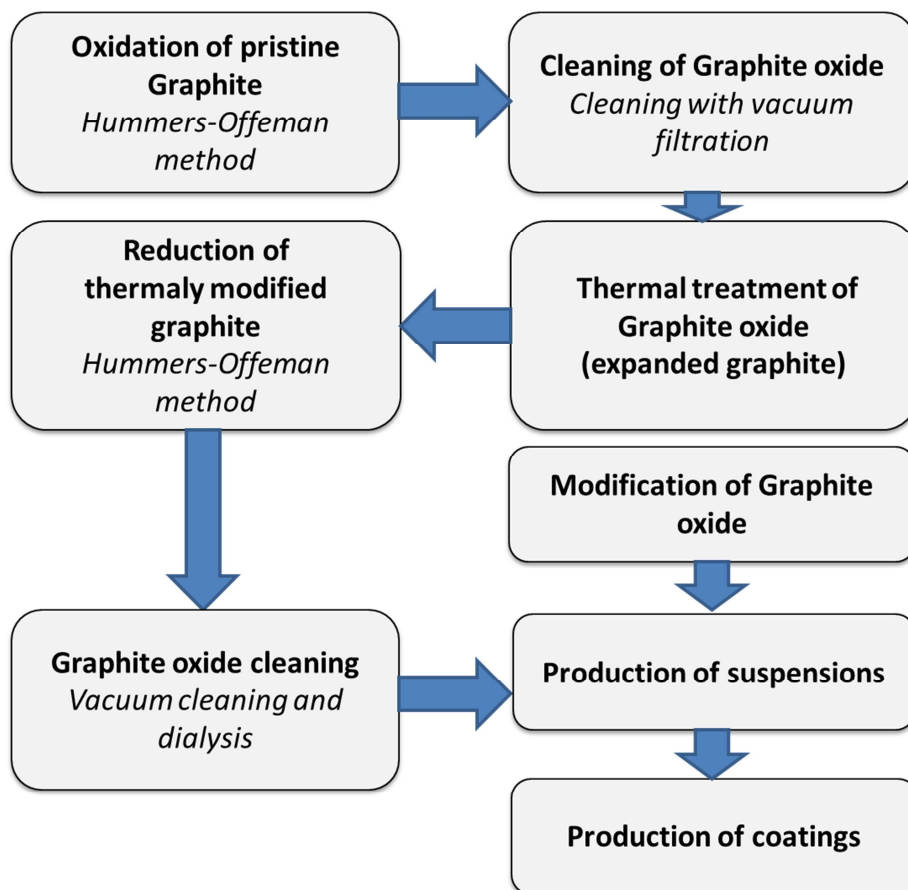
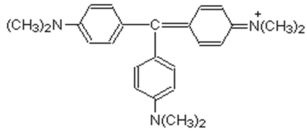
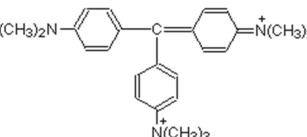
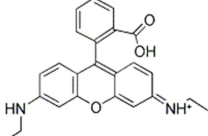
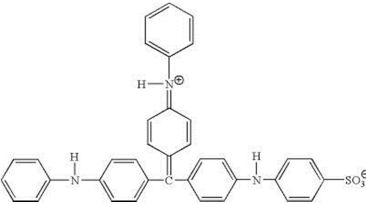
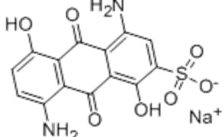
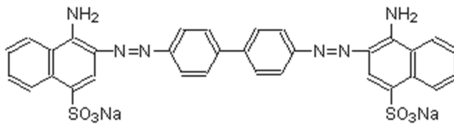


Fig. 17 Scheme of the two-step GO synthesis using thermally modified graphite.

Graphite oxide synthesis technique was developed and modified versions of this synthesis were created, and intermediate and final products of GO synthesis were analyzed. Synthesized products were modified using functional reagents (Table 2). Using the GO and its modified products, a graphite oxide coatings polymer processing technique was developed, and analysis of substrates for these coatings was performed.

Table 2 Functional reagents used in GO modification

Name	Structural formula
Crystal Violet	
Methyl Green	
Rhodamine G	
Alkali Blue 6B	
Acid Anthraquinone Blue	
Congo Red	

Two types of membrane filters with a different pore size and texture were selected for the experiments: Poly-carbonate (PC) and Nylon (MagnaNylon) with the mean pore diameter of 0.22  $\mu\text{m}$  and 0.45  $\mu\text{m}$ . After making a series of tests, it was found that the highest quality of the GO coatings was achieved on the polycarbonate membrane filters. The membrane filters with a rough surface can be used only as a substrate in formation of thick GO layers of sufficient quality.

An important step was the preparation of water-based coating suspensions for GO production. GO disperses to the aqueous phase relatively easy, without need of using additional chemical dispersing agents. For fabrication of coatings,  $5 \cdot 10^{-5}$  g/ml suspensions, which were prepared from a higher concentration ( $5 \cdot 10^{-3}$  g/ml) with dilution, were used. Before the suspensions were filtered, they were sonicated for 30 minutes (Sonic VibraCell, 12 mm diameter electrode, 13% amplitude). GO state in solution is sensitive to a base of the suspension (Fig. 18). Neutral and basic GO suspension (with steady-state concentration of KOH 0.02 M, 0.002 M and 0.0002 M) was used for coating preparation.

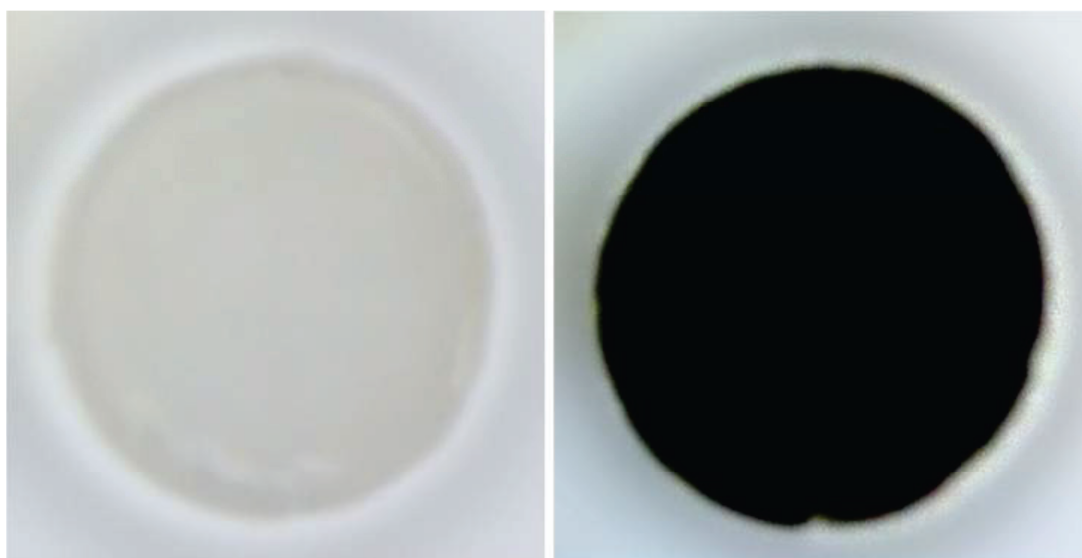


Fig. 18 GO coatings prepared on a polycarbonate membrane filters as a substrate. Thickness of the GO layer: 40 nm (left) and 400 nm (right), film diameter – 4 cm.

Coatings of GO and its modified products were formed by filtration of aqueous suspensions through the membrane filters in an aqueous medium. The pH of aqueous media was chosen as acidic, neutral or alkaline. Coatings of modified GO products were also prepared using this method.

Details for coatings used in laser induced reduction experiments are given in Table 3: GO-CRa, GO-CRb, GO-AB, GO-MN1, GO-MN2 and GO1.

Table 3 GO samples and their preparation procedures

Sample	Preparation procedure				
	Suspension	Filtration	Dopant	Substrate, Pore d	Film thickness
GO-CRa	H <sub>2</sub> O GO, concentration $1.5 \cdot 10^{-4}$ g/ml;	0.1 M KOH	Congo Red dye 0.001 M, 10 ml	PC, d=0.4 $\mu$ m	1200 nm
GO-CRb	H <sub>2</sub> O GO, concentration $5 \cdot 10^{-4}$ g/ml; sonicated 1 h;	H <sub>2</sub> O	Congo Red 0.001 M, 5 ml (c $5 \cdot 10^{-5}$ M)	PC, d=0.4 $\mu$ m	1200 nm
GO-AB	H <sub>2</sub> O GO, $1.5 \cdot 10^{-4}$ g/ml;	H <sub>2</sub> O	Alkali Blue dye 0.001 M, 0.5 ml	PC, d=0.4 $\mu$ m	1200 nm
GO-MN1	Neutral GO, $5 \cdot 10^{-5}$ g/ml	H <sub>2</sub> O	-	MagnaNylon, d=0.2 $\mu$ m	800 nm
GO-MN2	Neutral GO, $5 \cdot 10^{-5}$ g/ml	NaOH solution	-	MagnaNylon d=0.2 $\mu$ m	1200 nm
GO1	0.02 M KOH+GO, $5 \cdot 10^{-5}$ g/ml; Sonication for 30 min;	0.1 M KOH	-	PC, d=0.45 $\mu$ m	400 nm

### 3.1.2 SAMPLES USED IN GRAPHITE OXIDE WITH CONGO RED DYE REDUCTION

Graphite oxide was synthesized using the modified Hummers – Offeman method from a graphite precursor. Congo-Red dye (CR) was used as an additive [102]. Graphite oxide preserved the layered structure of its predecessor graphite. Functional reagents normally are used to arrange individual graphene sheets regularly and form larger graphene flakes. Such agents can be large organic molecules with certain functional groups that react with the functional groups existing in graphene or graphite oxide nanostructures, joining separate GO sheets into larger moieties. The use of organic Congo Red (CR) dye for this purpose was reported in [103]. While preparing the dye-modified GO suspensions, it was observed that positively charged organic molecules (Crystal Violet, Methyl Green, Rhodamine G, and Alkali Blue) reduced stability of the GO aqueous suspension. It was considered that this phenomenon occurred due to the interaction between the dye molecules and the negatively charged GO sheets. Meanwhile, the molecules with uneven positive and negative charge distribution (Acidic Anthraquinone Blue and Congo Red) can interact with the GO sheets by forming nanocomposite structures. This reaction resulted in a color change depending on the dye-to-GO ratio. The more important factors affecting the suspension color were the sonication and the treatment duration (Fig. 19 b-d).

Sonicated GO-CR suspensions were used to produce GO/CR nanocomposite films. The films with the thickness of 1200 nm were prepared on the polycarbonate membrane filters via slow filtration into alkaline media. Such thickness was chosen as from the previous experiments it was observed that higher GO reduction level is achieved in thicker samples. Obtained films were flexible in a wet ambient. Mechanical properties of the coatings were dependent on the GO-to-CR ratio. The samples with the higher CR content were more flexible and prone to curl.

Details for coatings, doped with different concentrations of Congo Red dye used in laser induced reduction experiments are given in Table 4: GO-CR1, GO-CR2, GO- CR3, GO- CR4.

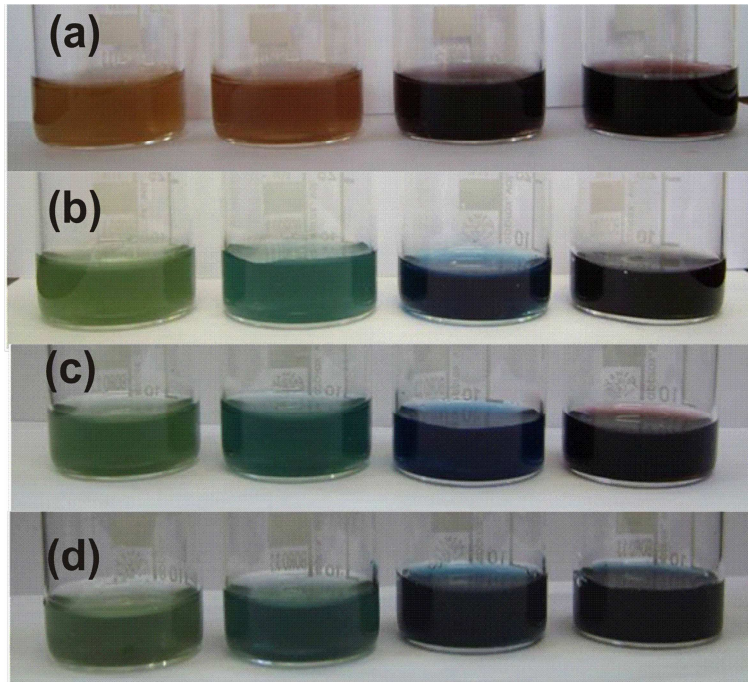


Fig. 19 Color change of the GO–CR aqueous mixtures. GO concentration– $1.5 \cdot 10^{-4}$  g/ml. CR concentrations (from left to right):  $5.0 \cdot 10^{-6}$  M;  $1.0 \cdot 10^{-5}$  M;  $5.0 \cdot 10^{-5}$  M;  $1.0 \cdot 10^{-4}$  M. Treatment of GO-CR mixtures: (a) – fresh prepared, without sonication; (b) – after 1 h sonication; (c) – after 48 h; (d) – after 48 h + 1 h sonication.

Table 4 GO-CR samples with different concentrations and their preparation procedures

Sample	Preparation procedure				
	Suspension	Filtration	Dopant	Substrate, Pore d	Film thickness
GO-CR1	H <sub>2</sub> O GO, $1.5 \cdot 10^{-4}$ g/ml,	H <sub>2</sub> O	Congo Red 0.001 M, 0.5 ml (2 %)	PC, d=0.4 $\mu$ m	1200 nm
GO-CR2	H <sub>2</sub> O GO, $1.5 \cdot 10^{-4}$ g/ml,	H <sub>2</sub> O	Congo Red 0.001 M, 1 ml (4 %)	PC, d=0.4 $\mu$ m	1200 nm



GO-CR3	H <sub>2</sub> O GO, 1.5·10 <sup>-4</sup> g/ml	H <sub>2</sub> O	Congo Red 0.001 M, 5 ml (19 %)	PC, d=0.4 μm	1200 nm
GO-CR4	H <sub>2</sub> O GO, 1.5·10 <sup>-4</sup> g/ml,	H <sub>2</sub> O	Congo Red 0.001 M, 10 ml (38 %)	PC, d=0.4 μm	1200 nm

### 3.1.3 SAMPLES USED IN GRAPHENE-CHITOSAN LASER TREATMENT EXPERIMENTS

Graphene flakes of 8 nm height were obtained from Graphene Supermarket (USA). ITO glass slides (100 x 100 mm<sup>2</sup>, resistivity of 12 Ω cm<sup>2</sup>) were purchased from Optical Filters (UK). The slides were laser cut into 2 x 2 cm<sup>2</sup> square electrodes.

K<sub>4</sub>Fe(CN)<sub>6</sub>•3H<sub>2</sub>O, CH<sub>3</sub>COOH, KCl, and chitosan from shrimp shells were obtained from Sigma Aldrich (Germany). H<sub>2</sub>SO<sub>4</sub>, HNO<sub>3</sub>, NaH<sub>2</sub>PO<sub>4</sub>•H<sub>2</sub>O, Na<sub>2</sub>HPO<sub>4</sub>, and NaOH were obtained from ROTH GmbH (Germany). All reagents used were of analytical grade. All solutions were prepared with ultrapure MilliQ-water (resistivity of 18.2 MΩ cm<sup>2</sup>) directly taken from Synergy 185 unit equipped with a UV lamp (Millipore, USA).

Chitosan matrix was chosen to ensure even distribution of graphene flakes through the electrode surface. Previous attempts to cover the surface of the electrode with uniform layer of graphene, using aqueous graphene suspensions failed due to forming of graphene agglomerates. Use of chitosan allowed to implement uniform distributions of graphene flakes and increased mechanical stability of the electrode.

Graphene flakes were additionally exfoliated to 2-3 nm and functionalized with hydroxy- and carboxy-groups by sonication 50 mg of graphene flakes in mixture of 5 mol/l H<sub>2</sub>SO<sub>4</sub> and HNO<sub>3</sub> 3:1 (V:V) at 40°C for

20 h; then the mixture was filtrated and neutralized with MiliQ water. Finally, solid precipitate was dried at 80°C for 24 h.

Firstly, aqueous solution of 0.5% chitosan was prepared. Chitosan was dissolved in aqueous 1% CH<sub>3</sub>COOH solution; then pH was adjusted to 5.0 with 20 % NaOH solution. Then functionalized graphene was added to the solution and sonicated for 2 h till a homogeneous dispersion. Suspensions of appropriate concentration (Table 5) were prepared in this way. These suspensions were spin-coated on the indium-tin-oxide (ITO) square electrodes with WS-650-23 spin-coater (Laurell Technologies Corporation, USA), at the 700 rpm rotation speed for the period of 1 min. and then 1800 rpm for 30 s (Fig. 20). The electrodes were left to dry overnight and then characterized applying Cyclic voltammetry (CV) and Electrochemical Impedance Spectroscopy (EIS). Thickness of the graphene-chitosan film was ~1 μm.

Table 5 Samples and their graphene suspensions concentrations.

Sample	G1	G2	G3	G4
Concentration	10 pg/ml	10 μg/ml	1 mg/ml	3 mg/ml

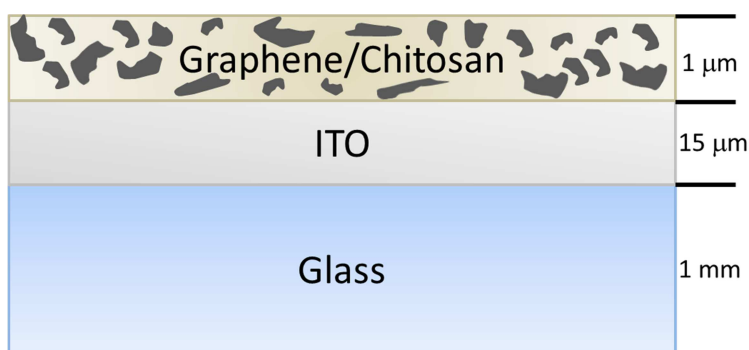


Fig. 20 Cross-sectional view of the graphene/chitosan sample.

### 3.2 LASER TREATMENT

Experiments on reduction of graphite oxide to graphene were performed using localized laser heating. The picosecond laser (Atlantic, 10 ps, 100 kHz, Ekspla) was used in the experiments. Experimental setup with a picosecond

laser included the laser, electro-optical shutter, nonlinear crystal for wavelength conversion, the beam expander and galvanometer scanners with focusing objectives (focus = 80 mm) for both 1064 nm and 532 nm wavelengths (Fig. 21).

The samples of graphite oxide / Congo-Red composite films were treated using the picosecond laser (Atlantic, 10 ps, 100 kHz, 1064 nm, Ekspla) (Fig. 21). During the tests, the average laser power was varied from 7 mW to 50 mW, which corresponded to the pulse energy from 0.07  $\mu\text{J}$  to 0.5  $\mu\text{J}$ . The diameter of the focused laser beam at surface of GO was 20  $\mu\text{m}$  ( $1/e^2$  level). Therefore, laser energy density (fluence) in the center of the laser spot was from 0.048  $\text{J}/\text{cm}^2$  to 0.32  $\text{J}/\text{cm}^2$ , respectively. The scanning speed was changed in the range of 5 – 100 mm/s. The pulse energy and the scanning speed both together determined the irradiation dose to the material.

The sample was placed inside a chamber with controllable ambient. Experiments were conducted with the GO/CR nanocomposite films in the nitrogen atmosphere to prevent the oxygen effect from the air. Areas of the GO films were modified by scanning the laser beam with a hatch between scanning lines equal to the beam diameter.

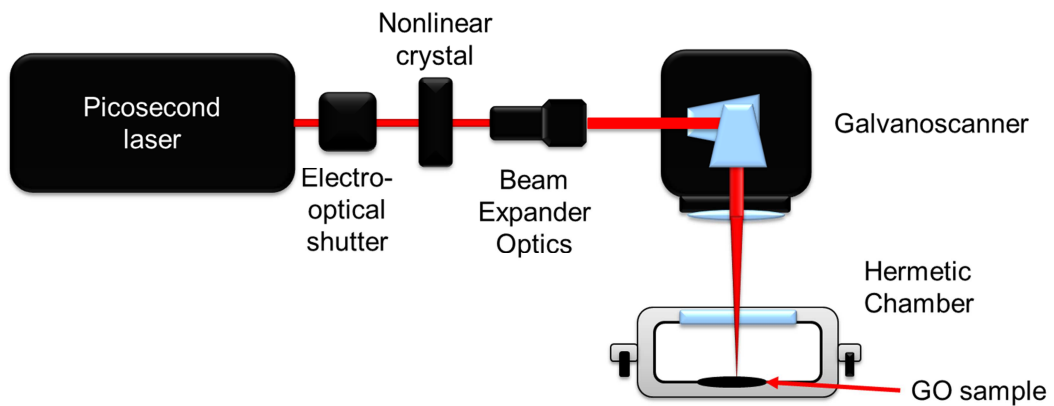


Fig. 21 Experimental setup for laser treatment of graphite oxide films.

Laser irradiation of graphene chitosan composite films was performed with the picosecond laser (Atlantic, 10 ps, 100 kHz, 1064 nm, and 532 nm Ekspla). The scanning speed was varied from 50 to 300 mm/s, and the applied mean laser power was varied from 50 mW to 200 mW. Any exceptional cases are specified in the text. Beam spot diameter at the focus was 20  $\mu\text{m}$ . GO/Chit

composite was modified by applying hatch pattern, which means that lines with a certain distance (hatch) between them (20  $\mu\text{m}$ ) were scribed on sample surface.

In order to achieve more uniform structuring, a different approach was chosen (Fig. 22). In this approach pulse overlapping was selected to be equally in both X and Y directions. In X direction, it was varied by means of changing the scanning speed and in Y – by changing the hatch period. A pitch parameter was introduced to reflect this type of overlapping. It stands for the distance between adjacent pulses in X/Y directions. The values of the used scanning speeds and hatch periods are shown in Table 6.

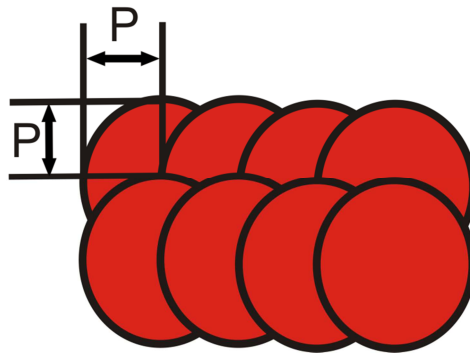


Fig. 22 Scheme of overlapping pattern with pitch parameter.

Seven values of pitch parameter were investigated (Table 6) and the laser power was varied from 10 mW to 500 mW. Radiation of picosecond laser at two different wavelengths (1064 nm and 532 nm) was used in these experiments.

Table 6 Pitch values and corresponding scanning speed and hatched period at the 100 kHz pulse repetition rate.

Pitch, $\mu\text{m}$	1	2	3	4	5	6	7
Scanning speed, mm/s	100	200	300	400	500	600	700
Hatch period, $\mu\text{m}$	1	2	3	4	5	6	7

### 3.3 CHARACTERIZATION

Raman spectroscopy and scanning electron microscopy (SEM) were used to characterize the samples. Raman measurements for GO characterization were performed with the 632.8 nm excitation (He-Ne laser) by using the confocal Raman spectrometer/microscope LabRam HR800 (Horiba Jobin Yvon) equipped with the 600 grooves/mm grating and a CCD camera cooled down to  $-132^{\circ}\text{C}$  working temperature. The laser power at the sample was restricted to 1 mW and the laser beam was focused to  $\sim 2\ \mu\text{m}$  diameter spot on the surface. Spectra were taken with the 50x objective lens. The overall integration time was 100 s. Raman spectra were captured from the center of laser scribed lines and untreated area of GO film for comparison.

Raman spectroscopy measurements for graphene/chitosan composite films were performed with the Raman microscope inVia (Renishaw, UK) equipped with thermoelectrically cooled CCD detector using four different excitation wavelengths: 442 nm (0.8 mW) line from a He-Cd laser, 532 nm (0.6 mW) from a diode-pumped solid state laser, 633 nm (0.5 mW) from a He-Ne laser, and 785 nm (1.8 mW) from a diode laser. Raman spectra were taken using a 50x/0.75 NA objective lens. Integration time was 50 s. Wavenumber axis was calibrated according to the Si line at  $520.7\ \text{cm}^{-1}$ . Frequencies and intensities of the Raman bands were determined by fitting the experimental contour with Gaussian-Lorentzian form components. Spectral analysis was performed by using GRAMS/A1 8.0 (Thermo Scientific, USA) software.

The scanning electron microscope JSM-6490 LV (JEOL) was used for investigation of surface morphology changes during the laser treatment. Samples without any additional preparation were used in the SEM microscopy.

Cyclic voltammetry (CV) and electrochemical impedance spectroscopy (EIS) measurements were conducted with CompactStat potentiostat/galvanostat with impedance module (Ivium Technologies, The Netherlands). Three-electrode system was used employing bare or graphene modified ITO as a working electrode, Pt wire was as a counter electrode and

Ag/AgCl (KCl sat.) electrode served as a reference one (Fig. 23). Electrochemical impedance spectroscopy (EIS) was performed with the same equipment at a constant applied potential, with a potential perturbation of 10 mV in the frequency range from 100 kHz to 0.1 Hz.

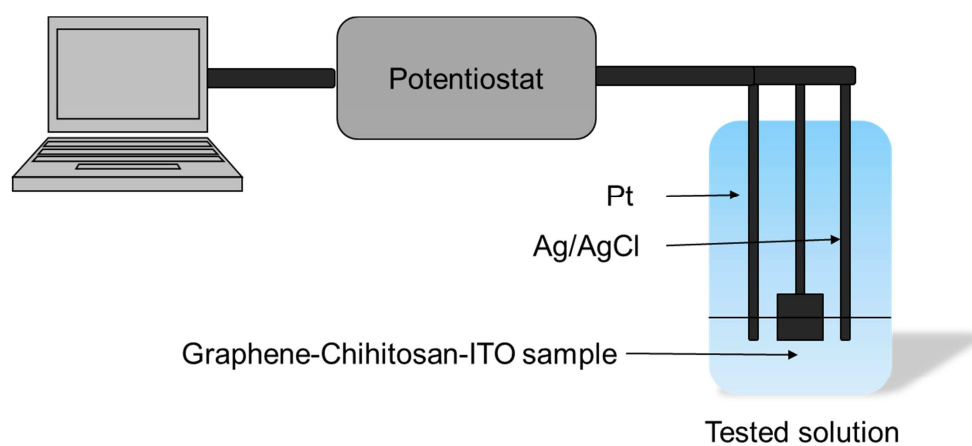


Fig. 23 Cyclic voltammetry (CV) and electrochemical impedance spectroscopy (EIS) measurement setup.

## **4 GRAPHITE OXIDE REDUCTION TO GRAPHENE USING PICOSECOND LASER IRRADIATION**

The aim of our experiments was modification of the graphite oxide film by converting it locally into graphene using laser irradiation. An effect of the process parameters and ambient atmosphere on properties of the laser reduced graphene was investigated. Results are presented in article A1.

Irradiation with the laser beam caused a change in morphology of the GO film. After laser processing, samples were at first investigated under the optical microscope (Olympus BX51TF). Further evaluation of the laser processed samples included scanning electron microscopy, measurement of electrical resistance and Raman spectroscopy.

The results presented in this chapter below were achieved using only the picosecond laser working at the fundamental wavelength of 1064 nm. Depending on the thickness of the sample and the scanning speed, the irradiated areas burned out when the infrared laser with average power of 100 mW and higher was applied. Use of the average laser power below 10 mW did not show any visible effects of the laser irradiation even in the thinnest samples, which were 10-40 nm in thickness.

SEM (JSM-6490 LV, JEOL) was used for precise evaluation of surface modifications of laser treated GO films. Characteristic SEM images are presented below.

Fig. 24, Fig. 25 and Fig. 26 present the laser modified lines in GO film doped with Congo-Red dye. The laser processing parameters were quite similar (the same irradiation dose). Surface of GO film was elevated when the low laser power at the low scanning speed was used. However, in case of the higher laser power even at the higher scanning speed, smoothening of the surface was accompanied by exfoliation of the graphite oxide layer. Keeping the same laser processing parameters but in nitrogen atmosphere, the visual effect of laser processing was similar (Fig. 27). The further increase in the mean laser power at the same scanning speed led to damage of the GO film in

the center of laser scan line where intensity of the laser beam was maximal due to the Gaussian distribution of the beam.

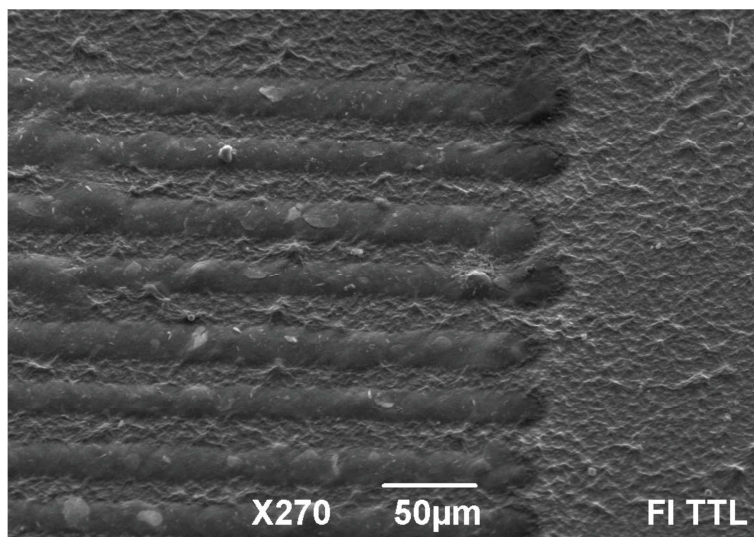


Fig. 24 SEM image of laser modified lines in GO film. Process parameters: laser Atlantic, wavelength 1064 nm; irradiation dose  $6.37 \text{ J/cm}^2$  (laser power 10 mW; scanning speed 10 mm/s); ambient air. Sample GO-CRa.

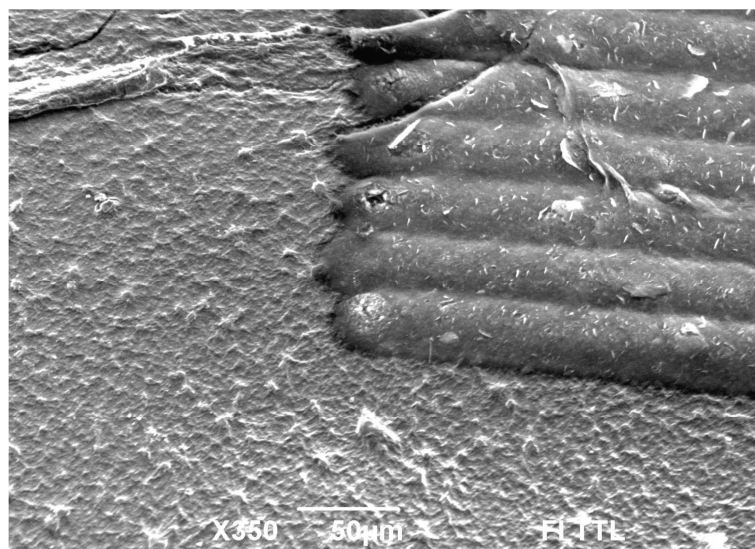


Fig. 25 SEM image of laser modified lines in GO film. Process parameters: laser Atlantic, wavelength 1064 nm; irradiation dose  $6.37 \text{ J/cm}^2$  (laser power 30 mW; scanning speed 30 mm/s); ambient air. Sample: GO-CRa.



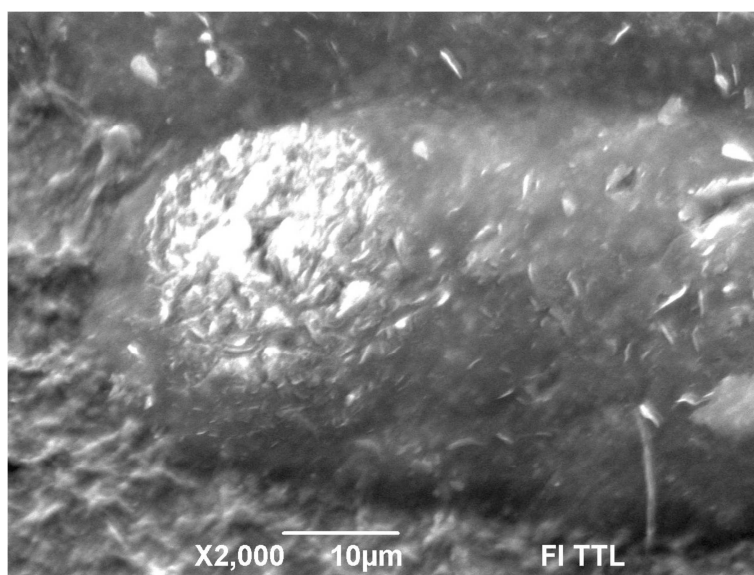


Fig. 26 SEM image of laser modified lines in GO film. Process parameters: laser Atlantic, wavelength 1064 nm; irradiation dose  $6.37 \text{ J/cm}^2$  (laser power 30 mW; scanning speed 30 mm/s); nitrogen atmosphere. Sample: GO-CRa.

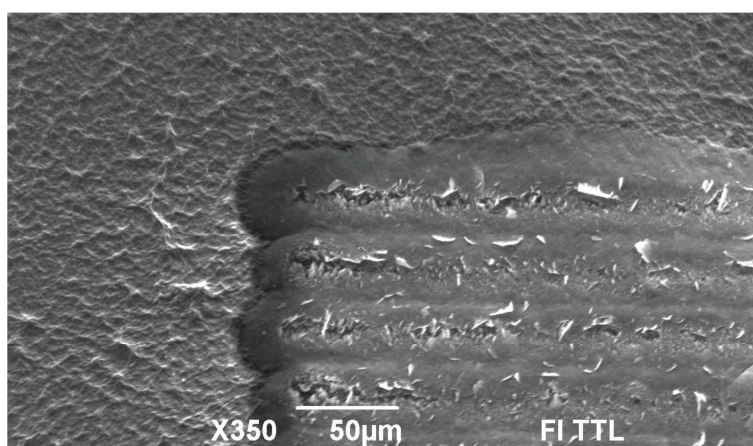


Fig. 27 SEM image of laser modified lines in GO film. Process parameters: laser Atlantic, wavelength 1064 nm; irradiation dose  $10.62 \text{ J/cm}^2$  (laser power 50 mW; scanning speed 30 mm/s); nitrogen atmosphere. Sample: GO-AB.

The used dopants modified the GO film and laser processing results were different in the same range of the process parameters. Fig. 27 and Fig. 28 present SEM images of laser modified lines in the GO film doped with Alkali-Blue dye.

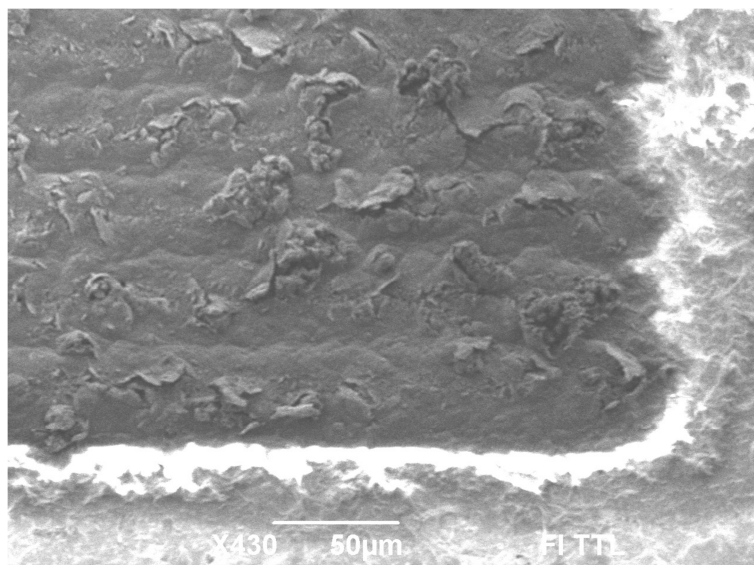


Fig. 28 SEM image of laser modified lines in GO film. Process parameters: laser Atlantic, wavelength 1064 nm; Irradiation dose  $2.55 \text{ J/cm}^2$  (laser power 20 mW; scanning speed 50 mm/s); argon atmosphere. Sample: GO-AB.

The surface of laser modified areas in samples doped with the Congo-Red dye was smooth and elevated, while the surface of laser irradiated areas in Alkali-Blue dye doped samples was notably damaged with irregular cracking patterns. The reason could be in the ability of Congo-Red to form larger moieties composed of the nano-platelets of graphene due to interaction between the amino groups in Congo-Red molecule and the functional groups of GO located on the edges of nano-platelets.

#### **4.1 ELECTRICAL RESISTANCE OF MODIFIED GO LAYER**

Graphite oxide and graphene possess completely different electrical and related thermal conductivity properties. GO is an isolating material, while graphene is well known as a highly conductive one. Therefore, measurements of electrical resistance were used as one of the means to evaluate reduction of GO to the graphene phase. The resistance was measured with an ohmmeter between edges of the laser modified GO area of  $4 \times 10 \text{ mm}^2$ . Results for the GO films with the initial thickness of 800-1200 nm are presented in Fig. 29. All films were prepared on MagnaNylon substrates, neutral suspensions ( $5 \cdot 10^{-5}$

<sup>5</sup> g/ml), for a 800 nm-thick film, the suspension was filtered into water, while for the 1200 nm-thick film, the suspension was filtered in NaOH solutions.

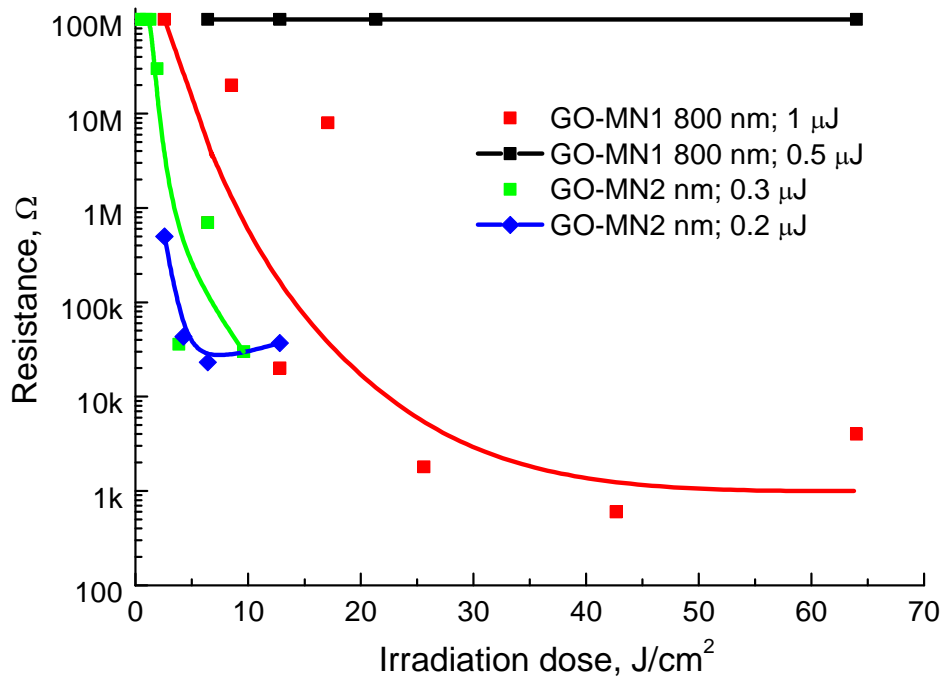


Fig. 29 Dependence of the GO film resistance on the irradiation dose for different GO films. Samples irradiated with the 1064 nm wavelength from the picosecond laser in air atmosphere. Solid lines are approximations of experimental data.

Electrical resistance of the GO films irradiated with the picosecond 1064 nm laser decreased by 4-5 orders from 100s of megaohms to one kilohm in a certain range of laser processing parameters, which depended on film preparation procedures as well. The irradiation dose was estimated from laser fluence in the center of the focused laser beam and beam overlap during scanning the beam across the surface. Rapid changes in the resistance were observed on the low-dose side, while minimum in resistivity was also pronounced in the GO sample with thickness of 1200 nm which was treated with 0.2 μJ pulse energy. For the GO film with thickness of 800 nm, it was identified that the low pulse energy (0.5 μJ) did not cause changes in resistivity of the film independent of the accumulated dose. The differences in response to laser irradiation of 1200 nm and 800 nm thick GO films evidence sensitivity of the initial materials to film preparation procedures (Table 3). Therefore,

further experiments were performed on samples prepared by the route similar to the 1200 nm-thick sample. Thickness of the GO film is important for quality of the reduction process, as temperature simulations presented later in section 5.3 show. Certain pulse energy is needed for effective GO reduction. However the film is heated up to 1400 K at those energy levels. In case of thinner film, polymer substrate would also heat up and deform from high temperature, causing addition strains and cracking formations in GO film.

## 4.2 SIMULATION OF HEAT TRANSFER VIA GRAPHENE CHANNELS

Simulation of heat transfer via graphene channels was performed using COMSOL Multiphysics software. Three materials having thermal contact in the scheme were investigated: graphene, graphite oxide and the substrate.

Table 7. Physical parameters of the materials, comprising heat transfer system, used in simulation

Material/ Parameter	Density $\rho$ , kg/m <sup>3</sup>	Thermal conductivity, W/m·K	Thermal capacity, J/kg·K
Graphene [104]	2260	5000	710
Graphite oxide	2260	28.8	710
Polycarbonate	1210	0.2	1250

The graphite oxide coating was modified by the laser to form a 1.2 mm wide and 44 mm long zigzag channels (Fig. 30, Fig. 31 a). One end of the channel was heated by soldering iron, the other end was connected to the massive copper radiator. Thermo-vision camera Fluke recorded temperature field in the sample (Fig. 31). The laser-reduced GO channel is clearly distinguished from the unmodified laser background material, indicating a significant difference in the thermal properties between the laser reduced and non-reduced GO surface sites.

For the thermal simulations, the heat conduction equation was solved using a method of finite element analysis. Temperature distribution was chosen to evaluate due to problematic evaluation of the exact heat flux absorbed by the material.

Whereas, layers of graphene and graphite oxide were very thin (reduced graphene~300 nm, according to modelling described in section 5.3, GO~1.2 μm) comparing to other two dimensions, thermal gradient in the direction of thickness was negligible. In this case, the simulation can be simplified to a two dimensional model. For this model, the heat conduction equation for thin films was used (1):

$$d_z \rho C_p \frac{\delta T}{\delta t} + d_z \rho C_p \nabla T = \nabla \cdot (d_z k \nabla T), \quad (1)$$

where  $d_z$  is the thickness of the layer,  $\rho$  is the density of the material,  $C_p$  is the heat capacity,  $t$  is time,  $k$  is the thermal conductivity and  $T$  is temperature. Temperature source of 200°C was added as a boundary condition to one contact pad (Fig. 30), the second contact pad on opposite end of the conductor was bonded to a heat sink of infinitive capacity. The boundary conditions for all other boundaries were selected as thermal insulation, because of significant difference in thermal conductivity of graphene  $k=5000 \text{ W/m}\cdot\text{K}$  and polycarbonate  $k=0.2 \text{ W/m}\cdot\text{K}$ .

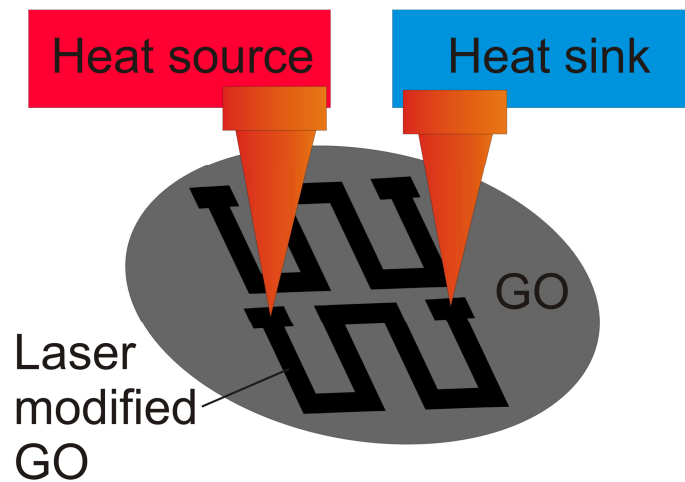


Fig. 30 Principal and at the same time schematic view of the setup used for thermal imaging of laser scribed graphene channels on GO substrate.

Results of simulations for similar geometrical dimensions are compared with the thermo-vision image in Fig. 31.

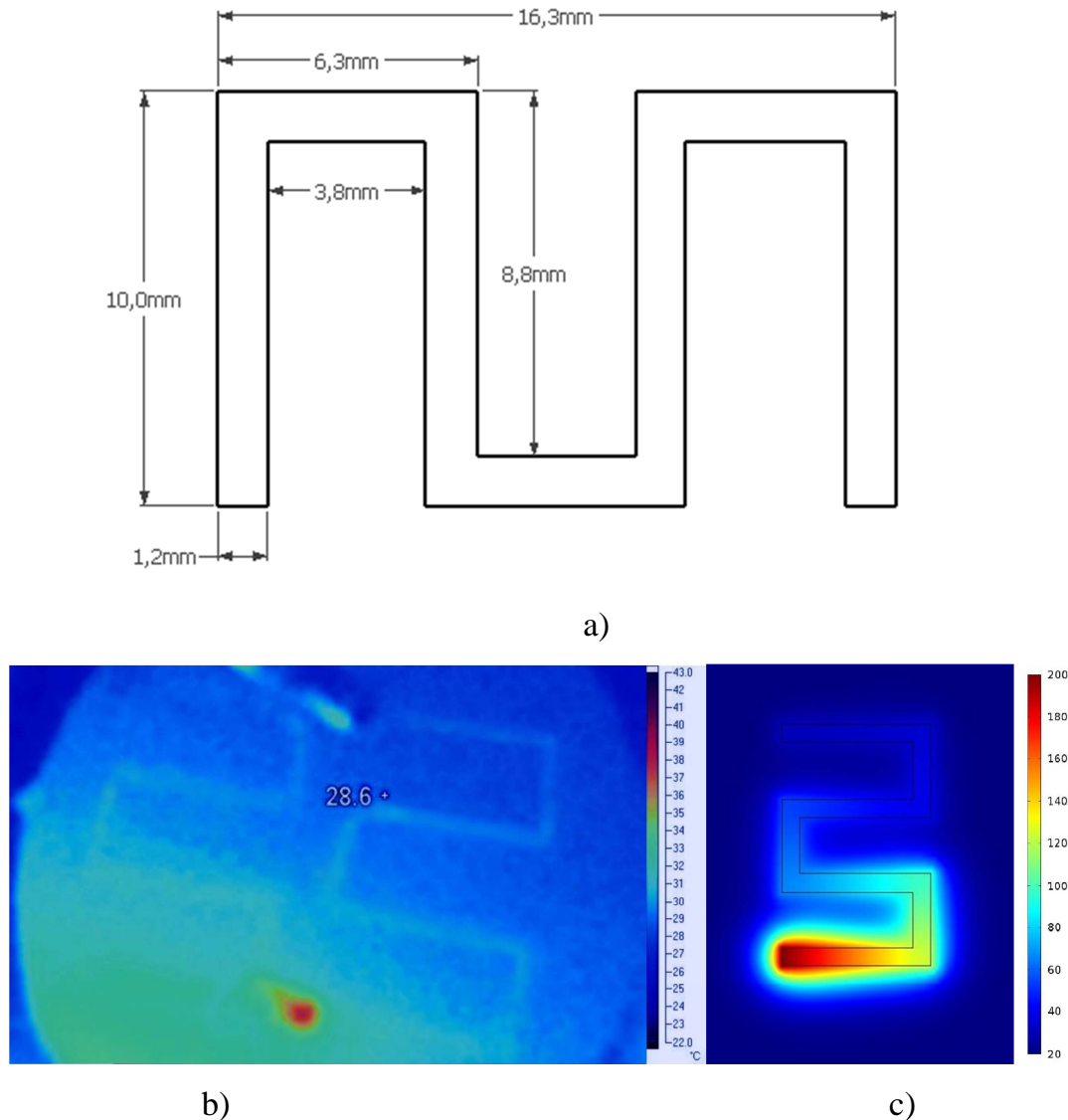


Fig. 31 a) Drawing and dimensions of the zigzag structure used in experiment and modeling; b) temperature distribution in the double zigzag structure of graphite oxide coating formed by localized laser reduction method measured by thermo-visual camera. Red dot is the contact point of the heater. The opposite end of the reduced conductor was connected to a massive copper radiator; c) Temperature distribution in graphene channel in graphite oxide layer in polycarbonate, simulated by COMSOL.

Thermal energy transferred through a conductor can be found by knowing the conductor geometry and the material thermal conductivity coefficient:

$$P = k \frac{\Delta T}{\Delta x} S \quad (2)$$

So, for a conductor which cross-sectional area  $S$ , the length  $\Delta x$  and heat transfer coefficient  $k$ , the temperature difference that exists between the heat source and the radiator is:

$$\Delta T = \frac{P\Delta x}{kS} = R_K P, \quad (3)$$

where  $R_K$  is the material thermal resistance:

$$R_K = \frac{\Delta x}{kS}. \quad (4)$$

One of potential applications for the graphene based heat conductor could be the heat removal from LED chips. Temperature settled in the heat source (e.g. LEDs) when it is connected by the conductor made of graphene and other materials of a certain cross-section with a radiator was evaluated. The objective was to evaluate the possibility of cooling the LED (conduct the heat away). Suppose LED emit 10 W of heat output. In the calculations we used parameters of metals with high thermal conductivity and graphene ("pure" and reduced) (Table 8).

Table 8 Evaluation of thermal power transmission in conductors and conductor temperature generated temperature drop  $\Delta T$ .  $k$  is the coefficient of thermal conductivity; conductor dimensions, conductor thermal resistance  $R_K$ ,  $P$  is the thermal power emitted by heat source (such as LEDs)  $\Delta T$  is the temperature difference between the ends of the conductor, when one end is connected to the heat source, and the other to the radiator of infinite capacity,  $D$  is the effective diameter of the heat conductor.

Conductor	$k$ , W/m·K	Length, mm	Width, mm	h, mm	$R_K$ , K/W	$P$ , W	$\Delta T$ , K	$D$ , $\mu\text{m}$
Graphene [104]	5000	10	1	0.001	2	10	20	35.69
Silver[105]	429	10	1	0.001	23.3	10	233.1	35.69
Coper[105]	401	10	1	0.001	24.9	10	249.4	35.69
Gold[105]	318	10	1	0.001	31.5	10	314.5	35.69
Graphene	1000	10	1	0.001	10	10	100	35.69
Graphene	1000	10	2	0.001	5	10	50	50.48
Graphene	1000	10	3	0.001	3.33	10	33.3	61.82

Graphene	1000	10	4	0.002	1.25	10	12.5	100.9
Graphene	1000	20	3	0.001	6.67	10	66.7	61.82
Graphene	5000	100	3	0.001	6.67	10	66.7	61.82

Semiconductor LED should be kept below 75°C. Simulation results in table 8 that a heat conductor made of graphene, with the length of 10 mm, the width of 1 mm and the thickness of 1 μm (our studied thickness) can keep the LED below the critical temperature. At the same time, metal conductors with the same dimensions are unable to remove efficiently heat. The problem with using reduced graphene coatings is that the thermal properties of the conductor are difficult to control over large dimensions, but it can be adapted to a local heat removal in a short distance, if the heat conductor gauges are limited.

### 4.3 RAMAN SPECTRA ANALYSIS

Laser irradiated samples of GO films were analyzed using Raman scattering spectroscopy. This technique is considered to be one of the most reliable means in identifying graphene allotrope [47]. Examples of the Raman spectra captured on the sample processed at various laser and scanning parameters are shown in Fig. 32.

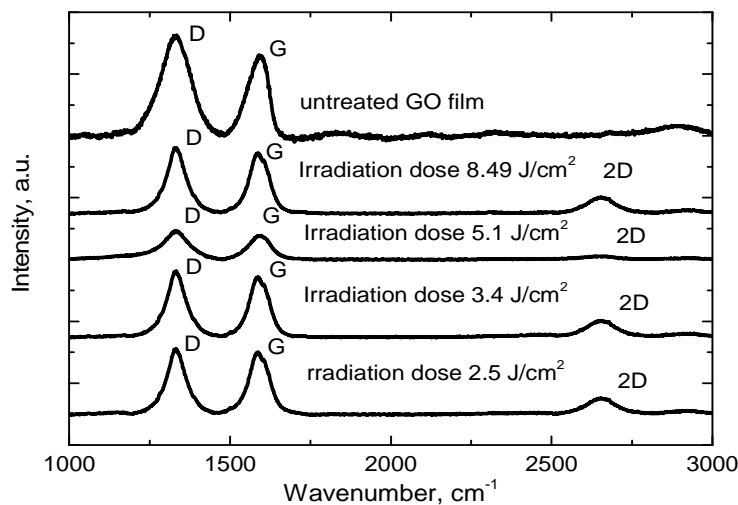


Fig. 32 Raman spectra of untreated by laser GO film and treated at various scanning parameters using 1064 nm radiation in nitrogen atmosphere Sample: GO1



Depending on the laser treatment parameters, the ratio  $I_D/I_G$  decreased, and the 2D-band, indicating graphene layers formation, appeared [13]. However, the D-line was observed in Raman spectra of all laser irradiated GO films, used in the investigations. This spectral line shows presence of packing irregularities [106], and the reason can be presence of oxygen during the experiments. The D-line was slightly reduced by irradiating GO in argon atmosphere [40]. Shift of the G-line to the higher wave numbers can be recognized in the spectra with the higher 2D-band intensity. Such shift corresponds to the decrease in the number graphene layers [107]. Therefore, experiments in an evacuated chamber filled with nitrogen or argon gas were also conducted. For samples, after irradiation GO with the picosecond laser in nitrogen or argon atmosphere, the  $I_D/I_G$  ratio was lower than in air atmosphere at the same laser treatment parameters. For more demonstrative identification of most suitable laser treatment parameters,  $I_{2D}/I_G$  ratios were calculated (Fig. 33). The highest value of this ratio means the best reduction results. According to this evaluation, the better results are achieved in argon and nitrogen atmosphere, when the irradiation dose was  $6.37 \text{ J/cm}^2$ .

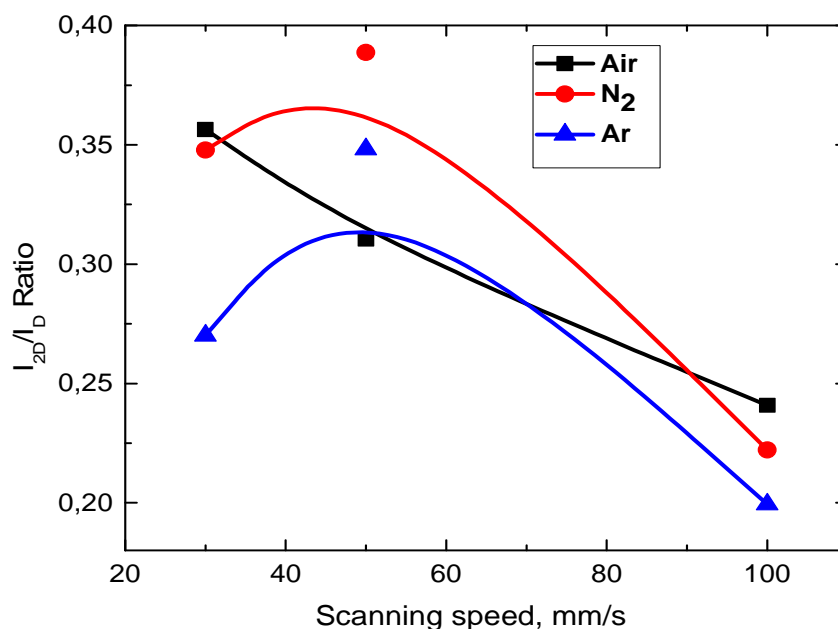


Fig. 33 The ratio of intensities in Raman lines  $I_{2D}/I_D$  versus scanning speed at the constant mean laser power of 50 mW ( $F=0.16 \text{ J/cm}^2$ ) in air, nitrogen and argon atmosphere. Experiments were conducted with 1064 nm radiation. Sample: GO-AB.

Similar behavior was observed for the GO film doped with Congo Red. The highest ratio between intensities of the Raman lines  $I_{2D}/I_D$  was achieved when laser irradiation was performed in the oxygen-free atmosphere (Fig. 34), however the optimal laser processing parameters shifted to the lower mean laser power, keeping the same irradiation dose.

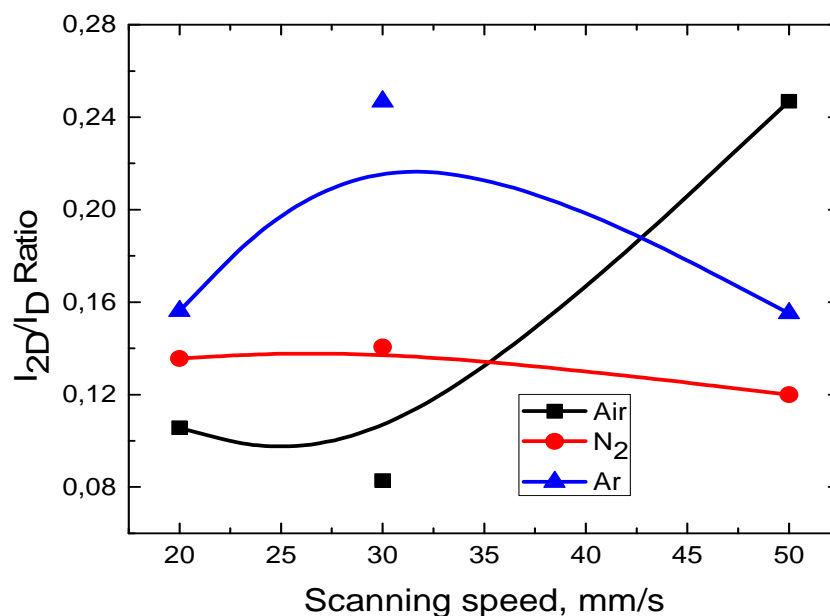


Fig. 34 The ratio of intensities of the Raman lines  $I_{2D}/I_D$  versus scanning speed at the constant 30 mW power ( $F=0.1 \text{ J/cm}^2$ ) in air, nitrogen and argon atmosphere. Experiments were conducted with 1064 nm radiation. Sample: GO-CRb.

#### 4.4 CONCLUSIONS

- Electrical resistivity of the 1200 nm-thick GO films irradiated with the picosecond laser at the wavelength of 1064 nm decreased in a certain range of the laser processing parameters and the 2D-line appeared in Raman spectra of the same samples after the laser treatment in ambient air indicating formation of the graphene phase.
- Reduction of Graphite oxide to graphene with laser irradiation allows forming the heat conductive channels which, according to the theoretical estimations, are more effective than metallic heat conductive systems at short (<10 mm) distances.

- The higher quality of GO reduction to graphene was achieved by conducting the laser irradiation experiments in nitrogen and argon atmosphere compared to air ambient, as the  $I_{2D}/I_D$  ratio in Raman spectra increase to 0.5 in the laser modified samples.

## **5 GRAPHITE OXIDE/ CONGO RED NANOCOMPOSITE COATINGS REDUCTION**

In this section results of the reduction of graphite oxide doped with the Congo-Red dye are presented. From previous experiments with various GO additives, Congo-Red dye was chosen as it delivered more effective reduction and less morphology changes after the laser treatment. Thus, influence of Congo-Red dye to GO reduction with laser irradiation was investigated in detail. Results are presented in articles A2 and A3 and presentations.

### **5.1 INVESTIGATION OF CONGO-RED DYE INFLUENCE ON GO REDUCTION**

Picosecond laser irradiation was applied to GO/CR nanocomposite coatings (thickness of 1200 nm) with different Congo-Red (CR) concentration. The mean laser power and scanning speed were varied to find out the optimal irradiation conditions for graphene phase formation (Fig. 35).  $I_D/I_G$  and  $I_{2D}/I_G$  ratios from Raman spectra was chosen as criteria for evaluation of laser induced reduction quality. The laser treatment was performed in argon ambient to prevent oxygen effect from the air. The laser treated areas of the samples were investigated by Raman spectroscopy.

The absolute best results in our experiments were obtained when the laser power was 40 mW and the scanning speed was 25 mm/s (irradiation dose –  $10.2 \text{ J/cm}^2$ ). Raman spectrum of laser processed area of the GO/CR nanocomposite with the CR concentration of 19 wt% is shown in Fig. 36.

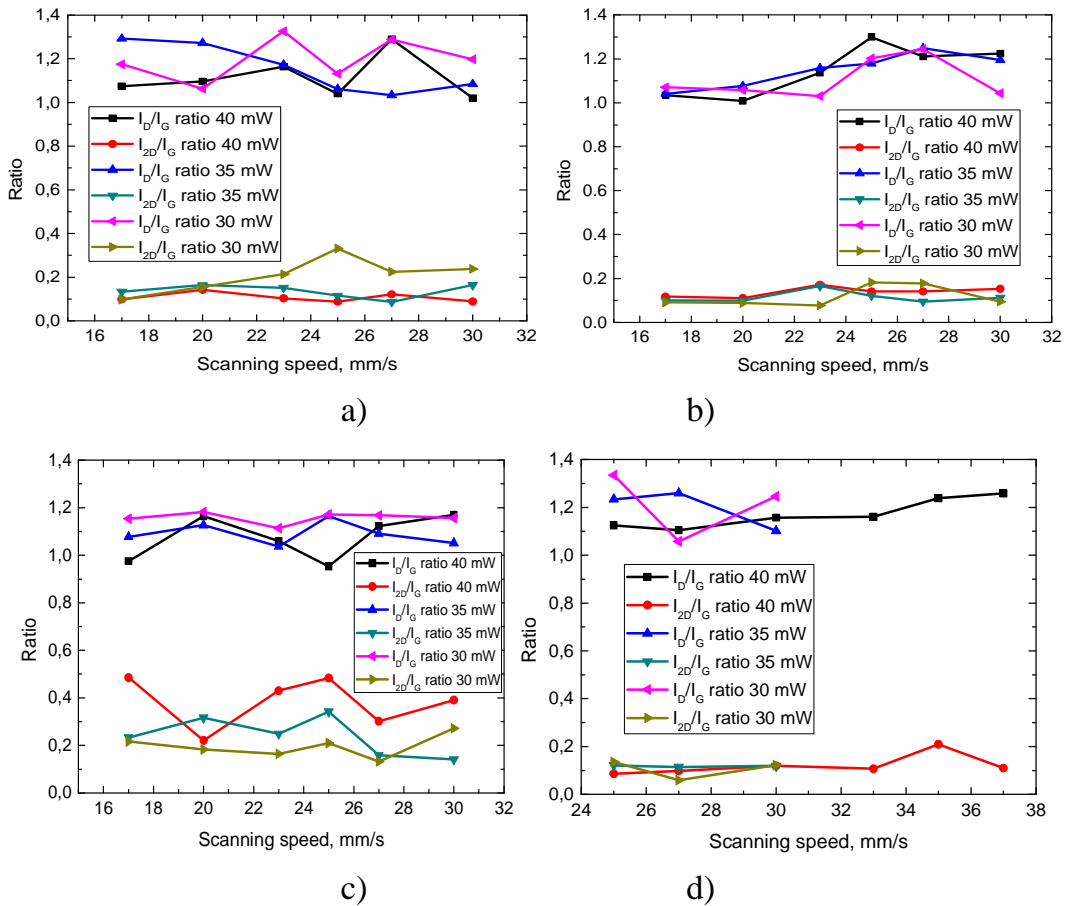


Fig. 35 Dependence of the  $I_D/I_G$  and  $I_{2D}/I_G$  ratios on the scanning speed using different average laser power for the reduction. GO suspensions, with different concentration of CR a) GO-CR1-2 %, b) GO-CR2-4 %. c) GO-CR3-19 %, d) GO-CR43.8 %.

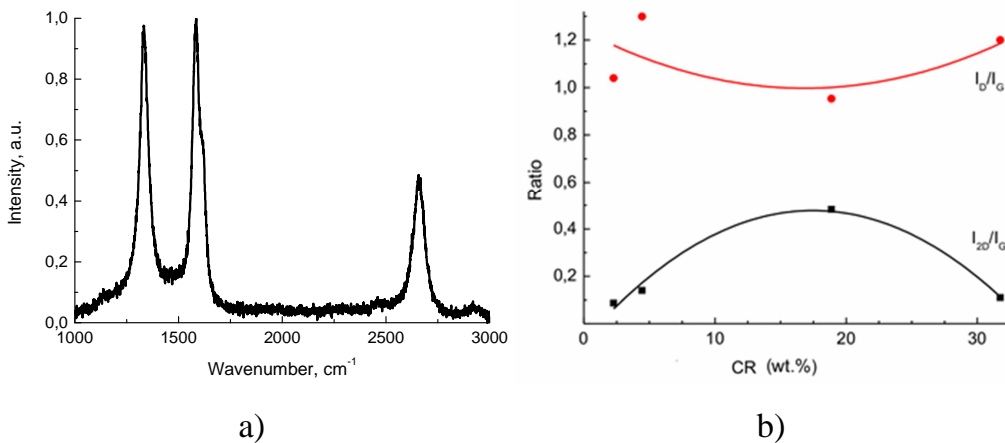


Fig. 36 a) Raman spectrum of the laser-treated GO/CR nanocomposite (GO-CR-3); b) dependence of the intensities ratio of the Raman lines D, G, and 2D on the CR concentration in laser-treated GO/CR nanocomposites. Laser process parameter: wavelength 1064 nm; mean laser power 40 mW, scanning speed 25 mm/s (dose –  $10 \text{ J/cm}^2$ ).

Presence of intense 2D-line indicates formation of the graphene-like structure due to the laser treatment of GO/CR film. The wavenumber of the symmetric 2D-band ( $2660\text{ cm}^{-1}$ ) coincides well with the estimated value for a single-layer graphene [106]. This band was approximated by the Lorentzian form and the bandwidth estimated. The full-width at a half maximum (FWHM) was found to be equal to  $55\text{ cm}^{-1}$ . This estimated value is about two times larger than expected for the perfect single graphene layer [108]. Relatively low  $I_{2D}/I_G$  ratio and intense D-band indicates presence of structure defects such as edge or vacancy defects and the structure composed of several graphene layers. Ratio of the intensities of the Raman lines depended on the CR concentration. Fig. 36 b presents results variation in  $I_D/I_G$  and  $I_{2D}/I_G$  depending on the CR concentration in the nanocomposites treated with the laser at identical conditions. Variation in the intensities ratios related to the quality of resulting graphene film indicate importance of the CR concentration on linkage of graphene sheets together and formation larger blocks with the increase in order. Existence of the optimal GO to CR ratio in the GO/CR nanocomposites is consistent with measurements of electrical conductivity and Raman scattering performed in this work. Therefore later experiments were conducted with the optimal concentration of the Congo-Red dye (19 wt%).

## **5.2 CHARACTERIZATION OF GO LASER TREATED FILMS WITH OPTIMAL CONGO-RED DYE CONCENTRATION**

Experiments presented in this section were conducted with the GO/CR nanocomposite films (aqueous GO suspension, doped with Congo-Red dye by 19 wt%) in the nitrogen atmosphere to prevent the oxygen effect from the air. Areas of the GO films were modified by scanning the laser beam with a hatch equal to the beam diameter. The sample was placed inside a chamber with controllable ambient.

Fig. 37 and Fig. 38 present SEM pictures of laser modified areas of the GO film. All samples in those pictures were irradiated with the same dose but

using different laser fluence. Reduction of GO to graphene normally should lead to a decrease in the film thickness. In Fig. 37 we can see that laser heating initiated intensive evaporation of volatile components from the film, and swelling of the film took place.

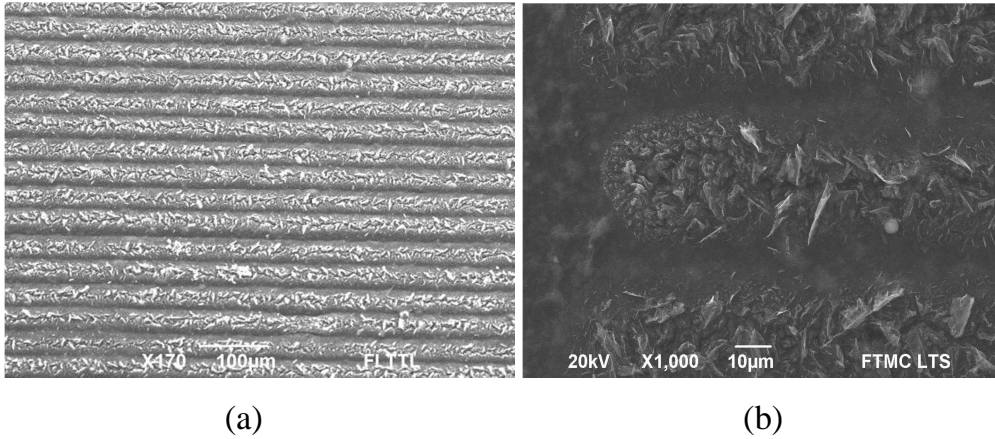


Fig. 37 SEM pictures of the laser-modified GO coating. The laser irradiation dose was  $3.18 \text{ J/cm}^2$ , laser fluence  $0.16 \text{ J/cm}^2$ : (a) low magnification image; (b) detailed view of the scan line ends at the higher magnification.

At lower laser fluence, the reduced region remained elevated, but no cracks in the film were observed (Fig. 38 a).

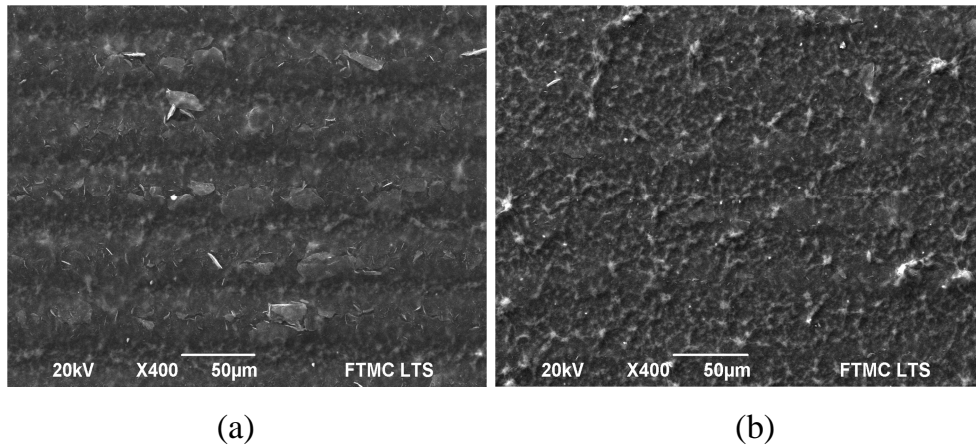


Fig. 38. SEM pictures of the laser-modified GO coating: (a) laser irradiation dose was  $2.5 \text{ J/cm}^2$ , fluence –  $0.06 \text{ J/cm}^2$ ; (b) laser irradiation dose –  $3.18 \text{ J/cm}^2$ , fluence –  $0.03 \text{ J/cm}^2$ .

Raman spectra of all samples were measured in the laser irradiated areas as well as in the untreated places. The Raman spectra measurements revealed dependence of the spectral line intensities on the laser processing parameters for different settings of the mean laser power and scanning speed. Variation of

those parameters affects the laser fluence (energy density) as well as the irradiation dose (time). Fig. 39 presents Raman spectra from the samples irradiated with the similar dose, but using different laser fluence. Differential spectra were obtained by extracting the Raman spectrum of the laser untreated GO film.

All spectra contain the D-band ( $1331\text{--}1338\text{ cm}^{-1}$ ), indicating the presence of structural defects, and the G-band ( $1586\text{--}1592\text{ cm}^{-1}$ ). The 2D-band ( $2653\text{ cm}^{-1}$ ) appearing in the spectra after laser treatment corresponds to the graphene formation due to the laser-induced GO reduction to graphene reaction. When the laser fluence was increased, the D-band intensity grew in respect to the G-band as laser heating released chemical bonds on edges of graphene sheets. Both D- and G-bands experienced narrowing as the fluence increased. Such behavior corresponds to decrease of disorder in the sample. Intensity of the 2D-band significantly increased at higher fluences (Fig. 39).

Differential spectra revealed intensification not only the 2D-band but also appearance of the D'-peak near  $1620\text{ cm}^{-1}$ . This band was previously attributed to the usually inactive Raman band activated due to the photon confinement effect induced by the generated defects [106,109]. Thus, the laser treatment induced defects which were responsible for the D'-band. This effect was especially pronounced in the case of the highest used laser power (Fig. 39 a).



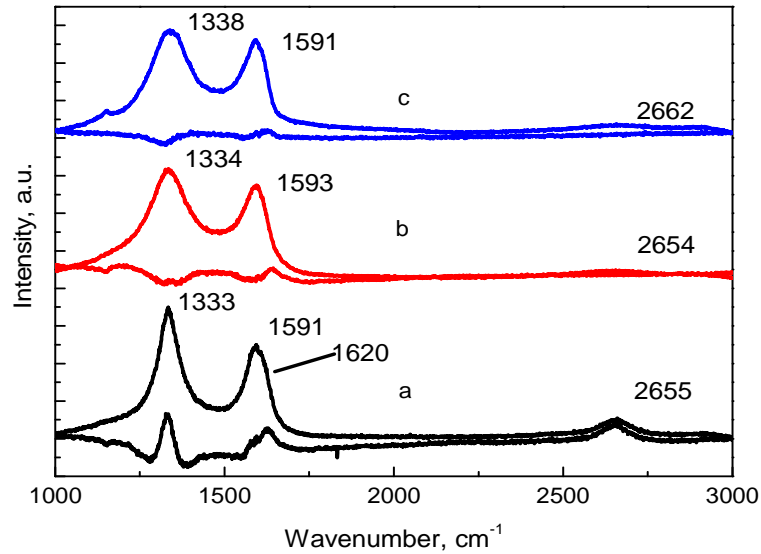


Fig. 39 Raman spectra normalized to the G-peak intensity and differential spectra obtained by extracting the spectrum of untreated GO: (a) laser irradiation dose was  $3.18 \text{ J/cm}^2$ , fluence –  $0.16 \text{ J/cm}^2$ ; (b) laser irradiation dose –  $2.5 \text{ J/cm}^2$ , fluence –  $0.06 \text{ J/cm}^2$ ; (c) laser irradiation dose –  $3.18 \text{ J/cm}^2$ , fluence –  $0.03 \text{ J/cm}^2$ . Spectra are shifted vertically to avoid their overlap in the figure.

At the laser fluence of  $0.1 \text{ J/cm}^2$ , bumping of the laser treated area was slightly lower. The reduced lines were smoother (Fig. 40 a) than using fluence of  $0.16 \text{ J/cm}^2$  (Fig. 37). At the lowest used fluence ( $0.03 \text{ J/cm}^2$ ), the reduced lines were smooth but more irregular (Fig. 40 b). This indicates that overlap of the scribing lines should be considered while changing the laser power in order to achieve the effective reduction.

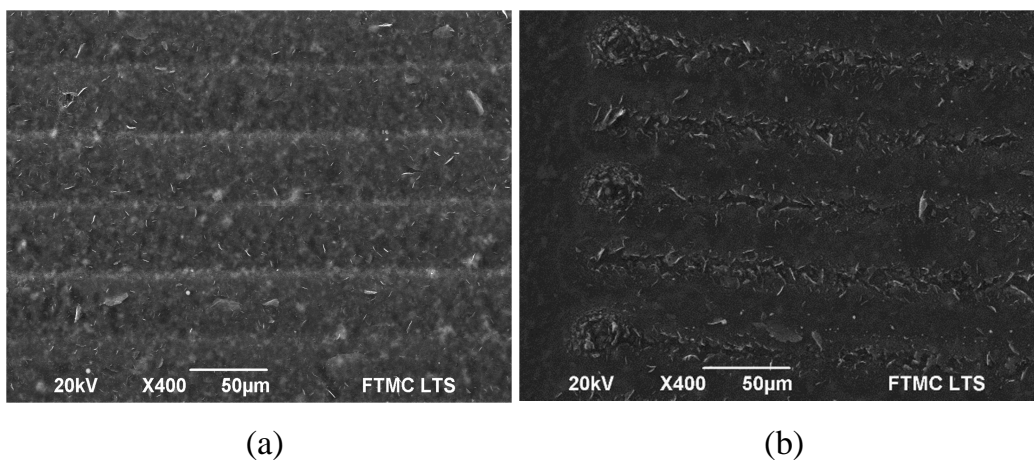


Fig. 40 SEM pictures of laser-modified GO coating: (a) the laser irradiation dose was  $6.4 \text{ J/cm}^2$ , fluence –  $0.1 \text{ J/cm}^2$  (b) laser irradiation dose –  $3.18 \text{ J/cm}^2$ , fluence –  $0.03 \text{ J/cm}^2$ .

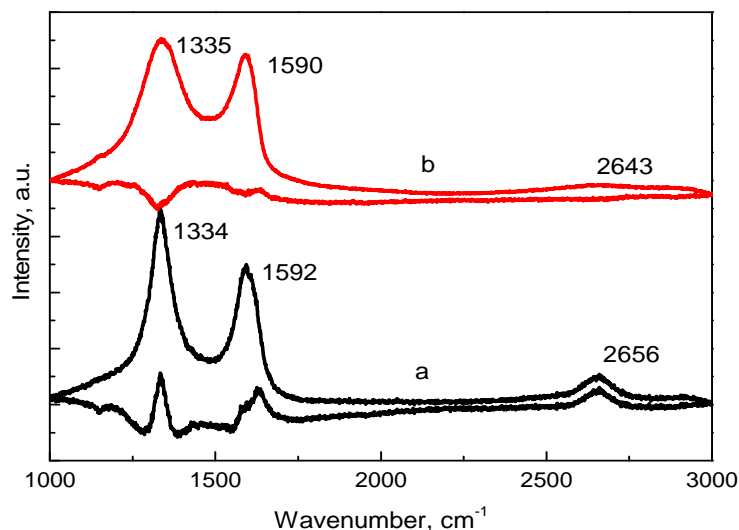


Fig. 41 Raman spectra normalized to the G-peak and differential spectra obtained by extracting the spectrum of laser untreated GO: (a) the laser irradiation dose was  $6.4 \text{ J/cm}^2$ , fluence –  $0.1 \text{ J/cm}^2$ ; (b) laser irradiation dose –  $3.18 \text{ J/cm}^2$ , fluence –  $0.03 \text{ J/cm}^2$ .

At the higher irradiation dose (lower scanning speed), a significant narrowing of the D-band and the rise of the 2D-band intensity were observed (Fig. 43). In Fig. 42 b., the scribed lines were irregular and indistinct. Raman spectroscopy confirmed a low degree of reduction (Fig. 43). At the low used laser power, no significant differences in the shape of the D- and G- Raman lines of the untreated and reduced GO were observed and the intensity of the 2D-band was low. The GO reduction was more effective using the laser fluence of  $0.16 \text{ J/cm}^2$ . A pronounced narrowing of the D-band and the rise in the intensity of the 2D-band compared to the results of Fig. 41 were observed. This indicates that not only the mean laser power, but also the scanning speed are important for the GO reduction process. At a lower scanning speed, GO was longer heated at higher temperatures, which caused an increase in efficiency of the reduction process.

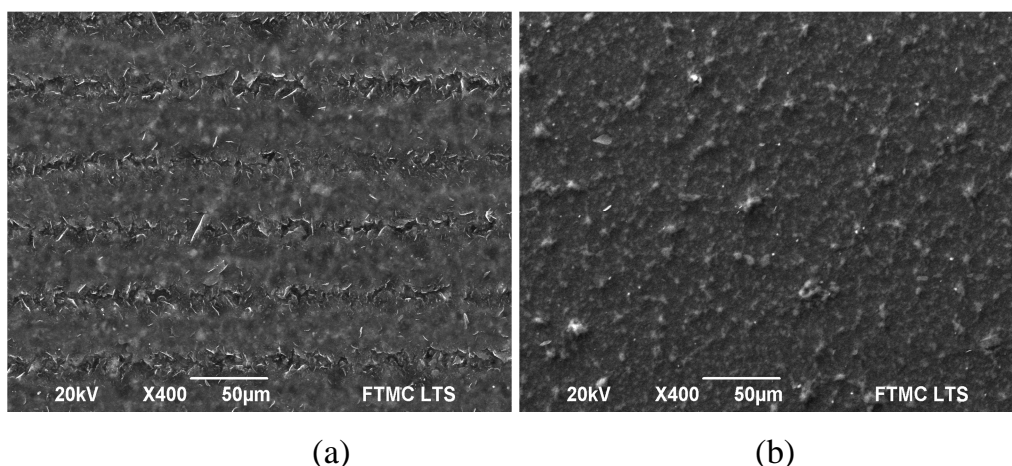


Fig. 42 SEM pictures of the laser-modified GO coating; (a) laser irradiation dose –  $10.06 \text{ J/cm}^2$ , fluence –  $0.16 \text{ J/cm}^2$ ; (b) laser irradiation dose –  $8.18 \text{ J/cm}^2$ , fluence –  $0.02 \text{ J/cm}^2$ .

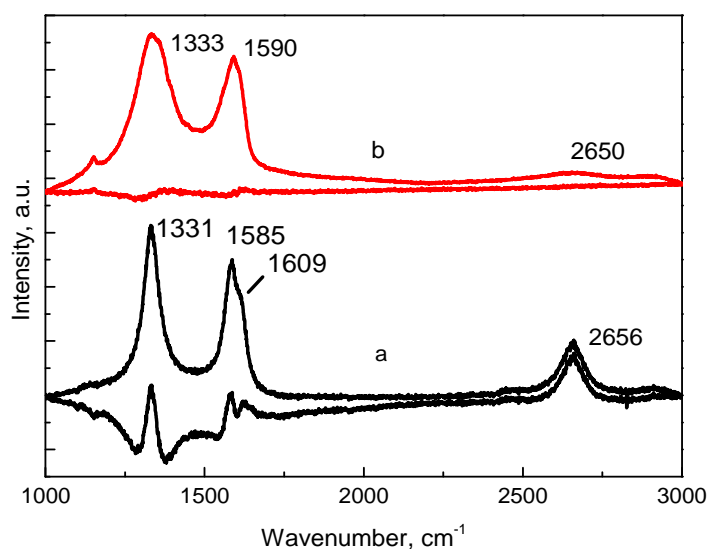


Fig. 43 Raman spectra normalized to the G-peak and differential spectra obtained by extracting the spectrum of the laser untreated GO: (a) laser irradiation dose –  $10.06 \text{ J/cm}^2$ , fluence –  $0.16 \text{ J/cm}^2$ ; (b) laser irradiation dose –  $8.18 \text{ J/cm}^2$ , fluence –  $0.02 \text{ J/cm}^2$ .

From Fig. 39, Fig. 41, Fig. 43, we can see that the use of the low laser fluence ( $0.02\text{--}0.06 \text{ J/cm}^2$ ) did not give any significant change in Raman spectra compared to the spectrum of the laser untreated GO. Differential spectra do not indicate any development of the 2D-band due to the laser treatment. The use of the  $0.09\text{--}0.16 \text{ J/cm}^2$  laser fluence caused a significant increase in the intensity of the 2D-peak, indicating formation of graphene. On

the other hand, a minor rise of the intensity and narrowing of the D-line were also observed (Fig. 41, Fig. 43). It can be explained by structural surface defects, which could be created by evaporating of water molecules and carboxyl, hydroxyl, and epoxide groups [85] from the GO film at high temperatures.

The best GO reduction results in our experiments were obtained when the laser power was 50 mW and the scanning speed was 30 mm/s (laser irradiation dose – 10.06 J/cm<sup>2</sup>, fluence – 0.16 J/cm<sup>2</sup>). Under these conditions, a minimal concentration of structural defects, represented by the low I<sub>D</sub>/I<sub>G</sub> ratio and the relatively largest intensity of the 2D-line, was obtained. Dependence of the D- and G-peak positions and widths determined as the full width at the half maximum (FWHM) on the of the pulse energy and the number of laser pulses per spot (Fig. 44). The experimental curves were fitted by:

$$y = y_0 + A \cdot \exp(R_0 \cdot x) \quad (5)$$

Table 9 Parameters of Eq. (5 for the D-band position (cm<sup>-1</sup>) and FWHM (cm<sup>-1</sup>), the G-band position (cm<sup>-1</sup>) and FWHM (cm<sup>-1</sup>), and the 2D-band FWHM (cm<sup>-1</sup>) dependences on the pulse energy and the irradiation dose product.

Parameter	D-band position	D-band FWHM	G-band position	G-band FWHM	2D-band FWHM
y <sub>0</sub>	1332	52	1585	47	69
A	23	164	9	65	98
R <sub>0</sub>	-0.89	-0.17	-0.25	-0.18	-0.17

Parameter y<sub>0</sub> for the D- and G-band positions can be described as a specific final value of the Raman shift as fitted curves were approaching this value exponentially by increasing the pulse energy and the number of laser pulses per spot product. Moreover, in the analysis of the G-peak position dependence, it was found that the curve was approaching the G-peak position of a monolayer graphene (Fig. 44 c, blue line). In the case of the line widths of the D- and G-peaks and the normalized 2D-band width, the parameter y<sub>0</sub> corresponds to the values which confirm the line widths of the monolayer

graphene. The parameter  $R_0$  shows an exponential rate of decrease for these quantities and A is amplitude of fitted curves.

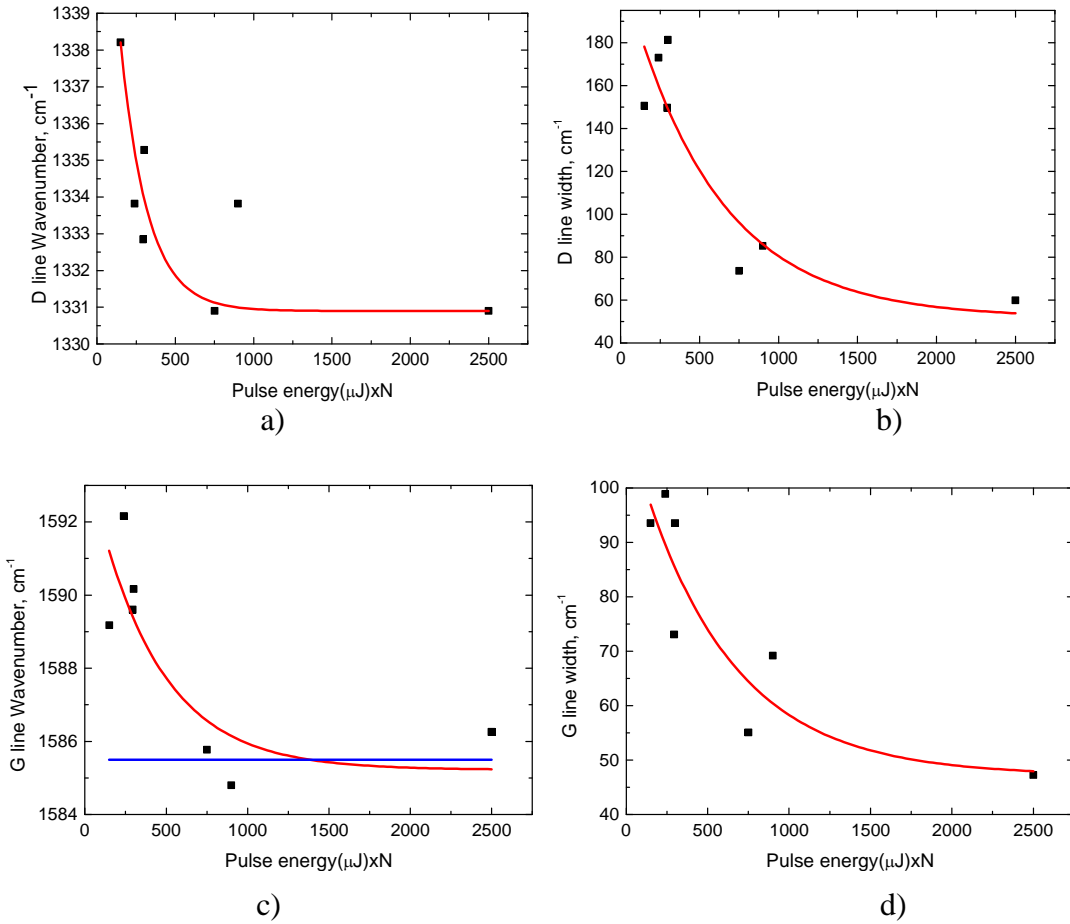


Fig. 44 Dependence of the D-peak position (a) and its FWHM (b), and the G-peak position (c) and its FWHM (d) on the pulse energy and the number of laser pulses per spot product.

By increasing the pulse energy, the D-and G-peaks moved to the shorter wavelengths. At higher pulse energies, the 2D-band intensity tended to grow, which corresponded to formation of a smaller number of graphene layers [110]. Similar behavior of dependence of the Raman peak positions on the number of graphene layers was observed by Rohl et al. [40], where the G- and 2D-peaks moved to shorter wavelengths when the number of graphene layers was decreasing. We found out that in our experiment the figure of merit for the GO reduction to graphene was the position and width of the Raman bands as a function of the product of the pulse energy and the number of laser pulses per spot. Both they determine the temperature in the irradiation zone and the time

how long the material is heated. The influence of the pulse energy is more crucial as reduction appears only from the certain pulse energy value while the irradiation dose is adding the number of laser pulses applied and determines the duration of the reduction process (when material is heated above a certain temperature). The dependence of the G-band position on the pulse energy and the number of laser pulses per spot product exponentially approaches the G-band peak position of the graphene monolayer [110,111] as it is shown in Fig. 44 c. FWHM of the D- and G-peaks tended to decrease as the pulse energy and the irradiation dose were increased. Such behavior corresponds to decreasing disorder in a sample [112,113].

FWHM of the 2D-band was also evaluated (Fig. 45). The dependence of FWHM showed an exponential decline (Eq.5) as the value of the product of the pulse energy and the number of laser pulses per spot increased. Such behavior also corresponds to the decreasing number of the graphene layers, probably due to ablation.

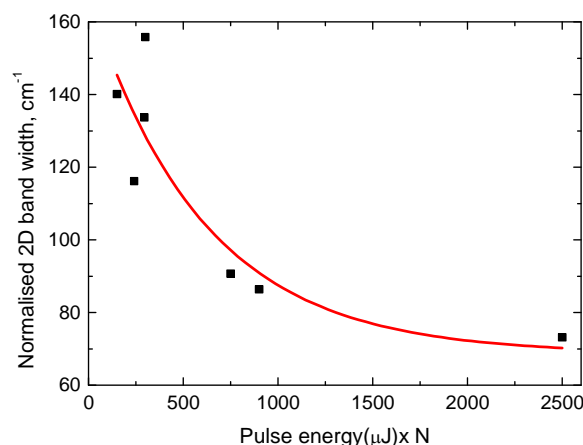


Fig. 45 Dependence of the 2D-peak width (FWHM) on the product of the pulse energy and the number of laser pulses per spot.

### 5.3 MODELING THE TEMPERATURE DYNAMICS DURING THE GO REDUCTION

Simulation of temperature dynamics after laser irradiation was carried out using COMSOL Multiphysics software. Transient temperature distribution in GO films was simulated using the pulsed laser irradiation with the 1064 nm wavelength and the Gaussian temporal beam profile (Fig. 46). The mean laser power (pulse energy) and the pulse overlapping (scanning speed) were varied between simulations.

The heat conduction equation was solved for the thermal simulations using method of finite element analysis. Heat transfer equation was modeled for GO layer with the thickness of 1.2  $\mu\text{m}$ , coated on polycarbonate film with the thickness of 10  $\mu\text{m}$ .

For this model, we used the heat conduction equation (6). All equations were simulated in the cylindrical coordinates system.

$$\rho C_p \frac{\delta T}{\delta t} - \nabla \cdot (k \nabla T) = Q \quad (6)$$

where  $\rho$  is the density of the material,  $C_p$  is the heat capacity and  $k$  is the thermal conductivity,  $Q$  is the heat source, which represents amount of laser energy absorbed by GO. Solution of (6) for  $Q$  is represented by equation (7)

$$Q = \frac{2(1-R)\alpha E_p}{t_p \pi \omega_0^2} \exp(-\alpha z) f_H\left(\frac{t}{t_p}\right) \exp\left(\frac{-2r^2}{\omega_0^2}\right), \quad (7)$$

where  $R$  is the reflectivity of GO film,  $\alpha$  is the linear GO absorption coefficient of,  $E_p$  is the pulse energy;  $t_p$  is the pulse width (at  $1/e^2$  level of intensity),  $\omega_0$  is the beam radius at the focal spot (at  $1/e^2$  level of intensity),  $z$  is the coordinate perpendicular to the surface of sample, the point of the surface is at  $z=0$ .  $f_H(t)$  is the Heaviside step function,  $r$  is transfer coordinate,  $t$  is time.

Boundary conditions for all boundaries were selected as thermal insulating, because of significant difference in thermal conductivity of GO and air. Constants and coefficients used in calculation are represented in Table 10.

Table 10. Constants and coefficients used in calculations of the temperature dynamics during the GO reduction

<b>Constant or coefficient</b>	<b>Symbol</b>	<b>Value</b>
GO density	$\rho$	2260 kg/m <sup>3</sup>
GO heat capacity (at const. pressure)	$C_p$	710 J/kg·K
Pulse energy	$E_p$	0.2 $\mu$ J, 0.3 $\mu$ J and 0.5 $\mu$ J
Beam radius at the focus ( $1/e^2$ )	$\omega_0$	20 $\mu$ m
Pulse width	$t_p$	10 ps
Linear absorption coefficient of GO	$\alpha$	$5.5 \cdot 10^6 \text{ m}^{-1}$ [114]
Thermal conductivity of GO	$k$	28.8 W/m·K [115]
Reflectivity of GO	$R$	0.05 %

Transient temperature distribution was found at different depths positions in GO film from the surface point. The GO absorption coefficient at the 1064 nm wavelength radiation is equal to  $\alpha=5.3 \cdot 10^4 \text{ cm}^{-1}$ , which corresponds to a penetration depth of 189 nm for the laser wavelength. Thus, all the laser radiation was absorbed by linear absorption in the GO layer [114]. The transient temperature distributions were calculated at the central point of the laser pulses for different depths in the GO film. Temperatures through the whole graphene sheet depth are shown in Fig. 46 and Fig. 47.



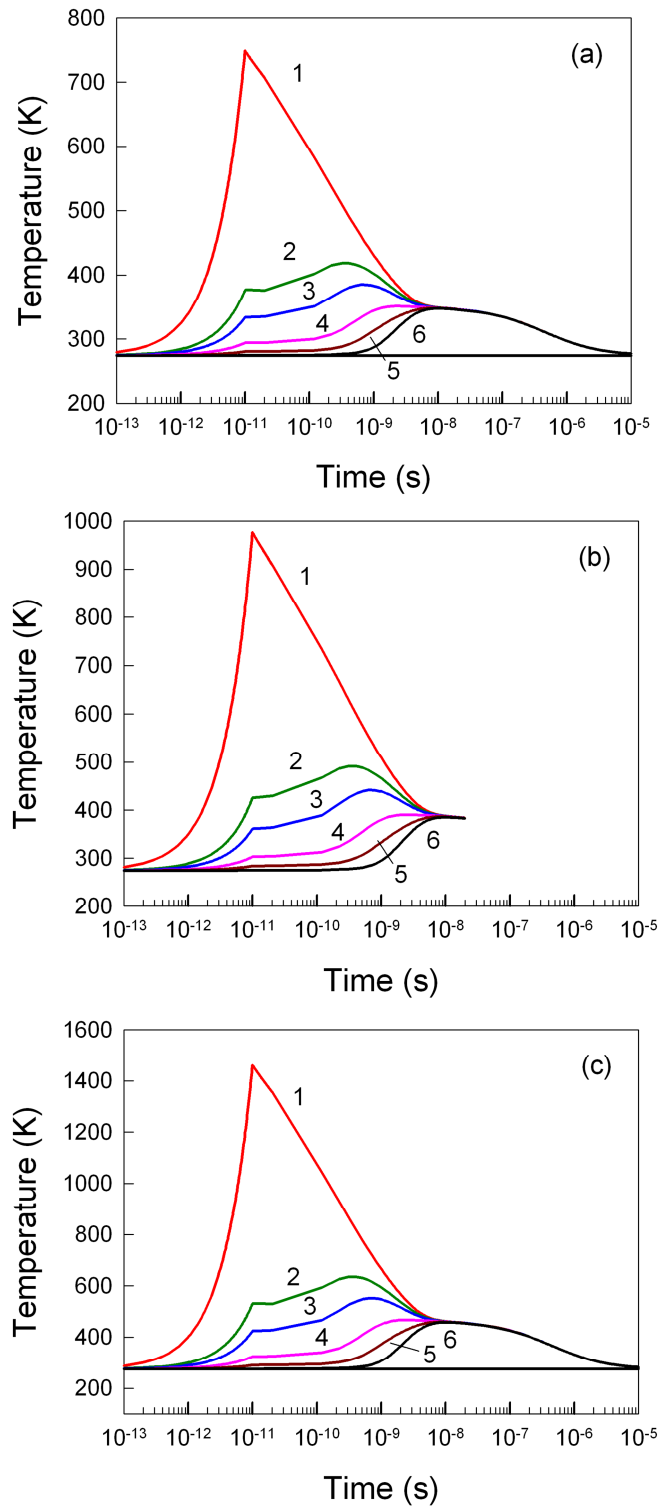


Fig. 46 Temporal temperature distribution after the first laser pulse at different depths inside the GO film: (a)  $0.2 \mu\text{J}$  (20 mW), (b)  $0.3 \mu\text{J}$  (30 mW), and (c)  $0.5 \mu\text{J}$  (50 mW). 1 – GO surface, 2 – 300 nm under the surface, 3 – 500 nm under the surface, 4 – 700 nm under the surface, 5 – 900 nm under the surface, 6 – at the GO and PC substrate boundary (1200 nm).

Absorption of the laser energy induced the temperature increase in the GO film and it decays fast with the depth and time. Based on the thermal simulation results, the time, how long the irradiated GO sample was heated above a certain temperature, was estimated from Fig. 46. Thermal simulation results showed that the surface of GO was heated to 1000°C for a few nanoseconds with a single laser pulse, when the pulse energy exceeded 0.3  $\mu\text{J}$  (30 mW). The heating was necessary for the effective thermal reduction of GO [74,76]. This time of “high temperature” was multiplied by the number of laser pulses per spot, depending on the scanning speed (at constant pulse repetition rate). Results are shown in Fig. 47. It can be considered that it is possible to achieve greater effectiveness of reduction at pulse energy and the number of laser pulses per spot product values of 900 and 2500, while the temperature of GO above 1000°C is kept for a certain time as long as 9 ns and 31 ns, respectively.

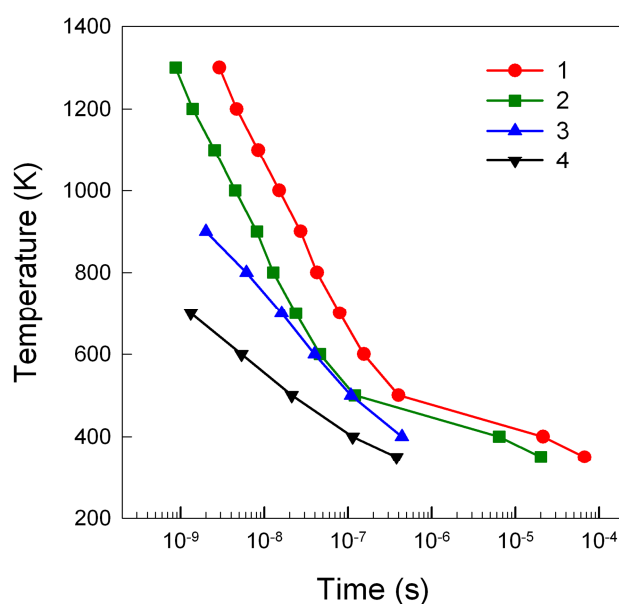


Fig. 47 Dependence of temperature on the accumulated time according to temporal temperature distribution simulations, which determines how long GO was heated with different laser irradiation parameters. Curve parameters specified in Table 11.

Table 11 Values of laser parameters to curves, displayed in Fig. 47.

	Pulse energy x number of laser pulses per spot	Average power, mW	Scanning speed, mm/s
1	2500	50	20
2	900	50	30
3	750	30	30
4	240	50	100

Since the experiment was conducted at the 100 kHz pulse repetition rate, the time interval between two pulses was longer than decay of the graphene temperature. Therefore, the cooling time of the GO sheet was shorter than the interval between pulses.

Under our experimental conditions, the GO surface was heated over 1400 K during the laser treatment. Laser irradiation mainly heated the surface of the GO film where the effective thermal reduction occurred. According to Wei et al. [80], the thermal reduction of GO occurs already at moderate temperatures (100 to 250°C). It is reported that GO reduction takes place in the temperature range from 100 to 1000°C [74,75,79,80,82-84]. According to Huh [85], vaporization of water molecules occurs at 200°C temperature, removal of carboxyl groups at ~200–600°C, removal of residual carboxyl and hydroxyl groups at ~800°C, removal of residual hydroxyl groups, and partial removal of the epoxy group and removal of aromatic C=C bonds at ~1000°C, which corresponds to the 50 mW irradiation power. Moreover, it should be noted that phenol groups stay in GO even after 1000°C treatment [83]. Ablation of graphene flakes is induced at high pulse energies, when temperature exceeds evaporation limit. The precise balance between removal of oxygen-containing groups and preserving the conjugation structure can be reached by control of the temperature conditions in the layer and by using appropriate ambient gases.

## 5.4 CONCLUSIONS

- Quality of GO-CR film reduction with laser irradiation strongly depends on the concentration of the Congo-Red molecules in the composite film.
- Irradiation of the GO films with the picosecond laser at 1064 nm wavelength induced significant changes in the material properties. A decrease in width of the G-, D-, and 2D- Raman bands was observed upon increasing product of the pulse energy and the number of laser pulses per spot, indicating a decrease in disorder of the laser treated film and the number of graphene sheets during the laser treatment.
- Best results of ps-laser reduction of graphite oxide to graphene were achieved by using the 50 mW mean laser power (fluence  $0.16 \text{ J/cm}^2$ , irradiation dose  $10.6 \text{ J/cm}^2$ ). Analysis of temperature dynamics revealed an increase in local temperature up to 1400 K for the GO surface irradiated 1064 nm laser at average power of 50 mW, and up to 600 K for the GO layer 300 nm under the surface. Such thermal effect was sufficient for reduction of GO to graphene.

## 6 GRAPHENE-CHITOSAN COMPOSITE FILM MODIFICATION USING PICOSECOND LASER IRRADIATION

In this section results of laser induced modification of graphene/chitosan-ITO films are presented. During experiments, laser irradiation power was varied and beam scanning speed was constant – 300 mm/s. Modified samples were investigated with SEM and Raman spectroscopy. For the electrochemical investigation of the modified composite films, methods of the Cyclic voltammetry and Electrochemical impedance spectroscopy were applied. These methods The results are published in article A5.

### 6.1 INVESTIGATION OF GRAPHENE-CHITOSAN FILM MORPHOLOGY

Laser irradiation induced the reduction in graphene/chitosan film thickness (Fig. 48). Thickness of the film strongly depended on the applied laser irradiation dose. Simultaneously, the surface morphology changes induced by laser irradiation increased with the increasing irradiation dose.

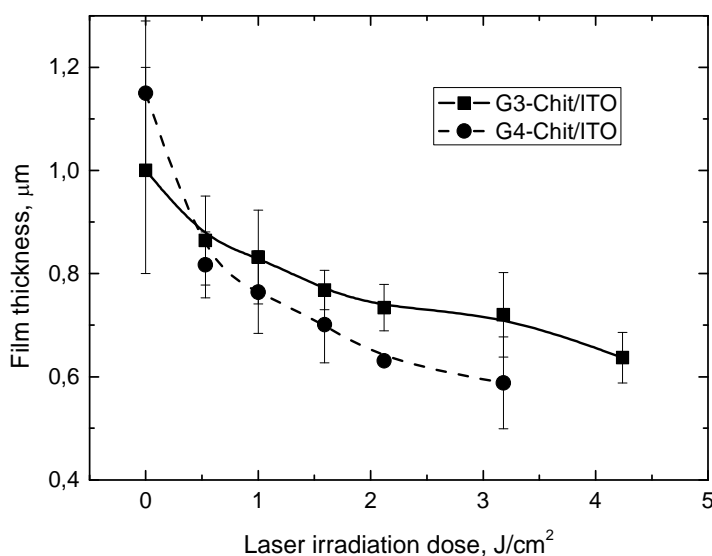


Fig. 48 Dependence of the graphene/chitosan film thickness on the laser irradiation dose.

The laser untreated film was not perfectly flat with clearly visible influence of the graphene concentration in the film, (Fig. 49a,b). Roughness of the film surface increased with the graphene concentration. The laser irradiation caused some changes in the surface morphology of the films. A couple of examples are presented in Fig. 49 c-f, where the increase of roughness of the films caused by the laser irradiation was evident. The higher laser irradiation dose led to the larger roughness of the film (Fig. 49c,e or d, f).

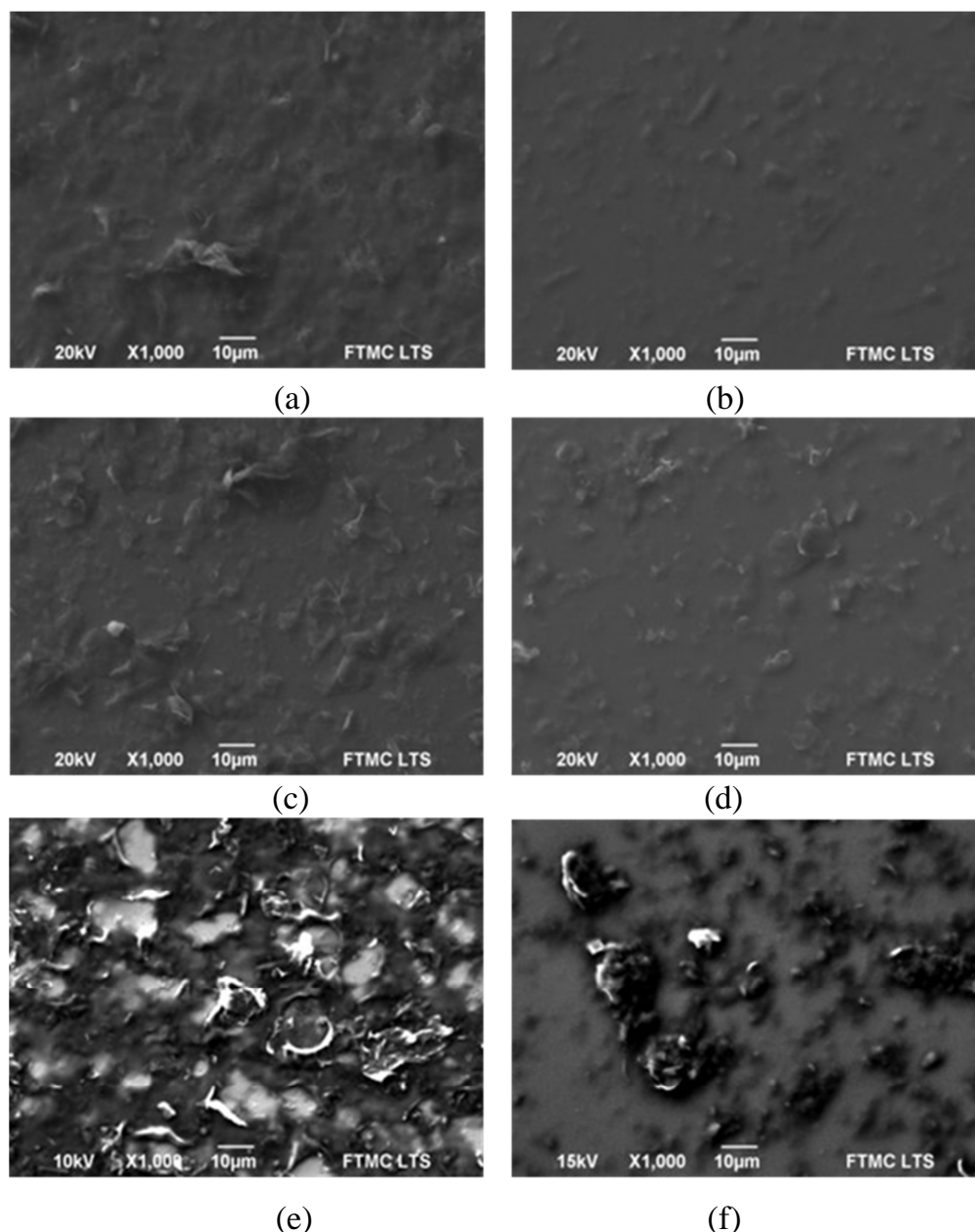


Fig. 49 SEM images of (a,c,e) G4-Chit/ITO and (b,d,f) G3-Chit/ITO take in (a,b) untreated and (c-f) picosecond laser irradiated areas with the laser pulse energy of 0.75  $\mu\text{J}$  (irradiation dose 1.67  $\text{J}/\text{cm}^2$ ) (c,d), and e, f 1.5  $\mu\text{J}$ . (irradiation dose 3.34  $\text{J}/\text{cm}^2$ ), using 300 mm/s scanning speed.

Chitosan was likely ablated by the laser irradiation and graphene flakes were exposed with the increase of the picosecond laser power. Since more graphene edges were opened, the D-band was enhanced in Raman spectra after the laser treatment. In addition, according to the Raman spectra, more edge defects were observed after the laser treatment, which is in good agreement with the SEM morphology images.

## **6.2 RAMAN SPECTROSCOPY MEASUREMENTS ON GRAPHENE - CHITOSAN COMPOSITE FILMS**

The laser treatment effect on the Raman spectra of G4-Chit/ITO and G3-Chit/ITO samples is demonstrated in Fig. 50 and Fig. 52, respectively. Intensity of the G-band decreased after the laser treatment because of the conversion of the initial relatively low-defected graphene structures to disordered forms. For example, the laser treatment with 200 mW (irradiation dose  $4.25 \text{ J/cm}^2$ ) radiation resulted in the decrease of the G-peak intensity by a factor of 0.50 for the sample G3-Chit/ITO (Fig. 52). Raman spectra revealed the development of broad D- and G-features using high average laser power. The width of the D- and G-bands determined as the full width at the half maximum (FWHM) was found to be  $306\text{--}364$  and  $116\text{--}153 \text{ cm}^{-1}$ , respectively. The FWHM of the G-band is a measure of the bond-angle disorder at  $\text{sp}^2$  hybridized carbon structures [116]. For example, the FWHM of around  $180 \text{ cm}^{-1}$  was detected for sputtered amorphous carbon film by using the 633 nm laser excitation line [117]. Thus, appearance of such broad bands evidenced laser treatment induced formation of highly disordered carbon clusters. In the case of sample G4-Chit/ITO (Fig. 50) at relatively low laser power (50 mW), the spectrum revealed development of one broad feature ( $\text{FWHM} = 430 \text{ cm}^{-1}$ ) centered at  $1487 \text{ cm}^{-1}$ . Such spectral shape can be explained by shift of the G-peak to lower wavenumbers. Detailed Raman spectroscopic analysis of amorphous and disordered carbon by using three stage model have revealed softening of the G-peak upon formation of amorphous carbon from

nanocrystalline graphite [116,117]. Similarly, a single broad Raman peak was observed recently upon amorphization of the functionalized graphene sample by treatment with focused ion beams [118]. Considerably lower wavenumber of the G-peak ( $1545\text{ cm}^{-1}$ ) comparing with initial sample ( $1581\text{ cm}^{-1}$ ) was also visible in the case of the treatment by 100 mW laser power (Fig. 50). At higher laser power, the presence of the D- and G-peaks was clearly visible and the  $I_D/I_G$  ratio was indicating formation of highly disordered nanocrystalline graphite (Fig. 51 Fig. 53).

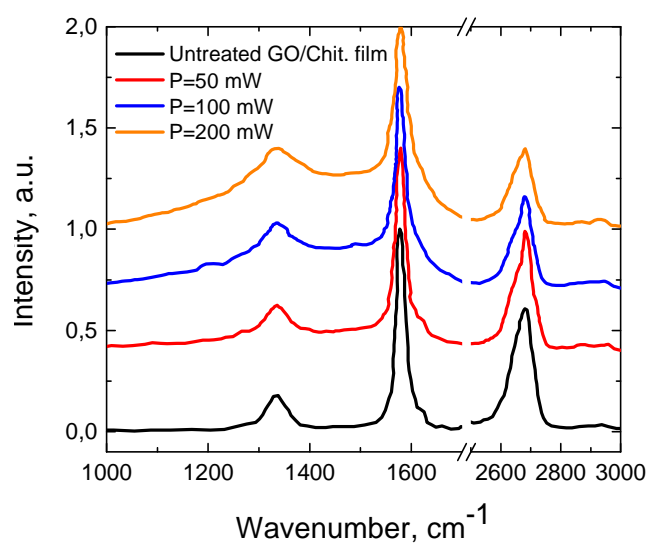


Fig. 50 Raman spectra of G4-Chit/ITO samples at different laser power applied.

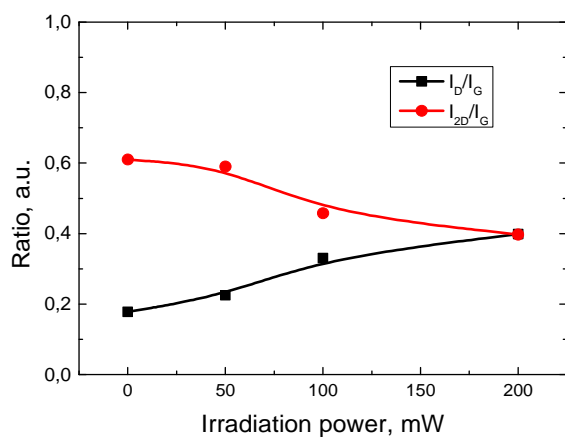


Fig. 51 Dependence of the  $I_D/I_G$  and  $I_{2D}/I_G$  ratios in the G4-Chit/ITO samples at different laser power applied.



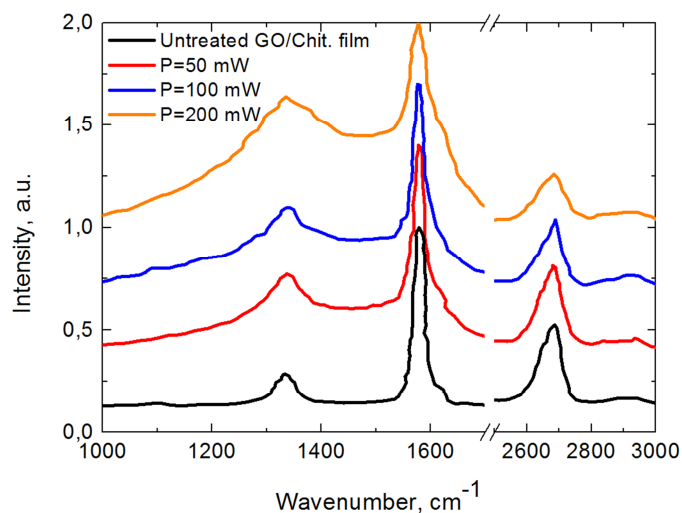


Fig. 52 Raman spectra of the G3-Chit/ITO samples at different laser power applied.

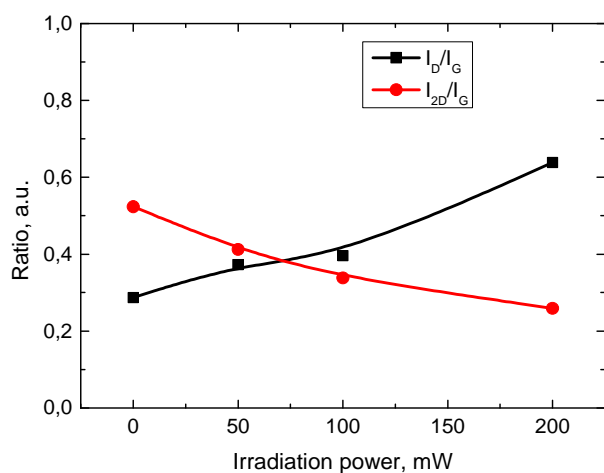


Fig. 53 Dependence of the  $I_D/I_G$  and  $I_{2D}/I_G$  ratios of the G3-Chit/ITO samples at different laser power applied.

Multi-wavelength Raman spectroscopy provides possibility to distinguish the degree of disorder in carbonaceous materials by dispersion analysis of the G-peak [116]. Only in highly disordered carbon, the G-peak shows dispersion which is proportional to the degree of disorder, while, no such dispersion was observed for crystalline graphite, nanocrystalline graphite or glassy carbon [116,119]. Fig. 54 compares the difference Raman spectra measured at four excitation wavelengths in the 900–2000  $\text{cm}^{-1}$  spectral region. Shift of the D-

band towards lower wavenumbers is clearly visible with increase in excitation wavelength; no such shift was detectable for the G-band. Quantitative analysis of the peak positions revealed the D-peak dispersion to be equal to  $\sim 53 \text{ cm}^{-1}/\text{eV}$ . This value is very similar to the dispersion ( $51 \text{ cm}^{-1}/\text{eV}$ ) observed for defected graphite obtained by irradiation with 2 MeV protons at a fluence of  $10^{18} \text{ ions/cm}^2$  [120]. Absence of the G-peak dispersion for the G3-Chit/ITO and G4-Chit/ITO samples indicated that the laser treatment with 200 mW pulsed radiation results in formation of the disordered nanocrystalline graphite, but not amorphous carbon.

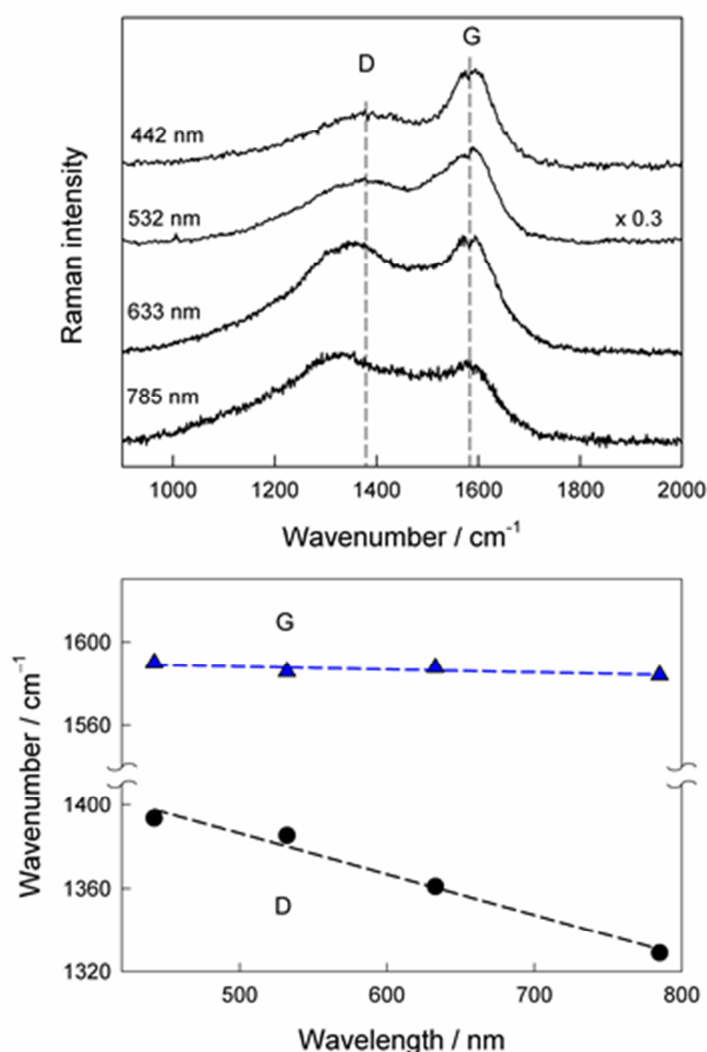


Fig. 54 Difference Raman spectra of G3-Chit/ITO sample measured with 442 nm (2.81 eV), 532 nm (2.33 eV) 633 nm (1.96 eV), and 785 nm (1.58 eV) (upper) and dependence of the peak wavenumbers of the G- and D-bands on the excitation wavelength (bottom). The sample was treated with 200 mW, scanning speed 300 mm/s (irradiation dose  $4.25 \text{ J/cm}^2$ ).

## 6.3 ELECTROCHEMICAL INVESTIGATION OF GRAPHENE-CHITOSAN MODIFIED ITO ELECTRODES

### 6.3.1 CYCLIC VOLTAMMETRY

Fig. 55 presents characteristics of the cyclic voltammetry of the bare and modified ITO recorded in 0.1 M KCl solution. The bare ITO electrode exhibited a reduction wave at ca. -0.8 V in the scan going towards negative potentials and this reduction was also observed at negative potentials in the backwards scan but it was shifted towards less negative potentials. The electrode modification with the G2-Chit film caused a shift of the position of this reduction wave to less negative potential values as seen from the red curve in Fig. 55, which was closer to reduction of carbon-oxy-species than that of ITO, indicating the presence of graphene. After the laser irradiation, the reduction peak decreased significantly indicating the ITO coverage but less carbon-oxy-species, maybe due to reduction of the modified graphene as was found in other works [95,121]. Moreover, in such a way an effective potential window of the electrode was extended.

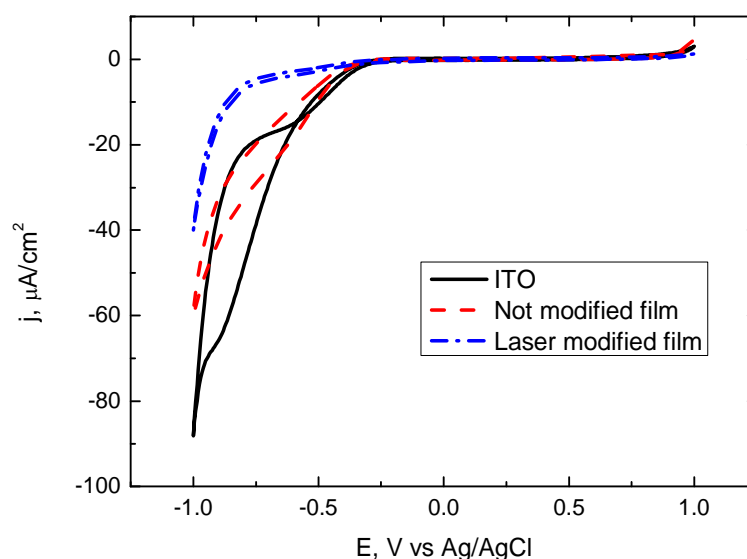


Fig. 55 CVs at ITO, G2-Chit/ITO and laser irradiated G2-Chit/ITO in 0.1 mol/l KCl. Potential scan rate was 100 mV/s, mean power 50 mW.

### 6.3.2 ELECTROCHEMICAL IMPEDANCE SPECTROSCOPY

Electrochemical Impedance Spectroscopy spectra were recorded at differently modified electrodes: bare ITO, G1-Chit/ITO, G2-Chit/ITO, G3-Chit/ITO, G4-Chit/ITO, and the same electrodes irradiated with picosecond-laser using various potentials over the whole potential range used in the CV investigation: -0.75; -0.50; 0.00; 0.50; 0.75; 1.00 V. Graphene load was varied from 0 to 3 mg/ml.

Fig. 56 presents the complex-plane impedance spectra at various potentials measured with differently modified electrodes before and after laser irradiation. The charge separation was dominating in the double-layer region at 0 V as Complex plane EIS spectra have linear shape (Fig. 56a) and all spectra of differently modified electrodes were similar. In all cases, the impedance values rose after the laser irradiation, especially clearly visible at low graphene loads.

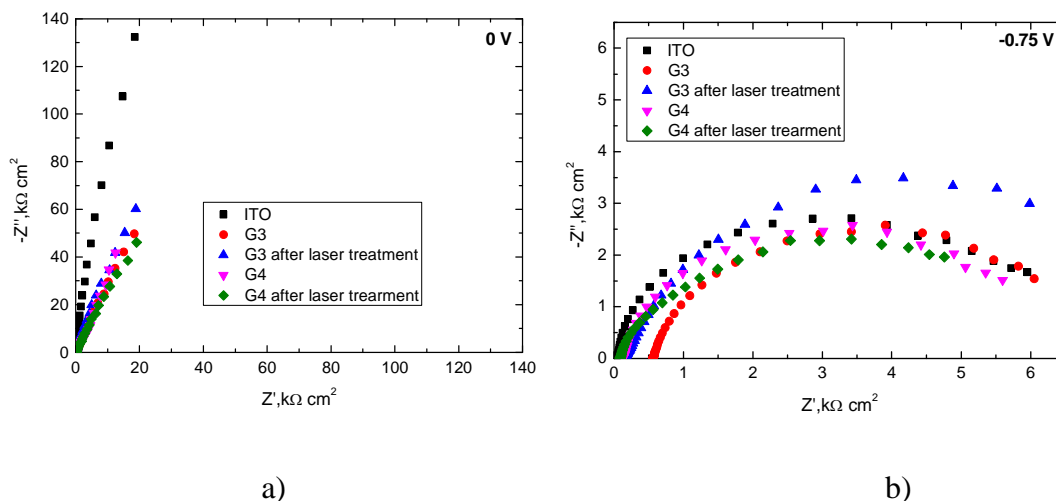


Fig. 56 Complex plane EIS spectra at ITO, untreated G-Chit/ITO, laser-treated G-Chit/ITO with different graphene load at different potentials in 0.1 M KCl. Laser irradiation dose 1 J/cm $^2$ .

As expected, the spectra showed more resistive behavior of the electrode in negative potential region, where reduction of ITO or graphene-oxy-species occurred. G3-Chit/ITO and G4-Chit/ITO had rather similar shape of the spectra to ITO containing semicircle meaning that a charge transfer is important at this potential, i.e. the electrochemical reaction occurs. In this case,

the semicircle appears due to reduction of superficial oxy-species. However, no clear semicircles were found at low graphene loads due to significantly lower concentration of oxy-species. At -0.75 V, the reduction of the oxy-species continued, and in all cases, clear semicircles were obtained. Also in the negative potential region, the impedance values increased after the laser treatment due to partial reduction of modified graphene during laser irradiation. The highest values were observed when graphene load was 1  $\mu\text{g/ml}$ . Probably, this film composition had an optimal components ratio and the modified graphene reduction was fastest under these conditions, while at the lower concentration, chitosan slowed down this process and at higher graphene loads less oxy-species was reduced during the laser irradiation.

The spectra were analyzed fitting to an electrical equivalent circuit (Fig. 57, Fig. 58). Almost all spectra except the double-layer region were analyzed, as usual for graphene modified electrodes, applying a modified Randles' equivalent circuit consisting on the cell resistance,  $R_{\Omega}$ , in series with the parallel combination of the constant phase element, CPE, and the charge transfer resistance,  $R_{ct}$ , and the open Warburg element,  $W_o$ , as a specific electrochemical element describing diffusion. CPE was modelled as non-ideal capacitor:

$$\text{CPE} = -1/(C_{dl}i\omega)^{\alpha}, \quad (8)$$

where  $C_{dl}$  means the double-layer capacitance;  $\omega$  is frequency; and the  $\alpha$  exponent shows the surface roughness.

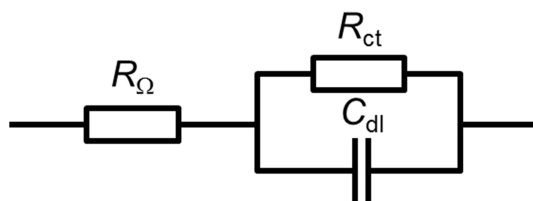


Fig. 57 Schematic diagram of Randles' equivalent circuit for double layer capacitance evaluation.

The spectra at the double-layer region were analyzed using all elements in series:  $-R_{\Omega}-CPE_{dl}-W_o-$  [40].

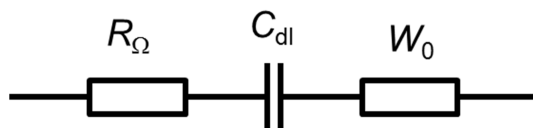


Fig. 58 Schematic diagram of Warburg equivalent circuit for double layer capacitance evaluation.

The capacitance  $C_{dl}$  of the double layer region increased also with the electrode modification and, especially, after the laser treatment. However, it slightly decreased after ITO modification with G-Chit film, depending on the electrode. This increase also depended on graphene load, as seen from Fig. 59. Capacitance increased with the increase in graphene load, and a significant increase in capacitance was observed after the laser treatment at different potentials (Fig. 59). Comparing capacitance changes at the same graphene load depending on different laser irradiation doses applied during irradiation, almost linear behavior was obtained (Fig. 60). This fact suggests that the laser treatment improves electrochemical properties of the G-Chit modified electrode due to creation the edge defects and formation of nanocrystalline structures from graphene flakes after laser.

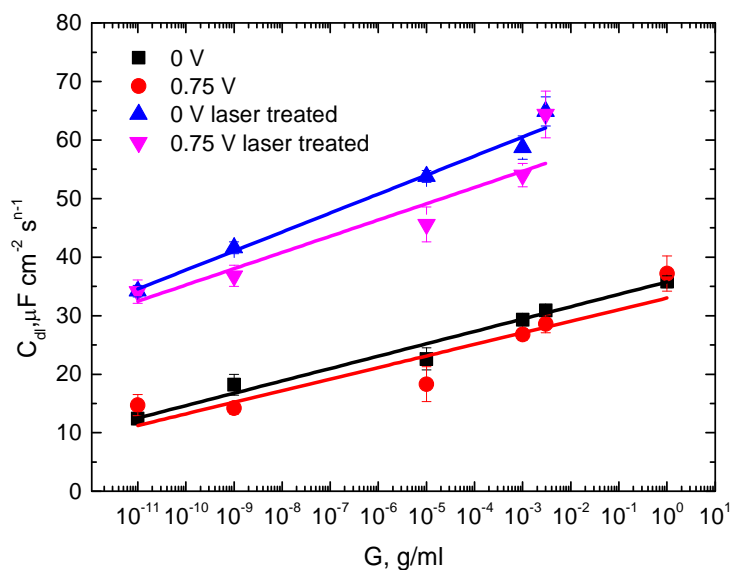


Fig. 59 Dependence of capacitance calculated from EIS data on graphene load, at 0 V and 0.75 V.

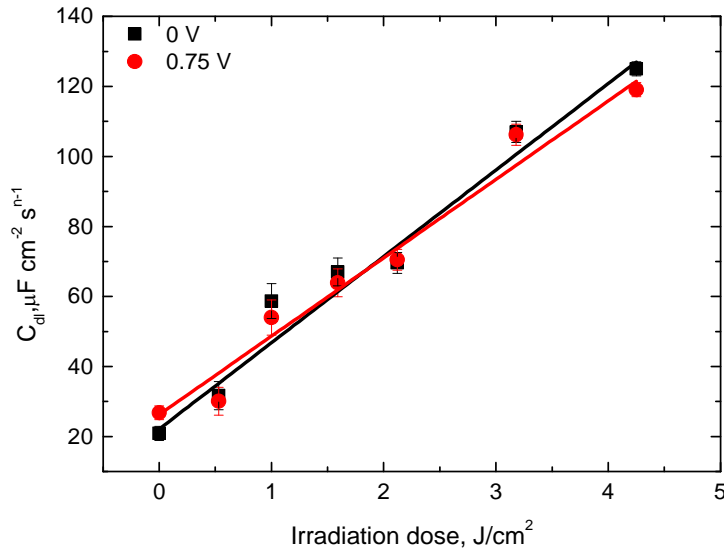


Fig. 60 Dependence of the capacitance calculated from EIS data at 0 V and 0.75 V on the laser irradiation dose in G3-Chit/ITO sample.

The data obtained are in a good agreement with the known fact that the laser interaction with carbon nanomaterial composite leads to cleaning of materials, morphological changes and removal of material at higher laser power density [122] and [16]. Efficiency of the laser processing strongly depends on the laser irradiation parameters such as the fluence and pulse overlap (irradiation dose) as has been found in [123,124].

#### 6.4 UNIFORM MODIFICATION OF GRAPHENE-CHITOSAN FILM

Uniform modification of graphene/chitosan film was implemented by picking such values of beam scanning speed and hatch, that pulse overlap would be homogeneous in scanning direction and in perpendicular direction. For such overlapping type the pitch parameter was introduced. It describes the distance between sequent pulses. The above described configuration of laser parameters allows minimization of process variables as variation of the pitch includes variation in scanning speed and hatch simultaneously. Therefore only laser power and pitch were changed during these experiments. Experiments were performed with 1064 nm and 532 nm irradiation of picosecond laser at constant pulse repetition rate of 100 kHz.

No significant changes in film morphology were observed at irradiation powers beneath 50 mW for both laser wavelengths. At laser power of 300 mW and higher, ablation of film took place. Significant changes in Raman spectra were observed at the 100 mW irradiation power using 1064 nm wavelength (Fig. 61, Fig. 62). When higher laser power was applied, Raman spectra corresponded to amorphous carbon spectra.

Increase of the D- and G-bandwidth was observed after the laser treatment. Such conditions correspond to increasing disorder. Meanwhile 2D-band intensity decreased. The  $I_D/I_G$  and  $I_{2D}/I_G$  ratios were evaluated to clarify defectiveness of the graphene-chitosan after the laser treatment (Fig. 62). The intensity of the 2D-band, corresponding to graphene phase was gradually rising as the pulse overlap decreased (pitch parameter increased). Opposite behavior was observed in the D-band intensity meaning the decrease of number of defects in irradiated film. Thus the defectiveness level can be controlled in fine manner with the picosecond laser irradiation using 100 mW mean power at 1064 nm wavelength.

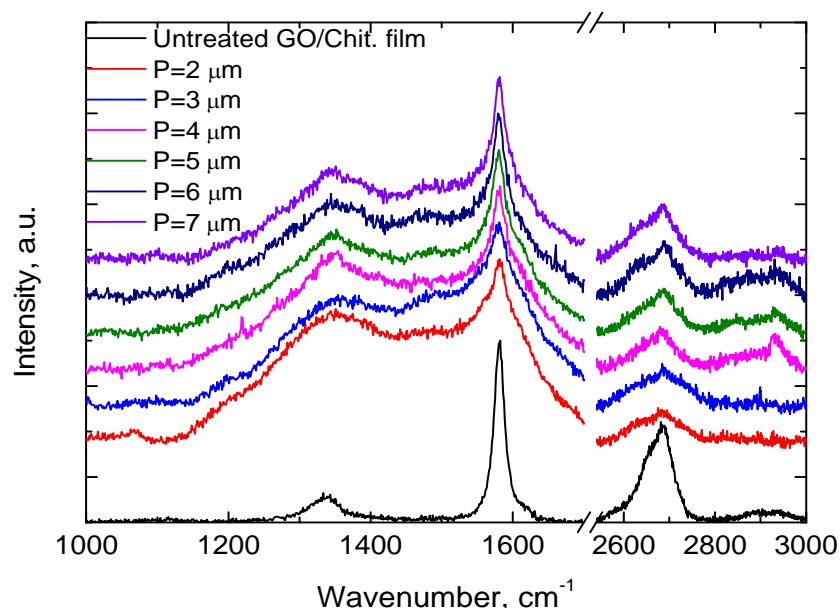


Fig. 61 Raman spectra dependence on the pitch parameter applying the 100 mW 1064 nm picosecond laser irradiation.



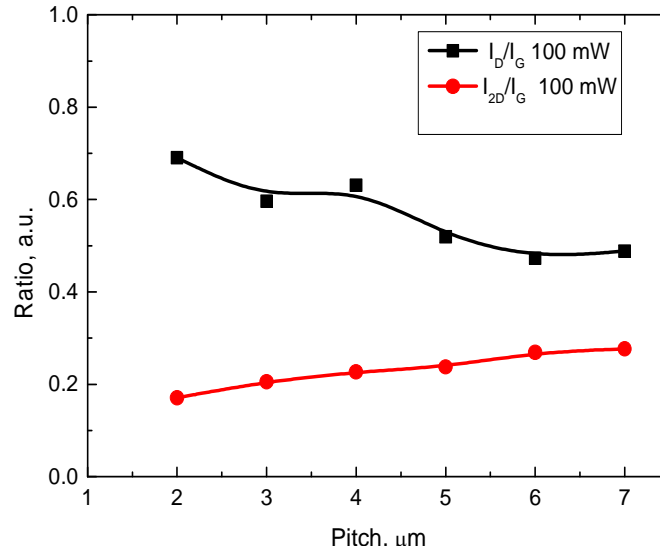


Fig. 62 Dependence of the  $I_D/I_G$  and  $I_{2D}/I_G$  ratios on the pitch applying 100 mW, 1064 nm picosecond laser irradiation.

Results differed in the case of 532 nm irradiation (Fig. 63, Fig. 64). Similar to 1064 nm irradiation, the broadening of the D- and G-bands was observed at the high pulse overlap conditions using the 100 mW average power. Yet the change of the D- and 2D-band intensities is not as regular as with 1064 nm irradiation (Fig. 64). The  $I_{2D}/I_G$  ratio decreased at the pitch of 3 μm, but then it increased more rapidly than after 1064 nm treatment. The value of  $I_{2D}/I_G$  ratio was twice higher at 6 μm and 7 μm pitch compared to 1064 nm. On the other hand, the  $I_D/I_G$  ratio dependence was more irregular using 532 nm irradiation.

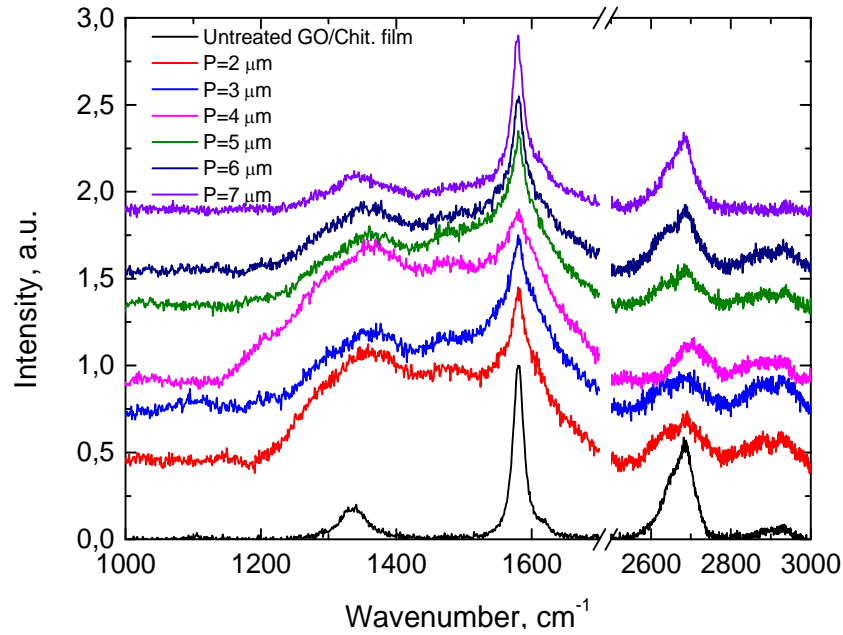


Fig. 63 Raman spectra dependence on the pitch parameter applying the 100 mW, 532 nm picosecond laser irradiation.

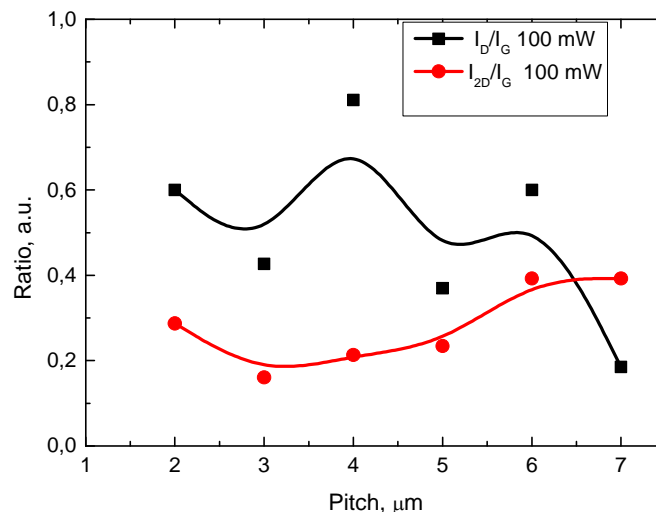


Fig. 64 Dependence of the  $I_D/I_G$  and  $I_{2D}/I_G$  ratios on the pitch parameter applying 100 mW, 532 nm picosecond laser irradiation.

At the mean laser power lower than 100 mW, no changes in the spectra were observed after the 1064 nm laser treatment while after the 532 nm treatment, the spectra differed from untreated graphene-chitosan film. Due to lower modification, the 2D-band intensity was higher than for the 100 mW modification, and fewer defects were present (Fig. 66). Dependence of the  $I_D/I_G$  and  $I_{2D}/I_G$  ratio on the pitch parameter was not as strong as with 100 mW irradiation.

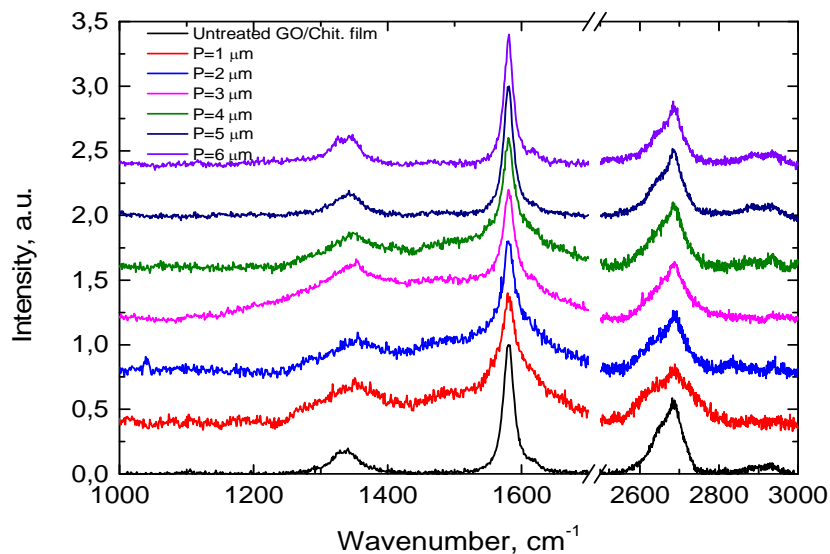


Fig. 65 Raman spectra dependence on the pitch parameter applying the 50 mW, 1064 nm picosecond laser irradiation.

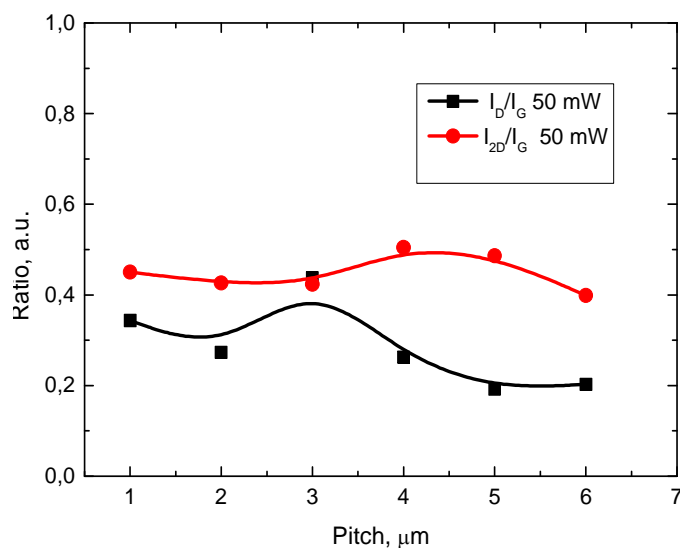


Fig. 66 Dependence of the  $I_D/I_G$  and  $I_{2D}/I_G$  ratios on the pitch parameter applying the 50 mW, 532 nm picosecond laser irradiation.

Morphology of the laser treated film area exhibited distinct differences depending on the laser irradiation wavelength. SEM images of 2 μm and 5 μm pitch were chosen to compare surface modifications. At the same irradiation power of 100 mW and 2 μm pitch, forming of porous structure was observed

Fig. 67). After the 532 nm irradiation treatments, density of the pores was much higher than that after the 1064 nm treatment. The border between the

laser treated and untreated zone was sharper after the 523 nm irradiation (Fig. 68). In case of 1064 nm irradiation, the treated zone had smoother surface than untreated film despite the forming of porous structure.

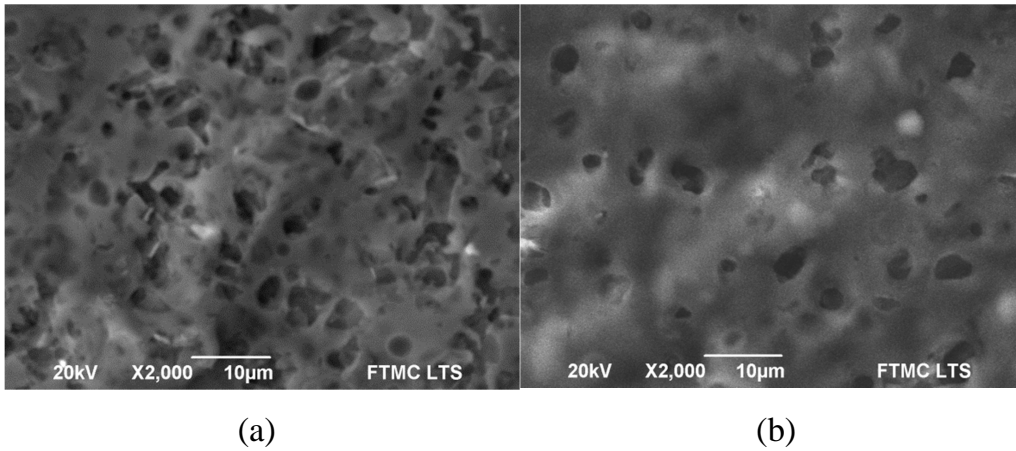


Fig. 67 SEM image of the laser treated graphene-chitosan film. Laser parameters: 100 mW, pitch-2 µm: a) 532 nm; b) 1064 nm.

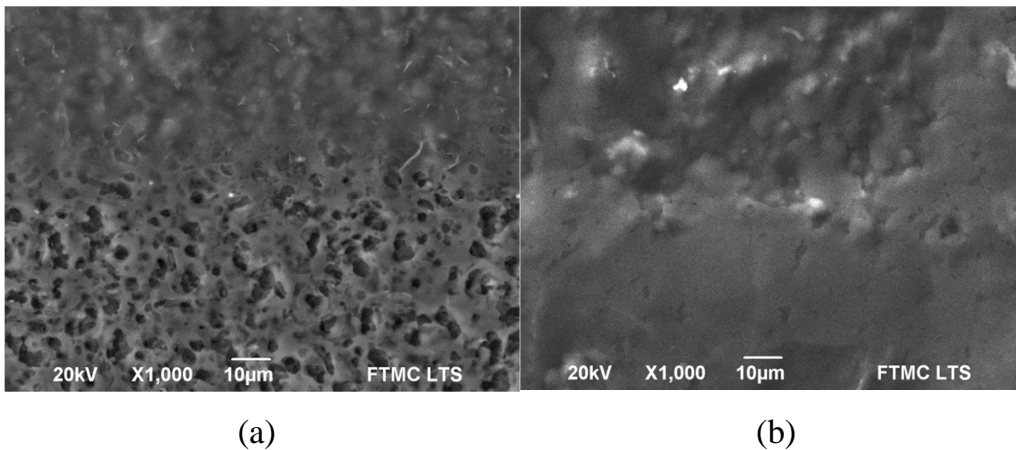


Fig. 68 SEM image of a border between the laser-treated graphene-chitosan film and untreated film. Laser parameters: 100 mW, pitch-2 µm: a) 532 nm; b) 1064 nm.

Using the same laser power but lower pulse overlap (the pitch was equal to 5µm), the morphology changes were also observed (Fig. 69, Fig. 70). Size of pores increased, but their density decreased after the 523 nm irradiation (Fig. 69). The number of pores also decreased after the 1064 m irradiation, also the border between treated and untreated zones became less intense in both cases.

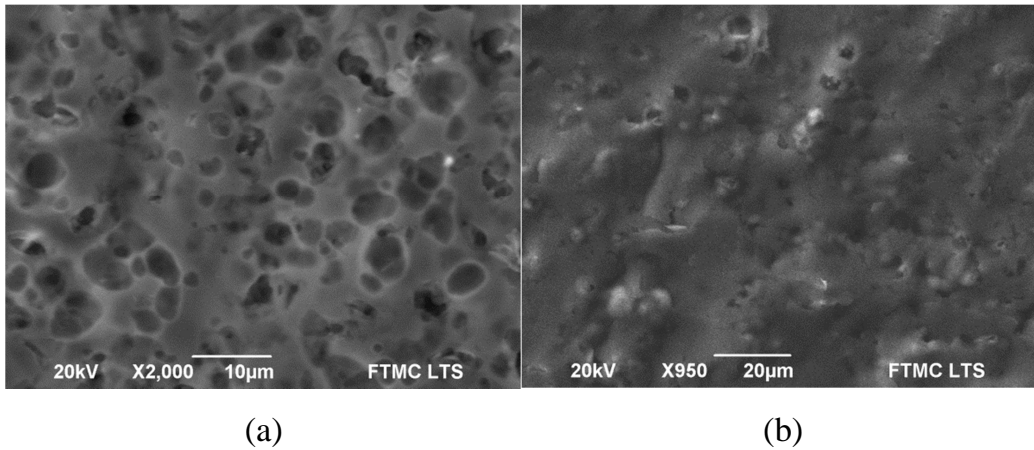


Fig. 69 SEM image of the laser treated graphene-chitosan film. Laser parameters: 100 mW, pitch-5  $\mu\text{m}$ : a) 532 nm; b) 1064 nm.

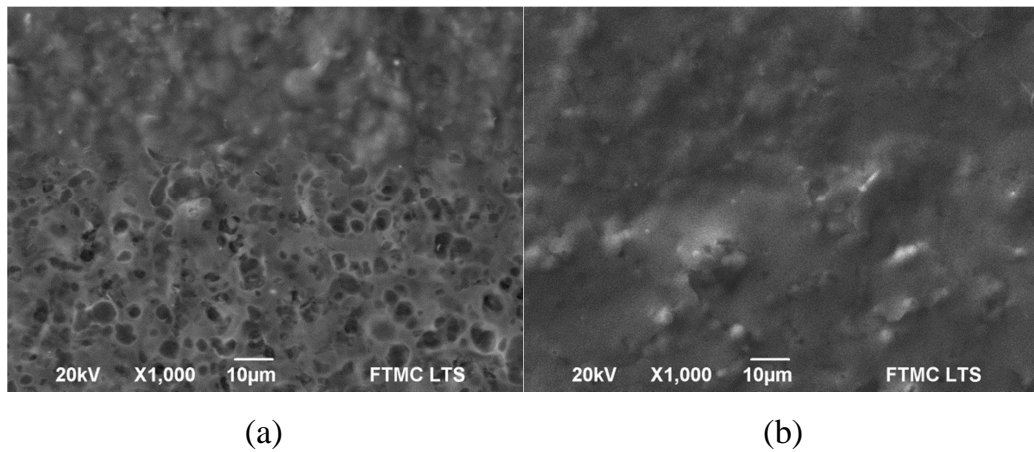


Fig. 70 SEM image of a border between the laser-treated graphene-chitosan film and untreated film. Laser parameters: 100 mW, pitch-5  $\mu\text{m}$ : a) 532 nm; b) 1064 nm.

More significant changes of the surface morphology between 2  $\mu\text{m}$  and 5  $\mu\text{m}$  pitch are visible after 1064 nm treatment. It corresponds to more gradual change of the  $I_D/I_G$  and  $I_{2D}/I_G$  ratios depending on the pulse overlap (Fig. 62). The size and density of pores determine the structural defects of graphene-chitosan film. On the other hand, porous structure indicates an increase of the surface area, which is very helpful feature in sensing applications.

## 6.5 CONCLUSIONS

- The Raman spectroscopy showed that laser irradiation can cut out graphene sheets in graphene-chitosan composites into smaller pieces inducing more edge defects and the higher graphene load – the larger amount of side defects appeared after laser treatment. The high laser irradiation dose resulted in the nanocrystalline graphene formation and significant reduction in thickness of the graphene-chitosan film.
- Picosecond laser irradiation caused an increase in capacitance at the electrode surface due to formation of graphene nanocrystals. Electrochemical investigation of the laser treated G-Chit/ITO samples proved that such composite electrodes are promising material to use as a substrate to sensor development.
- Uniform modification of graphene-chitosan composites allowed gradual controlling of defectiveness level in films using lower average powers of laser irradiation.

## LIST OF CONCLUSIONS

- Electrical resistivity of the 1200 nm-thick GO films irradiated with the picosecond laser at the wavelength of 1064 nm decreased in a certain range of the laser processing parameters and the 2D-line appeared in Raman spectra of the same samples after the laser treatment in ambient air indicating formation of the graphene phase.
- Reduction of graphite oxide to graphene with laser irradiation allows forming the heat conductive channels which, according to the theoretical estimations are more effective than metallic heat conductive systems at short (<10 mm) distances.
- The higher quality of GO reduction to graphene was achieved by conducting laser irradiation experiments in nitrogen and argon atmosphere compared to air ambient, as the  $I_{2D}/I_D$  ratio in Raman spectra increase to 0.5 in the laser modified samples.
- Quality of GO-CR film reduction with laser irradiation strongly depended on the concentration of the Congo-Red molecules in the composite film.
- Irradiation of the GO films with the picosecond laser at 1064 nm wavelength induced significant changes in the material properties. A decrease in width of the G-, D-, and 2D- Raman bands was observed upon increasing (pulse energy and the number of laser pulses per spot) indicating a decrease in disorder of the laser treated film and the number of graphene sheets during the laser treatment.
- Best results of ps-laser reduction of graphite oxide to graphene were achieved by using the 50 mW mean laser power (fluence  $0.16 \text{ J/cm}^2$ , irradiation dose  $10.6 \text{ J/cm}^2$ ). Analysis of temperature dynamics revealed an increase in local temperature up to 1400 K for 1064 nm (50 mW) irradiated the GO surface, and up to 600 K for the GO layer 300 nm under the surface. Such a thermal effect is sufficient for reduction of GO to graphene.

- The Raman spectroscopy showed that laser irradiation can cut out graphene sheets in graphene-chitosan composites into smaller pieces inducing more edge defects and the higher graphene load – the larger amount of side defects after laser treatment. High laser irradiation dose resulted to nanocrystalline graphene formation and significant thinning of the graphene-chitosan film.
- Picosecond laser irradiation caused an increase in capacitance at the electrode surface due to formation of nanocrystals of graphene. Electrochemical investigation of laser treated G-Chit/ITO samples proved that such composite electrodes are promising material to use as a substrate to sensor development.
- Uniform modification of graphene-chitosan composites allowed gradual controlling of defectiveness level in films using lower average powers of laser irradiation.



## SUMMARY

In this thesis research results on application of laser irradiation for forming and modification of graphene layers are presented.

Graphite oxide films on polycarbonate substrate were prepared using Hummers-Offeman method. Composition of films differed by thickness, additives and their concentration. Picosecond laser irradiation was applied to form heat conductive graphene channels. Laser power, beam scanning speed and atmosphere gases was varied during the experiments.

Raman spectroscopy was applied for graphene identification. Spectroscopy measurements showed that reduction level of GO to graphene depends on various factors: applied optical power, scanning speed, concentration of GO additives (Congo Red) and ambient atmosphere.

Forming of heat conductive channels was also confirmed by drop of resistance in treated films and thermo-vision measurements.

Temperature dynamics of GO film after picosecond laser pulse was modeled. The results of modelling together with Raman spectroscopy measurements confirmed that optimal laser power for GO reduction is 50 mW at 100 kHz pulse repetition rate.

Graphene/chitosan composite film on ITO contact was modified with picosecond laser irradiation. Raman spectroscopy showed, that laser treatment increase the disorder in composite film. EIS spectra measurements confirmed that rise of capacitance occurs in samples after laser treatment. The capacitance of modified electrodes is proportional to average power of applied laser irradiation.

## REFERENCES

- [1] Novoselov K. S., A. K. Geim, S. V. Morozov, D. Jiang, Y. Zhang, S. V. Dubonos, I. V. Grigorieva & A. A. Firsov. Electric Field Effect in Atomically Thin Carbon Films. *Science* **306** (2004) 666-9
- [2] Castro Neto A. H., F. Guinea, N. M. R. Peres, K. S. Novoselov & A. K. Geim. The electronic properties of graphene. *Reviews of Modern Physics* **81** (2009) 109-62
- [3] Pop E., V. Varshney & A. K. Roy. Thermal properties of graphene: Fundamentals and applications. *MRS Bulletin* **37** (2012) 1273-81
- [4] Falkovsky L. A. Optical properties of graphene. *JPCS* **129** (2008) 012004
- [5] Lee C., X. Wei, J. W. Kysar & J. Hone. Measurement of the Elastic Properties and Intrinsic Strength of Monolayer Graphene. *Science* **321** (2008) 385-8
- [6] Schwierz F. Graphene transistors. *Nat Nano* **5** (2010) 487-96
- [7] Zhan B., C. Li, J. Yang, G. Jenkins, W. Huang & X. Dong. Graphene Field-Effect Transistor and Its Application for Electronic Sensing. *Small* **10** (2014) 4042-65
- [8] Kim K. S., Y. Zhao, H. Jang, S. Y. Lee, J. M. Kim, K. S. Kim, J.-H. Ahn, P. Kim, J.-Y. Choi & B. H. Hong. Large-scale pattern growth of graphene films for stretchable transparent electrodes. *Nature* **457** (2009) 706-10
- [9] Nayak T. R., H. Andersen, V. S. Makam, C. Khaw, S. Bae, X. Xu, P.-L. R. Ee, J.-H. Ahn, B. H. Hong, G. Pastorin & B. Özyilmaz. Graphene for Controlled and Accelerated Osteogenic Differentiation of Human Mesenchymal Stem Cells. *ACS Nano* **5** (2011) 4670-8
- [10] Reina A., X. Jia, J. Ho, D. Nezich, H. Son, V. Bulovic, M. S. Dresselhaus & J. Kong. Large Area, Few-Layer Graphene Films on Arbitrary Substrates by Chemical Vapor Deposition. *Nano Lett.* **9** (2008) 30-5

- [11] Pei S.H.-M. Cheng. The reduction of graphene oxide. *Carbon* **50** (2012) 3210-28
- [12] El-Kady M. F., V. Strong, S. Dubin & R. B. Kaner. Laser Scribing of High-Performance and Flexible Graphene-Based Electrochemical Capacitors. *Science* **335** (2012) 1326-30
- [13] Strong V., S. Dubin, M. F. El-Kady, A. Lech, Y. Wang, B. H. Weiller & R. B. Kaner. Patterning and Electronic Tuning of Laser Scribed Graphene for Flexible All-Carbon Devices. *ACS Nano* **6** (2012) 1395-403
- [14] Bae S., H. Kim, Y. Lee, X. Xu, J.-S. Park, Y. Zheng, J. Balakrishnan, T. Lei, H. Ri Kim, Y. I. Song, Y.-J. Kim, K. S. Kim, B. Ozyilmaz, J.-H. Ahn, B. H. Hong & S. Iijima. Roll-to-roll production of 30-inch graphene films for transparent electrodes. *Nat Nano* **5** (2010) 574-8
- [15] Berger C., Z. Song, T. Li, X. Li, A. Y. Ogbazghi, R. Feng, Z. Dai, A. N. Marchenkov, E. H. Conrad, P. N. First & W. A. de Heer. Ultrathin Epitaxial Graphite: 2D Electron Gas Properties and a Route toward Graphene-based Nanoelectronics. *The Journal of Physical Chemistry B* **108** (2004) 19912-6
- [16] Celiešiūtė R., G. Grincienė, Š. Vaitekoniš, T. Venckus, T. Rakickas & R. Pauliukaitė. Application of carbon electrodes modified with graphene and chitosan to electrochemical sensing of ascorbate. *Chemija* **24** (2013) 296-306
- [17] Guo H.-L., X.-F. Wang, Q.-Y. Qian, F.-B. Wang & X.-H. Xia. A Green Approach to the Synthesis of Graphene Nanosheets. *ACS Nano* **3** (2009) 2653-9
- [18] Hong J.-Y.J. Jang. Micropatterning of graphene sheets: recent advances in techniques and applications. *Journal of Materials Chemistry* **22** (2012) 8179-91
- [19] Joh H.-I., S. Lee, T.-W. Kim, S. Y. Hwang & J. R. Hahn. Synthesis and properties of an atomically thin carbon nanosheet similar to graphene

- and its promising use as an organic thin film transistor. *Carbon* **55** (2013) 299-304
- [20] Kumar A., A. L. M. Reddy, A. Mukherjee, M. Dubey, X. Zhan, N. Singh, L. Ci, W. E. Billups, J. Nagurny, G. Mital & P. M. Ajayan. Direct Synthesis of Lithium-Intercalated Graphene for Electrochemical Energy Storage Application. *ACS Nano* **5** (2011) 4345-9
- [21] Zhi-Bo L. et al. Direct patterning on reduced graphene oxide nanosheets using femtosecond laser pulses. *Journal of Optics* **13** (2011) 085601
- [22] Zhu Y., Z. Sun, Z. Yan, Z. Jin & J. M. Tour. Rational Design of Hybrid Graphene Films for High-Performance Transparent Electrodes. *ACS Nano* **5** (2011) 6472-9
- [23] Geim A. K.K. S. Novoselov. The rise of graphene. *Nat Mater* **6** (2007) 183-91
- [24] Zhang Y., T.-T. Tang, C. Girit, Z. Hao, M. C. Martin, A. Zettl, M. F. Crommie, Y. R. Shen & F. Wang. Direct observation of a widely tunable bandgap in bilayer graphene. *Nature* **459** (2009) 820-3
- [25] Lui C. H., Z. Li, K. F. Mak, E. Cappelluti & T. F. Heinz. Observation of an electrically tunable band gap in trilayer graphene. *Nat Phys* **7** (2011) 944-7
- [26] Son Y.-W., M. Cohen & S. Louie. Energy Gaps in Graphene Nanoribbons. *Physical Review Letters* **97** (2006) 216803
- [27] Yang L., C.-H. Park, Y.-W. Son, M. Cohen & S. Louie. Quasiparticle Energies and Band Gaps in Graphene Nanoribbons. *Physical Review Letters* **99** (2007) 186801
- [28] Chen Z., Y.-M. Lin, M. J. Rooks & P. Avouris. Graphene nano-ribbon electronics. *Physica E: Low-dimensional Systems and Nanostructures* **40** (2007) 228-32
- [29] Kan E., Z. Li & J. Yang. Nanotechnology and Nanomaterials, Physics and Applications of Graphene - Theory (InTech, 2011), 331-48.

- [30] Wu J., H. A. Becerril, Z. Bao, Z. Liu, Y. Chen & P. Peumans. Organic solar cells with solution-processed graphene transparent electrodes. *Appl. Phys. Lett.* **92** (2008) 263302
- [31] Zhu Y., S. Murali, W. Cai, X. Li, J. W. Suk, J. R. Potts & R. S. Ruoff. Graphene and Graphene Oxide: Synthesis, Properties, and Applications. *Advanced Materials* **22** (2010) 3906-24
- [32] Balandin A. A., S. Ghosh, W. Bao, I. Calizo, D. Teweldebrhan, F. Miao & C. N. Lau. Superior Thermal Conductivity of Single-Layer Graphene. *Nano Lett.* **8** (2008) 902-7
- [33] Goli P., S. Legedza, A. Dhar, R. Salgado, J. Renteria & A. A. Balandin. Graphene-enhanced hybrid phase change materials for thermal management of Li-ion batteries. *Journal of Power Sources* **248** (2014) 37-43
- [34] Renteria J., D. Nika & A. Balandin. Graphene Thermal Properties: Applications in Thermal Management and Energy Storage. *Applied Sciences* **4** (2014) 525-47
- [35] Choi W., I. Lahiri, R. Seelaboyina & Y. S. Kang. Synthesis of Graphene and Its Applications: A Review. *Critical Reviews in Solid State and Materials Sciences* **35** (2010) 52-71
- [36] Blake P., E. W. Hill, A. H. Castro Neto, K. S. Novoselov, D. Jiang, R. Yang, T. J. Booth & A. K. Geim. Making graphene visible. *Appl. Phys. Lett.* **91** (2007) 063124
- [37] Ni Z., Y. Wang, T. Yu & Z. Shen. Raman spectroscopy and imaging of graphene. *Nano Res.* **1** (2008) 273-91
- [38] Ferrari A. C., J. C. Meyer, V. Scardaci, C. Casiraghi, M. Lazzeri, F. Mauri, S. Piscanec, D. Jiang, K. S. Novoselov, S. Roth & A. K. Geim. Raman Spectrum of Graphene and Graphene Layers. *Physical Review Letters* **97** (2006) 187401
- [39] Wang Y. y., Z. h. Ni, T. Yu, Z. X. Shen, H. m. Wang, Y. h. Wu, W. Chen & A. T. Shen Wee. Raman Studies of Monolayer Graphene: The Substrate Effect. *J. Phys. Chem. C* **112** (2008) 10637-40

- [40] Rohrl J., M. Hundhausen, K. V. Emtsev, T. Seyller, R. Graupner & L. Ley. Raman spectra of epitaxial graphene on SiC(0001). *Appl. Phys. Lett.* **92** (2008) 201918
- [41] Das A., B. Chakraborty & A. K. Sood. Raman spectroscopy of graphene on different substrates and influence of defects. *Bulletin of Material Science* **31** (2008) 579-84
- [42] Hong J., M. K. Park, E. J. Lee, D. Lee, D. S. Hwang & S. Ryu. Origin of New Broad Raman D and G Peaks in Annealed Graphene. *Sci. Rep.* **3** (2013) 2700
- [43] Stankovich S., D. A. Dikin, R. D. Piner, K. A. Kohlhaas, A. Kleinhammes, Y. Jia, Y. Wu, S. T. Nguyen & R. S. Ruoff. Synthesis of graphene-based nanosheets via chemical reduction of exfoliated graphite oxide. *Carbon* **45** (2007) 1558-65
- [44] Xia Z. Y., S. Pezzini, E. Treossi, G. Giambastiani, F. Corticelli, V. Morandi, A. Zanelli, V. Bellani & V. Palermo. The Exfoliation of Graphene in Liquids by Electrochemical, Chemical, and Sonication-Assisted Techniques: A Nanoscale Study. *Advanced Functional Materials* **23** (2013) 4684-93
- [45] Sutter P. Epitaxial graphene: How silicon leaves the scene. *Nat Mater* **8** (2009) 171-2
- [46] Tzalenchuk A., S. Lara-Avila, A. Kalaboukhov, S. Paolillo, M. Syvajarvi, R. Yakimova, O. Kazakova, T. J. B. M. Janssen, V. Fal'ko & S. Kubatkin. Towards a quantum resistance standard based on epitaxial graphene. *Nat Nano* **5** (2010) 186-9
- [47] Cappelli E. et al. Nano-graphene growth and texturing by Nd:YAG pulsed laser ablation of graphite on Silicon. *JPCS* **59** (2007) 616
- [48] Dreyer D. R., S. Park, C. W. Bielawski & R. S. Ruoff. The chemistry of graphene oxide. *Chemical Society Reviews* **39** (2010) 228-40
- [49] He H., J. Klinowski, M. Forster & A. Lerf. A new structural model for graphite oxide. *Chemical Physics Letters* **287** (1998) 53-6

- [50] Brodie B. C. Sur le poids atomique du graphite. *Ann. Chim. Phys.* **59** (1860) 466–72
- [51] Staudenmaier L. Verfahren zur Darstellung der Graphitsäure. *Berichte der deutschen chemischen Gesellschaft* **31** (1898) 1481-7
- [52] Hummers W. S.R. E. Offeman. Preparation of Graphitic Oxide. *J. Am. Chem. Soc.* **80** (1958) 1339
- [53] Park S.R. S. Ruoff. Chemical methods for the production of graphenes. *Nat Nano* **4** (2009) 217-24
- [54] Buchsteiner A., A. Lerf & J. Pieper. Water Dynamics in Graphite Oxide Investigated with Neutron Scattering. *The Journal of Physical Chemistry B* **110** (2006) 22328-38
- [55] Stankovich S., R. D. Piner, X. Chen, N. Wu, S. T. Nguyen & R. S. Ruoff. Stable aqueous dispersions of graphitic nanoplatelets via the reduction of exfoliated graphite oxide in the presence of poly(sodium 4-styrenesulfonate). *Journal of Materials Chemistry* **16** (2006) 155-8
- [56] Jung I., M. Pelton, R. Piner, D. A. Dikin, S. Stankovich, S. Watcharotone, M. Hausner & R. S. Ruoff. Simple Approach for High-Contrast Optical Imaging and Characterization of Graphene-Based Sheets. *Nano Lett.* **7** (2007) 3569-75
- [57] Si Y.E. T. Samulski. Synthesis of Water Soluble Graphene. *Nano Lett.* **8** (2008) 1679-82
- [58] Eda G., G. Fanchini & M. Chhowalla. Large-area ultrathin films of reduced graphene oxide as a transparent and flexible electronic material. *Nat Nano* **3** (2008) 270-4
- [59] Wang X., L. Zhi & K. Müllen. Transparent, Conductive Graphene Electrodes for Dye-Sensitized Solar Cells. *Nano Lett.* **8** (2007) 323-7
- [60] Xu Y., H. Bai, G. Lu, C. Li & G. Shi. Flexible Graphene Films via the Filtration of Water-Soluble Noncovalent Functionalized Graphene Sheets. *J. Am. Chem. Soc.* **130** (2008) 5856-7

- [61] Park S., J. An, R. D. Piner, I. Jung, D. Yang, A. Velamakanni, S. T. Nguyen & R. S. Ruoff. Aqueous Suspension and Characterization of Chemically Modified Graphene Sheets. *Chem. Mat.* **20** (2008) 6592-4
- [62] Chen H., M. B. Müller, K. J. Gilmore, G. G. Wallace & D. Li. Mechanically Strong, Electrically Conductive, and Biocompatible Graphene Paper. *Advanced Materials* **20** (2008) 3557-61
- [63] Ng Y. H., A. Iwase, A. Kudo & R. Amal. Reducing Graphene Oxide on a Visible-Light BiVO<sub>4</sub> Photocatalyst for an Enhanced Photoelectrochemical Water Splitting. *J. Phys. Chem. Lett.* **1** (2010) 2607-12
- [64] Cote L. J., R. Cruz-Silva & J. Huang. Flash Reduction and Patterning of Graphite Oxide and Its Polymer Composite. *J. Am. Chem. Soc.* **131** (2009) 11027-32
- [65] Gao X., J. Jang & S. Nagase. Hydrazine and Thermal Reduction of Graphene Oxide: Reaction Mechanisms, Product Structures, and Reaction Design. *J. Phys. Chem. C* **114** (2009) 832-42
- [66] Gao W., N. Singh, L. Song, Z. Liu, A. L. M. Reddy, L. Ci, R. Vajtai, Q. Zhang, B. Wei & P. M. Ajayan. Direct laser writing of micro-supercapacitors on hydrated graphite oxide films. *Nat Nano* **6** (2011) 496-500
- [67] Zhang Y., L. Guo, S. Wei, Y. He, H. Xia, Q. Chen, H.-B. Sun & F.-S. Xiao. Direct imprinting of microcircuits on graphene oxides film by femtosecond laser reduction. *Nano Today* **5** (2010) 15-20
- [68] Trusovas R., G. Račiukaitis, J. Barkauskas & R. Mažeikienė. Laser Induced Graphite Oxide/Graphene Transformation. *Journal of Laser Micro/Nanoengineering* **7** (2012) 49-53
- [69] Barkauskas J., J. Dakševič, R. Juškėnas, R. Mažeikienė, G. Niaura, G. Račiukaitis, A. Selskis, I. Stankevičienė & R. Trusovas. Nanocomposite films and coatings produced by interaction between graphite oxide and Congo red. *J. Mater. Sci.* **47** (2012) 5852-60



- [70] Zhang H.Y. Miyamoto. Graphene production by laser shot on graphene oxide: An ab initio prediction. *Phys. Rev.* **85** (2012) 033402
- [71] Sokolov D. A., K. R. Shepperd & T. M. Orlando. Formation of Graphene Features from Direct Laser-Induced Reduction of Graphite Oxide. *J. Phys. Chem. Lett.* **1** (2010) 2633-6
- [72] Santanu Das W. C. Graphene: Synthesis and Applications Nanomaterials and Their Applications(Crc Press Llc, 2011), 27-63.
- [73] Fan X., W. Peng, Y. Li, X. Li, S. Wang, G. Zhang & F. Zhang. Deoxygenation of Exfoliated Graphite Oxide under Alkaline Conditions: A Green Route to Graphene Preparation. *Advanced Materials* **20** (2008) 4490-3
- [74] Dubin S., S. Gilje, K. Wang, V. C. Tung, K. Cha, A. S. Hall, J. Farrar, R. Varshneya, Y. Yang & R. B. Kaner. A One-Step, Solvothermal Reduction Method for Producing Reduced Graphene Oxide Dispersions in Organic Solvents. *ACS Nano* **4** (2010) 3845-52
- [75] McAllister M. J., J.-L. Li, D. H. Adamson, H. C. Schniepp, A. A. Abdala, J. Liu, M. Herrera-Alonso, D. L. Milius, R. Car, R. K. Prud'homme & I. A. Aksay. Single Sheet Functionalized Graphene by Oxidation and Thermal Expansion of Graphite. *Chem. Mat.* **19** (2007) 4396-404
- [76] Wu Z.-S., W. Ren, L. Gao, J. Zhao, Z. Chen, B. Liu, D. Tang, B. Yu, C. Jiang & H.-M. Cheng. Synthesis of Graphene Sheets with High Electrical Conductivity and Good Thermal Stability by Hydrogen Arc Discharge Exfoliation. *ACS Nano* **3** (2009) 411-7
- [77] Lv W., D.-M. Tang, Y.-B. He, C.-H. You, Z.-Q. Shi, X.-C. Chen, C.-M. Chen, P.-X. Hou, C. Liu & Q.-H. Yang. Low-Temperature Exfoliated Graphenes: Vacuum-Promoted Exfoliation and Electrochemical Energy Storage. *ACS Nano* **3** (2009) 3730-6
- [78] Chen W., L. Yan & P. R. Bangal. Preparation of graphene by the rapid and mild thermal reduction of graphene oxide induced by microwaves. *Carbon* **48** (2010) 1146-52

- [79] Zhou Y., Q. Bao, L. A. L. Tang, Y. Zhong & K. P. Loh. Hydrothermal Dehydration for the “Green” Reduction of Exfoliated Graphene Oxide to Graphene and Demonstration of Tunable Optical Limiting Properties. *Chem. Mat.* **21** (2009) 2950-6
- [80] Wei Z., D. Wang, S. Kim, S.-Y. Kim, Y. Hu, M. K. Yakes, A. R. Laracuenta, Z. Dai, S. R. Marder, C. Berger, W. P. King, W. A. de Heer, P. E. Sheehan & E. Riedo. Nanoscale Tunable Reduction of Graphene Oxide for Graphene Electronics. *Science* **328** (2010) 1373-6
- [81] Xu J.-L., X.-L. Li, Y.-Z. Wu, X.-P. Hao, J.-L. He & K.-J. Yang. Graphene saturable absorber mirror for ultra-fast-pulse solid-state laser. *Opt. Lett.* **36** (2011) 1948-50
- [82] Yang D., A. Velamakanni, G. Bozoklu, S. Park, M. Stoller, R. Piner, S. Stankovich, I. Jung, D. Field & C. Ventricejr. Chemical analysis of graphene oxide films after heat and chemical treatments by X-ray photoelectron and Micro-Raman spectroscopy. *Carbon* **47** (2009) 145-52
- [83] Ganguly A., S. Sharma, P. Papakonstantinou & J. Hamilton. Probing the Thermal Deoxygenation of Graphene Oxide Using High-Resolution In Situ X-ray-Based Spectroscopies. *J. Phys. Chem. C* **115** (2011) 17009-19
- [84] Wang H., J. T. Robinson, X. Li & H. Dai. Solvothermal Reduction of Chemically Exfoliated Graphene Sheets. *J. Am. Chem. Soc.* **131** (2009) 9910-1
- [85] Huh S. H. Physics and Applications of Graphene - Experiments (InTech, 2011), 73-90.
- [86] Zhou Y., Q. Bao, B. Varghese, L. A. L. Tang, C. K. Tan, C.-H. Sow & K. P. Loh. Microstructuring of Graphene Oxide Nanosheets Using Direct Laser Writing. *Advanced Materials* **22** (2010) 67-71
- [87] Tao Y., B. Varghese, M. Jaiswal, S. Wang, Z. Zhang, B. Oezylmaz, K. Loh, E. Tok & C. Sow. Localized insulator-conductor transformation of

- graphene oxide thin films via focused laser beam irradiation. *Appl. Phys. A* **106** (2012) 523-31
- [88] Sokolov D. A., C. M. Rouleau, D. B. Geohegan & T. M. Orlando. Excimer laser reduction and patterning of graphite oxide. *Carbon* **53** (2013) 81-9
- [89] Yung K. C., H. Liem, H. S. Choy, Z. C. Chen, K. H. Cheng & Z. X. Cai. Laser direct patterning of a reduced-graphene oxide transparent circuit on a graphene oxide thin film. *J. Appl. Phys.* **113** (2013) 244903
- [90] Mukherjee R., A. V. Thomas, A. Krishnamurthy & N. Koratkar. Photothermally Reduced Graphene as High-Power Anodes for Lithium-Ion Batteries. *ACS Nano* **6** (2012) 7867-78
- [91] Orabona E., A. Ambrosio, A. Longo, G. Carotenuto, L. Nicolais & P. Maddalena. Holographic patterning of graphene-oxide films by light-driven reduction. *Optics Letters* **39** (2014) 4263-6
- [92] Li Y.-C., T.-F. Yeh, H.-C. Huang, H.-Y. Chang, C.-Y. Lin, L.-C. Cheng, C.-Y. Chang, H. Teng & S.-J. Chen. Graphene oxide-based micropatterns via high-throughput multiphoton-induced reduction and ablation. *Opt. Express* **22** (2014) 19726-34
- [93] Kumar P., K. S. Subrahmanyam & C. N. R. Rao. Graphene Produced By Radiation-Induced Reduction Of Graphene Oxide. *International Journal of Nanoscience* **10** (2011) 559-66
- [94] Huang L., Y. Liu, L.-C. Ji, Y.-Q. Xie, T. Wang & W.-Z. Shi. Pulsed laser assisted reduction of graphene oxide. *Carbon* **49** (2011) 2431-6
- [95] Chang H.-W., Y.-C. Tsai, C.-W. Cheng, C.-Y. Lin & P.-H. Wu. Reduction of graphene oxide in aqueous solution by femtosecond laser and its effect on electroanalysis. *Electrochemistry Communications* **23** (2012) 37-40
- [96] Ghadim E. E., N. Rashidi, S. Kimiagar, O. Akhavan, F. Manouchehri & E. Ghaderi. Pulsed laser irradiation for environment friendly reduction of graphene oxide suspensions. *Applied Surface Science* **301** (2014) 183-8

- [97] Xiong W., Y. S. Zhou, W. J. Hou, L. J. Jiang, Y. Gao, L. S. Fan, L. Jiang, J. F. Silvain & Y. F. Lu. Direct writing of graphene patterns on insulating substrates under ambient conditions. *Sci. Rep.* **4** (2014) 4892
- [98] Han G. H., S. J. Chae, E. S. Kim, F. Güneş, I. H. Lee, S. W. Lee, S. Y. Lee, S. C. Lim, H. K. Jeong, M. S. Jeong & Y. H. Lee. Laser Thinning for Monolayer Graphene Formation: Heat Sink and Interference Effect. *ACS Nano* **5** (2010) 263-8
- [99] Piazzzi M., L. Croin, E. Vittone & G. Amato. Laser-induced etching of few-layer graphene synthesized by Rapid-Chemical Vapour Deposition on Cu thin films. *SpringerPlus* **1** (2012) 52
- [100] Dhar S. A new route to graphene layers by selective laser ablation. *AIP Advances* **1** (2011) 022109
- [101] Krauss B., T. Lohmann, D. H. Chae, M. Haluska, K. von Klitzing & J. H. Smet. Laser-induced disassembly of a graphene single crystal into a nanocrystalline network. *Phys. Rev.* **79** (2009) 165428
- [102] Barkauskas J., I. Stankevičienė, J. Dakševič & A. Padarauskas. Interaction between graphite oxide and Congo red in aqueous media. *Carbon* **49** (2011) 5373-81
- [103] Li F., Y. Bao, J. Chai, Q. Zhang, D. Han & L. Niu. Synthesis and Application of Widely Soluble Graphene Sheets. *Langmuir* **26** (2010) 12314-20
- [104] Chen S., A. L. Moore, W. Cai, J. W. Suk, J. An, C. Mishra, C. Amos, C. W. Magnuson, J. Kang, L. Shi & R. S. Ruoff. Raman Measurements of Thermal Transport in Suspended Monolayer Graphene of Variable Sizes in Vacuum and Gaseous Environments. *ACS Nano* **5** (2010) 321-8
- [105] John H. Lienhard IV J. H. L. V. A Heat Transfer Textbook, (Phlogiston Press, 2005), 49-98.
- [106] Amini S., J. Garay, G. Liu, A. A. Balandin & R. Abbaschian. Growth of large-area graphene films from metal-carbon melts. *J. Appl. Phys.* **108** (2010) 094321-7

- [107] Graf D., F. Molitor, K. Ensslin, C. Stampfer, A. Jungen, C. Hierold & L. Wirtz. Raman imaging of graphene. *Solid State Commun.* **143** (2007) 44-6
- [108] Gupta A., G. Chen, P. Joshi, S. Tadigadapa & Eklund. Raman Scattering from High-Frequency Phonons in Supported n-Graphene Layer Films. *Nano Lett.* **6** (2006) 2667-73
- [109] Tsu R., J. González H & I. Hernández C. Observation of splitting of the  $E_{2g}$  mode and two-phonon spectrum in graphites. *Solid State Commun.* **27** (1978) 507-10
- [110] Graf D., F. Molitor, K. Ensslin, C. Stampfer, A. Jungen, C. Hierold & L. Wirtz. Spatially resolved raman spectroscopy of single- and few-layer graphene. *Nano Lett.* **7** (2007) 238-42
- [111] Duhee Yoon H. M. a. H. C. J. S. C., Jung Ae Choi and Bae Ho Park. Variations in the Raman Spectrum as a Function of the Number of Graphene Layers. *J. Korean Phys. Soc.* **55** (2009) 1299-303
- [112] Jorio A., E. H. M. Ferreira, M. V. O. Moutinho, F. Stavale, C. A. Achete & R. B. Capaz. Measuring disorder in graphene with the G and D bands. *physica status solidi (b)* **247** (2010) 2980-2
- [113] Jorio A., E. h. m. Ferreira, L. G. Cançado, C. A. Achete & R. B. Capaz. Physics and Applications of Graphene - Experiments (InTech, 2011), 439-54.
- [114] Kumar S., M. Anija, N. Kamaraju, K. S. Vasu, K. S. Subrahmanyam, A. K. Sood & C. N. R. Rao. Femtosecond carrier dynamics and saturable absorption in graphene suspensions. *Appl. Phys. Lett.* **95** (2009) 191911
- [115] Mu X., X. Wu, T. Zhang, D. B. Go & T. Luo. Thermal Transport in Graphene Oxide – From Ballistic Extreme to Amorphous Limit. *Sci. Rep.* **4** (2014) 3909
- [116] Ferrari A. C.J. Robertson. Interpretation of Raman spectra of disordered and amorphous carbon. *Phys. Rev.* **61** (2000) 14095-107
- [117] Ferrari A. C.J. Robertson. Resonant Raman spectroscopy of disordered, amorphous, and diamondlike carbon. *Phys. Rev.* **64** (2001) 075414

- [118] Lobo D. E., J. Fu, T. Gengenbach & M. Majumder. Localized Deoxygenation and Direct Patterning of Graphene Oxide Films by Focused Ion Beams. *Langmuir* **28** (2012) 14815-21
- [119] Wang Z., X. Huang, R. Xue & L. Chen. Dispersion effects of Raman lines in carbons. *J. Appl. Phys.* **84** (1998) 227-31
- [120] Mathew S., T. K. Chan, D. Zhan, K. Gopinadhan, A. Roy Barman, M. B. H. Breese, S. Dhar, Z. X. Shen, T. Venkatesan & J. T. L. Thong. Mega-electron-volt proton irradiation on supported and suspended graphene: A Raman spectroscopic layer dependent study. *J. Appl. Phys.* **110** (2011) 084309
- [121] Trusovas R., K. Ratautas, G. Račiukaitis, J. Barkauskas, I. Stankevičienė, G. Niaura & R. Mažeikienė. Reduction of graphite oxide to graphene with laser irradiation. *Carbon* **52** (2013) 574-82
- [122] Milovan J., S. Milesa, K. Branka, B. Slobodan, D. Dragan, D. Mirko & K. Aleksander. Characterization of laser beam interaction with carbon materials. *Laser Physics* **23** (2013) 056002
- [123] Wu C. H., S. Y. Chen & P. Shen. Polyynes and flexible Si-H doped carbon nanoribbons by pulsed laser ablation of graphite in tetraethyl orthosilicate. *Carbon* **67** (2014) 27-37
- [124] Dittmar H., F. Gäbler & U. Stute. UV-laser Ablation of Fibre Reinforced Composites with Ns-Pulses. *Physics Procedia* **41** (2013) 266-75